

8. SITE 1177¹

Shipboard Scientific Party²

SITE SUMMARY

The science objective of Site 1177 was to study the stratigraphic, geochemical, and physical properties framework of a reference site along the Ashizuri Transect. This transect includes Sites 297, 298, 582, and 583.

We recognized five lithostratigraphic units at Site 1177. Unit I (upper Shikoku Basin facies) is Pliocene in age (300.20 to 401.76 meters below seafloor [mbsf]) and consists mainly of weakly indurated hemipelagic mud interbedded with fresh volcanic ash. Unit II (lower Shikoku hemipelagic facies) is late Miocene in age (401.76 to 449.30 mbsf) and is composed almost entirely of a more strongly indurated hemipelagic mudstone than that of Unit I. Unit III (lower Shikoku turbidite facies) is early to late Miocene in age (449.30 to 748.35 mbsf) and consists of turbidite sand, silty sand, gravel, mudstone-clast conglomerate, and hemipelagic mudstone, plus a few thin layers of carbonate-cemented claystone and siliceous claystone. There are four sand-rich packets within this facies, and most of the siliciclastic sands contain abundant woody plant fragments. Mudstones display vivid color contrasts because of variations in clay mineralogy. Sediment dispersal evidently occurred through a broad system of coalescing submarine fans. Unit IV (volcaniclastic-rich facies) is early Miocene in age (748.35 to 831.08 mbsf). This unit consists of variegated mudstone to claystone, volcanic ash, and silt turbidites with both volcaniclastic and siliciclastic compositions. Many of the mudstone beds are enriched in expandable clay minerals. Unit V is basaltic basement (831.08 to 832.13 mbsf) and is probably early Miocene in age. The basalt contains one pillow structure, and an intrusive contact with overlying sediment is highly altered.

Deformation structures at this site, oceanward of the prism, are very sparse, more so than at the reference site at the Muroto Transect. This near absence at Site 1177 of structures and bedding dips $>10^\circ$ may result

¹Examples of how to reference the whole or part of this volume.

²Shipboard Scientific Party addresses.

from slower rates of sedimentation, slight differences in lithology, or differences in topography of the substrate. Early soft-sediment compaction-related structures are present between 748 and 831 mbsf; the main tectonic structure is a faulted and diagenetically altered interval between 579.45 and 581.10 mbsf. The basalt at the bottom of Hole 1177A, at 831 mbsf, exhibits glassy rinds at its contact with the overlying sediment and networks of veins bearing calcite and/or chlorite in complex interrelationships.

Biostratigraphic age control was provided by calcareous nannofossils, although their abundance and states of preservation were generally poor throughout the sequence; major intervals are barren of nannofossils. A total of 11 biostratigraphic events were identified. The continuous sedimentary section spans the time interval from the Pliocene (Zone NN18) through the early Miocene (Zones NN4–NN2). The biostratigraphic age estimates indicate an average sedimentation rate for the late Pliocene of 87 m/m.y. and a lower sedimentation rate of 28.7 m/m.y. for the lower Miocene to Pliocene sediments.

Magnetic inclination data of Hole 1177A after alternating-field (AF) demagnetization at 30 mT were useful for interpretation of geomagnetic polarity changes from the early Miocene to Pliocene. The Brunhes/Matuyama boundary is expected to occur above the initial coring depth of 300 mbsf. The Reunion Event (2.14 Ma) of the Matuyama Chron is interpreted to occur at 301.85 mbsf. The Matuyama/Gauss (2.581 Ma) and Gauss/Gilbert (3.58 Ma) boundaries are interpreted to occur at 328.55 and 384.25 mbsf, respectively. The beginning of Chron C3A (5.894 Ma) is identified to occur at 427.45 mbsf.

Sharp chemical discontinuities between and within lithostratigraphic units, particularly intense in the Cl, Na, K, sulfate, and alkalinity concentrations, and a high-sulfate turbidite unit in the middle half of the section are outstanding characteristics of Site 1177 pore fluid concentration-depth profiles. Discontinuities within lithostratigraphic units are unique for this site and were not observed at Sites 1173, 1174, or 808. The chemical discontinuities correspond to discontinuities in physical properties, suggesting that solute and fluid transport out of specific sediment intervals may be retarded. Alternatively, these zones may reflect the recent onset of diagenetic reactions in compositionally distinct layers, such as ashes. The sharpest discontinuity occurs at ~410 mbsf, at the boundary between lithostratigraphic Units I and II. The concentration-depth profiles are therefore only continuous in Units I and II but show unusual variance in Units III and IV. The most conspicuous interval of this character was identified close to the bottom of the sediment section (775–805 mbsf).

Within Unit III there is a general decrease in Cl concentration; the minimum value is ~7% fresher than modern seawater concentration. This freshening is most plausibly produced by in situ smectite dehydration in combination with Cl uptake by an authigenic hydrous silicate. Na and K profiles show similar trends, but to a lesser extent. Sulfate reduction is complete in Units I and IV, driven by microbial activity. In Unit III, sulfate concentration is high, ~86% of the modern seawater value, indicating that since burial little microbial activity has occurred. This is probably the result of the very low content of nonwoody, labile organic matter available for microbial activity in the turbidites. Most of the labile organic matter was microbially oxidized when the turbidites were at or close to the seafloor and sulfate diffused into this section.

The important diagenetic reactions are ash alteration, particularly reflected in the Ca, Na, and K profiles; carbonate formation as reflected in

the Ca and alkalinity profiles; and opal-A dissolution as reflected in the Si profile.

The total organic carbon (TOC) contents ranged from 0.03 to 1.62 wt%, with an average value of 0.45 wt%. The highest carbon values were measured in the Shikoku turbidite facies sediments (Unit III), which contained a terrestrial component characterized by plant detritus and pieces of wood. The sulfur content ranged from 0 to 0.81 wt%, with the highest concentrations occurring between 400–520 mbsf and 650–770 mbsf. The C/N ratios indicated that a mixture of both marine and terrigenous sources were contributing to the overall sediment composition. Unlike Sites 1175 and 1176, the inorganic carbon (~0.78 wt%) and carbonate contents (~2.7 wt%) were low with the exception of some thin-bedded carbonate-cemented layers (up to 65 wt%) in the Shikoku turbidite facies (Unit III).

Methane concentrations in sediments below the sulfate reduction zone (~4.5 m down to 734 mbsf) are consistent with a bacterial origin. The $C_1/(C_1+C_2)$ ratio for hydrocarbons in sediments below 750 mbsf plot within the mixing zone, suggesting that more than one source of hydrocarbons may be present.

Microorganisms were enumerated in 23 samples collected from 300 to 830 mbsf. Bacteria are present in all but two samples (687 and 830 mbsf) at abundances that are generally lower than expected based on results from previous Ocean Drilling Program (ODP) sites. A small but statistically significant increase in bacterial populations occurs from 380 to ~740 mbsf that correlates with elevated sulfate concentrations in the interstitial water between these depths. The continued presence of sulfate is unexpected when bacteria are present at $\sim 10^6$ cells/cm³ and may be related to very low organic carbon concentrations in the sediment preventing significant amounts of bacterial sulfate reduction. A total of 21 whole-round cores were taken for shipboard enrichment cultures, cell viability, and shore-based microbiological analysis to measure potential bacterial activities, culture microorganisms, characterize nucleic acids, and investigate fatty acid biomarkers.

Variations in physical properties at Site 1177 correlate well with the lithostratigraphic units. Units I and II are both characterized by low scatter in porosity. Unit I maintains a nearly constant porosity of 60%–65%. At the top of Unit II (402 mbsf), porosities begin to decrease rapidly with depth, decreasing to 45%–53% by 450 mbsf. Unit III is characterized by a gradual decrease in porosity with depth and by increased scatter that may be due to lithologic variations in this turbidite-rich sequence. Unit IV exhibits significant scatter and shows no clear trend with depth. An excursion to lower porosity (~40%) at 475–510 mbsf within Unit III occurs in a sandy section. Anomalously high porosity (~8%–15% higher than in surrounding sediments) within Unit IV occurs in a 30-m-thick zone between 765 and 795 mbsf. Low vertical *P*-wave velocities and formation factors also characterize this zone.

Most gas permeameter determinations at Site 1177 range around the values given by the background hemipelagites. Carbonate-cemented claystones at 540 and 591 mbsf give slightly higher values, as do the altered ashes of Unit IV, but the increase is small. The upper sands in Unit III account for all of the high measurements at the site. Numerous wood-bearing silty sands were measured in the lower part of Unit III, but most give identical results to the background hemipelagites, suggesting blockage of the pore connections, perhaps by smectite.

In addition to serving as the reference site for the Ashizuri Transect, Site 1177 provides a comparison to the Muroto reference site (Site

1173). Comparison of the two sites will aid our understanding of the evolution of the Nankai Trough accretionary prism in two different geologic settings characterized by differing angles of prism taper.

OPERATIONS

Transit from Site 1176 to Proposed Site WNT-01B (Site 1177)

Before starting the transit to proposed Site WNT-01B (Site 1177), normal operations were interrupted for 3.25 hr so that the hydraulic umbilical of the active heave compensator (AHC), which was leaking, could be inspected. A hole in one of the high-pressure supply lines was found but could not be repaired on board. The ship began the transit at 1700 hr on 29 June. During the transit, the ship stopped for another 2 hr (2000 to 2200 hr) to finish securing the AHC hydraulic umbilical in the derrick. The 70-nmi transit was made in 7 hr. A seafloor positioning beacon was deployed at 0222 hr on 30 June, initiating Site 1177.

Hole 1177A

The precision depth recorder indicated a drilling depth of 4851.4 meters below rig floor (mbrf). A standard rotary core barrel (RCB) bottom hole assembly was made up and run down to the seafloor. At 1500 hr on 30 June, the driller detected the seafloor by a reduction in drill-string weight at 4844.3 meters below sea level (mbsl) (4856 mbrf). Hole 1177A was then spudded and drilled to 300.2 mbsf (5156.2 mbrf) (Tables T1, T2). Davis-Villinger temperature probe (DVTP) measurements were taken at 50.5 mbsf (4906.5 mbrf) and 120 mbsf (4976.0 mbrf) but did not obtain good data. Hole 1177A was then cored from 300.2 to 833.9 mbsf (Cores 1R to 56R) and recovered 282.74 m (53%).

Coring was stopped after basalt was recovered in Core 56R. The bit was then tripped out of the hole. Once the bit had cleared the seafloor, the drill line was slipped and cut. The seafloor positioning beacon was released and recovered at 0910 hr on 5 July. The bit cleared the rig floor at 1730 hr on 5 July, ending operations at Site 1177.

Transit from Site 1177 to Proposed Site ENT-10A (Site 1178)

The transit to proposed Site ENT-10A (Site 1178) began at 1930 hr on 5 July. Typhoon Kirogi was approaching our location from the south and was predicted to pass close to the drill site. Although the weather in the vicinity of the vessel was good, a heavy swell was coming out of the south, causing excessive pitch and roll of the vessel. Because of the deep water at proposed Site ENT-10A (~4554 mbsl), we decided not to deploy the drill string and to suspend operations until the weather would allow safe operations. While the vessel was on standby, 20 stands of 5-in drill pipe were removed from the riser hold, made up, and placed in the middle bay of the pipe racker. The leaking AHC hydraulic umbilical was removed and placed on pallets on the main deck, and the coaxial cable was removed from the vibration-isolated television frame winch in preparation for installation of the new cable during the Yokohama port call after the leg.

T1. Coring summary, p. 57.

T2. Coring summary by section, p. 58.

At 1045 hr on 7 July, we decided to move the vessel out of the path of typhoon Kirogi and maintain at least a 250-nmi distance from it. The vessel was moved ~98 nmi to the west and looped around behind the typhoon. Because of the loss in operations time as a result of the typhoon, all of the proposed Site ENT-10A objectives could not be accomplished. Therefore, we decided to core at alternate proposed Site ENT-09A (Site 1178) instead.

LITHOSTRATIGRAPHY

We recognized five lithostratigraphic units at Site 1177 (Fig. F1). Table T3 shows their relation to correlative units at ODP Sites 808, 1173, and 1174.

Unit I (Upper Shikoku Basin Facies)

Unit I is Pliocene in age and at least 101 m thick. The unit extends from 300.20 mbsf, where coring began, to 401.76 mbsf (Section 190-1177A-11R-5, 6 cm). Unit I consists of weakly indurated hemipelagic mudstone (silty claystone to clayey siltstone) interlayered with thin beds of volcanic ash (Fig. F2). The ash contains fresh or partially altered shards of volcanic glass. The base of Unit I is located below the deepest volcanic ash with minimal alteration. Unit I at Site 1177 is equivalent to the upper Shikoku Basin facies at Sites 808, 1173, and 1174 (Table T3).

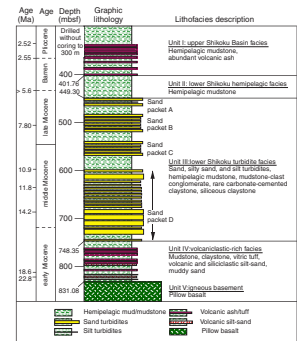
Unit II (Lower Shikoku Hemipelagic Facies)

Unit II is early Pliocene(?) to late Miocene in age and 47.54 m thick (Table T3). An interval barren of microfossils makes identification of the Pliocene/Miocene boundary uncertain. We placed the lithofacies boundaries at 401.76 mbsf (Section 190-1177A-11R-5, 6 cm) and 449.30 mbsf (Section 16R-4, 90 cm). Unit II consists of hemipelagic mudstone (silty claystone to clayey siltstone) with a few scattered laminae of siliceous claystone. The transition into Unit II coincides with a sharp decrease in amount of volcanic ash, but there is also a superimposed effect of mudstone compaction and diagenesis, as shown by porosity data (see "Physical Properties," p. 21). The mudstone is more strongly indurated than equivalent strata in Unit I, and X-ray diffraction (XRD) data show higher concentrations of expandable clay minerals (Table T4). The lower unit boundary occurs at a contact between hemipelagic mudstone and sandy turbidites (Fig. F1). Unit II at Site 1177 is equivalent to the upper part of the lower Shikoku Basin facies at Sites 808, 1173, and 1174 (Table T3).

Unit III (Lower Shikoku Turbidite Facies)

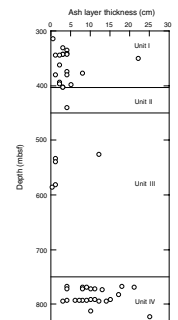
Unit III is 327.28 m thick and early to late Miocene in age (Fig. F1). Microfossils are sparse. The oldest dated horizon (691 mbsf) is 17.3–17.9 Ma (see "Biostratigraphy," p. 10). An equivalent turbidite facies does not exist at Sites 808, 1173, or 1174 (Table T3). The boundaries of Unit III are located at the top and bottom of two turbidite sand packets (Sections 190-1177A-16R-4, 90 cm, and 47R-5, 25 cm). Interbeds of sand, silty sand, and hemipelagic mudstone are the most characteristic feature of Unit III; these couplets occur together with scattered beds of

F1. Stratigraphic column, p. 27.



T3. Summary of stratigraphic relations, p. 64.

F2. Distribution and thickness of volcanic-ash layers, p. 28.



T4. Peak intensities and peak areas from XRD analysis, p. 65.

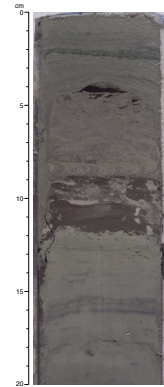
gravel, mudstone-clast conglomerate, carbonate-cemented claystone, and siliceous claystone. The sandy deposits are compacted but not cemented; this weak state of induration inhibited core recovery. Four discrete packets of sand-rich strata are present at depths of 449.30–472.80, 483.90–521.50, 540.10–569.06, and 598.16–748.35 mbsf (Fig. F1).

The hemipelagic mudstone typical of Unit III (silty claystone to clayey siltstone) has pronounced color banding, with colors varying from greenish gray to brownish gray, brown, and green. The colors, in part, reflect variations in the content of expandable clay minerals (Table T4). Higher contents of smectite also resulted in considerable amounts of sediment expansion once cores were split. Strata range from structureless to plane-parallel laminated or mottled by bioturbation. *Zoophycos* (Fig. F3) and *Chondrites* trace fossils are present locally. The mudstone is composed predominantly of clay minerals, silt-sized quartz, feldspar, sedimentary or metasedimentary lithic fragments, and minor amounts of volcanic glass (see “Site 1177 Smear Slides,” p. 57). Calcareous nannofossils are scarce. Disseminated wood and plant fragments are also present (Fig. F4), especially in the lower part of the unit. Laminae and thin beds of siliceous claystone vary in color from dark gray to dark green and probably formed by alteration of volcanic glass. Also scattered throughout the unit are thin beds of pale brown carbonate-cemented silty claystone and sand. Some of these zones have sharp contacts and are probably layered concretions.

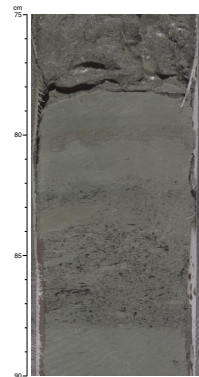
Deposits of silty sand, sand, gravel, and muddy sand range from laminae to thick beds. Lower contacts are sharp, and upper contacts are diffuse. Normal size grading is typical. Plane-parallel laminae are common in the upper parts of beds, and ripple cross-laminae are present locally (Fig. F5). The sandy deposits contain subrounded to angular grains of quartz, feldspar (including microcline), fine-grained metamorphic and sedimentary rock fragments, volcanic rock fragments, rare volcanic glass, and nannofossils (see “Site 1177 Smear Slides,” p. 57). Perhaps the most striking characteristic of Unit III turbidites is the unusual abundance of woody plant material. The organic matter usually is concentrated in the upper parts of sand beds together with intraformational mud clasts (Figs. F5, F6, F7). Core 190-1177A-46R contains a noteworthy example of mudstone-clast conglomerate with angular clasts, disorganized fabric, no size grading, and sandy matrix. Maximum clast size is 5–6 cm. Immediately above the conglomerate, numerous rip-up clasts of brown and green mudstone are dispersed through beds of sandy silt and sandy mud.

Unit III was deposited through a combination of hemipelagic settling, siliciclastic turbidity currents, and debris flows. The paucity of calcareous nannofossils in hemipelagic interbeds implies that the sediment was deposited close to or below the calcite compensation depth. Nannofossils are more common in the turbidites because of their rapid deposition. The abundance of quartz, sedimentary and metasedimentary lithic fragments, and woody organic matter indicates that the turbidites were derived from a landmass of significant size. Higher contents of disseminated smectite in the hemipelagic mudstones also indicate frequent influx of pyroclastic debris. The most likely detrital provenance is the central to southwest portion of Japan. That geologic domain was probably emergent during the middle to late Miocene as indicated by the presence of a major unconformity surface (Kano et al., 1991). Unlike the modern Nankai trench-wedge facies, however, the Miocene turbidites of the Shikoku Basin must have spread out over an impressive surface area of the abyssal floor. Transverse sediment dis-

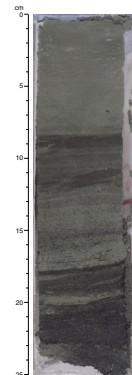
F3. *Zoophycos* in silty claystone from Unit III, p. 29.



F4. Wood fragments in silty claystone from Unit III, p. 30.



F5. Wood-rich sandy turbidite from Unit III interbedded with silty claystone, p. 31.



persal probably occurred through a broad system of coalescing submarine fans instead of a narrow axial-channel system typical of the modern trench.

Unit III at Site 1177 is lithologically similar to Unit 4 at Deep Sea Drilling Project (DSDP) Site 297 (Shipboard Scientific Party, 1975b), but there are also some important differences. Site 297 is located ~85 km to the south, and the turbidite section there is ~240 m thick (as compared to 299 m at Site 1177). Barren specimens precluded identification of the Pliocene/Miocene boundary at Site 297, but the upper part of Unit 4 does contain early Pliocene microfossils. In comparison, the age of the turbidite succession at Site 1177 falls entirely within the Miocene. Thus, the available biostratigraphic control shows that the two turbidite successions are not the same age. Considerable overlap of correlative Miocene strata seems likely between the respective units, but this inference cannot be proven using existing biostratigraphic data.

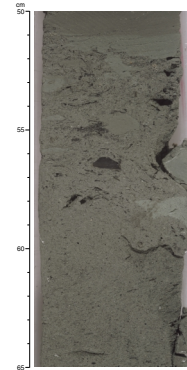
Farther to the northeast, Sites 1173 and 1174 are located above a structural high in the igneous basement that is associated with the Kinan Seamount chain. Temporal equivalents to the Miocene turbidite facies within that transect area are composed exclusively of hemipelagic mudstone. Evidently, seafloor relief along higher segments of the seamount chain was enough to prevent upslope deposition by sandy turbidity currents. We also note, however, that seismic reflection data from southeast of Site 1173 show an expanded Miocene section above a basement low along the axis of the seamount chain (Fig. F6, p. 14, in the "Data Report: Structural Setting of the Leg 190 Muroto Transect" chapter). Continuous high-amplitude reflectors within this interval of the reflection profile could represent lateral equivalents of the lower Shikoku turbidite facies, as recovered at Site 1177. If this interpretation is correct, the Kinan Seamount chain did not form a continuous barrier to sediment gravity flows moving from the paleomargin of central Japan toward the southeast.

Unit IV (Volcaniclastic-Rich Facies)

Unit IV is early Miocene in age and 82.73 m thick. The unit extends from 748.35 mbsf (Section 190-1177A-47R-5, 25 cm) to 831.08 mbsf (Section 56R-3, 0 cm). Its upper part (748.35–766.58 mbsf) consists predominantly of silty claystone with local silt laminae. The most distinguishing characteristics of Unit IV include the common occurrence of relatively fresh volcanic ash (Fig. F8), variegated mudstone to claystone with disseminated volcanic glass, and sandy to silty siliciclastic and volcaniclastic beds without terrigenous organic matter. Small-scale recumbent folds and chaotic bedding also indicate that slumping has affected some of the finer-grained sediments (Fig. F9). Examples of soft-sediment deformation are present in the following intervals: 190-1177A-50R-1, 67–74 cm, and 110–116 cm; 50R-2, 18–31 cm; 55R-2, 112–115 cm; and 55R-3, 16–20 cm.

The hemipelagic mudstone to claystone of Unit IV varies in color from brownish gray to greenish gray and green. Variations among tones of green are vivid, and many of the boundaries among thicker color zones are sharp. As in Unit III, these color variations are caused by changes in clay mineralogy (Table T4), and high concentrations of smectite caused significant amounts of core expansion upon splitting. The fine-grained deposits range from massive to laminated or bioturbated, and *Zoophycos* trace fossils are present locally. The mineral constituents are predominantly clay minerals. Disseminated volcanic glass

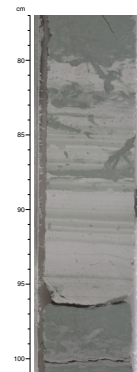
F6. Siliciclastic turbidite from Unit III containing plant material and rip-up clasts, p. 32.



F7. Siliciclastic turbidite from Unit III with rip-up clasts, p. 33.



F8. Laminated and bioturbated volcanic ash from Unit IV, p. 34.



is also common, as are quartz, feldspar, and lithic fragments (see “[Site 1177 Smear Slides](#),” p. 57). Microfossils are less common, but nanofossils are present in the lower part of the unit.

Most of the volcanic ash deposits are in the middle of Unit IV between 766.58 mbsf (Section 190-1177A-49R-4, 78 cm) and 793.33 mbsf (52R-3, 3 cm). These ash layers are interbedded with massive mudstone-claystone and laminated glass-rich silt. The volcanic ash is present in beds as thick as 18 cm (Fig. [F2](#)). Color varies from white to green, grayish green, and brown. The ash beds have sharp bases, diffuse to bioturbated tops, and plane-parallel laminae (Fig. [F8](#)). The ash contains clear, fresh volcanic glass, as well as some shards that are partially altered to clay. Most of the crystal constituents are composed of quartz and feldspar (Table [T5](#)). The lower part of Unit IV, between 793.33 and 831.08 mbsf, consists of massive or laminated silty claystone interbedded with volcanic ash and both siliciclastic and volcanoclastic sand to silt (interval 190-1177A-52R-3, 3 cm, to 56R-3, 0 cm). These weakly lithified, relatively coarse-grained lithologies vary in thickness from a few millimeters to 70 cm. The thicker silt and sandy mudstone beds are typically laminated, with sharp bases and normal grading. Composition of the silt- and sand-sized fragments varies considerably. Most of the sands contain abundant volcanic glass mixed with quartz, clay minerals, and altered volcanic lithic clasts. Some of the silts also contain abundant fragmented glass shards, whereas others are rich in quartz, altered lithic clasts, and clay minerals, with only traces of volcanic glass (see “[Site 1177 Smear Slides](#),” p. 57).

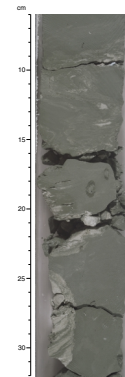
Unit IV formed through a combination of hemipelagic settling, fallout of volcanoclastic material, turbidity currents, and local remobilization through slumps. Nanofossils in the lower part of the unit also indicate that deposition occurred above the calcite compensation depth. This relatively shallow depth is consistent with deposition above juvenile igneous basement close to the Shikoku Basin spreading ridge.

The volcanoclastic-rich facies at Site 1177 appears to be correlative with Unit 5 at DSDP Site 297 (Shipboard Scientific Party, 1975b). Fine-grained vitric ash and ash-rich claystone at Site 297 is also late early Miocene to middle Miocene in age; basal sediments at Site 1177 are 18.6–23.2 Ma. On the other hand, coring at Site 297 was terminated ~80 m above igneous basement. This means that the probable thickness of the ash-rich claystone unit is nearly 210 m at Site 297, whereas the cored thickness at Site 1177 is only 82.73 m.

A true stratigraphic equivalent to Unit IV does not occur within the eastern Nankai Trough transect area that includes Sites 1173 and 1174. The rhyolitic tuff deposits at Site 808, although similar in some lithologic respects, are no older than 13.6 Ma (Shipboard Scientific Party, 1991). The volcanoclastic facies at Site 808, moreover, contains impressively thick beds of coarse-grained white to gray tuff. The early Miocene ash beds at Site 1177, in contrast, are older (by 5–9 m.y.), thinner, finer grained, and interbedded with volcanic and siliciclastic silt and sand. These differences make a rigorous stratigraphic correlation between the two units dubious.

Periodic influx of volcanoclastic material certainly affected the early stages of sedimentation within the western Shikoku Basin, but the source area of this volcanic and siliciclastic material remains uncertain. One possibility for the detrital source is the geologic domain of central to southwest Japan. Provenance of the sandy deposits of Unit IV, however, differs from the provenance of Unit III in that volcanic glass is common to abundant in many such beds and terrigenous plant debris

[F9](#). Contorted interbeds of volcanic ash and silty claystone of Unit IV, p. 35.



[T5](#). XRD analysis of volcanic ash, p. 68.

is scarce. Another possible detrital source is the Kyushu-Palau Ridge; this remnant arc is Paleogene in age and forms the western edge of Shikoku Basin (Karig, 1971). The oldest sedimentary strata recovered from DSDP Site 296 on Kyushu-Palau Ridge consist of lower(?) to upper Oligocene volcanic tuff, lapilli tuff, volcanic sandstone, and siltstone (Shipboard Scientific Party, 1975a). Based on this similarity in overall lithology, we suggest that the quartz and lithic-rich sand-silt beds of Unit IV originated from subaerial weathering of volcanic and volcanoclastic rocks that were exposed on the same subsiding remnant arc during early Miocene time.

Unit V (Basalt Basement)

Basalt of Unit V is probably early Miocene in age. We cored only 1.05 m into igneous basement, from 831.08 mbsf (Section 190-1177A-56R-3, 0 cm) to 832.13 mbsf (56R-3, 105 cm). The first occurrence of basalt displays a sharp contact with altered silty claystone (Fig. F10). The basalt is dark gray to black in color and aphyric to sparsely plagioclase phyric. The upper 30 cm of basalt has upper and lower chilled margins that are ~1 cm thick and concave. We interpret this geometry to be part of a pillow structure. A third chilled margin is straight. Alteration imparted a yellowish brown and grayish purple color to the interior and rim of the uppermost basalt. Fibrous veins of calcite and chlorite are common. We believe that the basalt formed through submarine lava flows and/or injection of sills near the spreading ridge that created the oceanic lithosphere of Shikoku Basin.

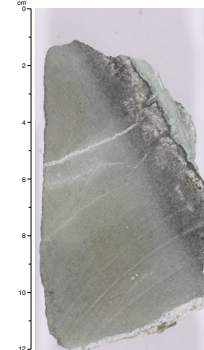
X-Ray Diffraction Mineralogy

The results of XRD analyses of bulk-sediment powders are shown in Figure F11. Data for two ash layers are in Table T5. Normalized relative mineral abundances within Unit I are similar to what we documented in equivalent deposits at Sites 1173 and 1174 (i.e., upper Shikoku Basin facies). Average values of total clay minerals, quartz, plagioclase, and calcite are 48%, 34%, 14%, and 3%, respectively (Table T6). The content of total clay minerals increases in Unit II to an average of 55%, and there is also an apparent decrease in the amount of cristobalite relative to quartz. This compositional boundary between Units I and II is fundamental because it also shows up as a pronounced shift in porosity values (see “Physical Properties,” p. 21). The scattered values of all constituents within Unit III are a consequence of interstratification among hemipelagic mud, turbidite mud and silt, and rare carbonate beds. The average content of total clay minerals within Unit III is 53%, but smectite content varies erratically (Table T4). The total clay value increases to 59% within Unit IV. In addition, Unit IV displays a significant increase in the ratio of cristobalite to quartz. Alteration of disseminated volcanic glass within the mudstone and claystone of Unit IV probably caused the apparent increase in cristobalite and total clay, particularly smectite-group minerals.

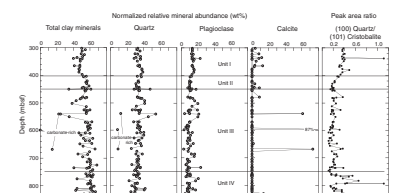
STRUCTURAL GEOLOGY

Deformation structures at Site 1177 are very sparse oceanward of the prism, as expected for a site designed to be a reference site. Bedding dips are <10° in the entire hole (Table T7). Intralayer folds and sedimentary

F10. Contact between green basal mudstone (Unit IV) and basalt (Unit V), p. 36.



F11. Abundances of total clay minerals, quartz, plagioclase, and calcite, p. 37.



T6. Mineral abundances based on XRD analysis of bulk-sediment powders, p. 69.

T7. Structural data, p. 71.

breccias, seen mostly between 748 and 831 mbsf (lithostratigraphic Unit IV) (see “**Lithostratigraphy**,” p. 5), are interpreted as early soft-sediment structures probably related to slope instabilities. The main later structure observed is a faulted interval from 579.45 to 581.10 mbsf that includes a healed normal fault and a few slickenlined fractures with greenish alteration walls (Fig. F12). Minor structures include web-like features with normal displacements at 502.45 mbsf in silty sand and stylolites at 537.00 mbsf in carbonate-cemented silty claystone.

The most surprising fact at Site 1177, compared with the other reference sites at the Nankai Trough (DSDP Site 582, Shipboard Scientific Party, 1986; also see “**Structural Geology**,” p. 9, in the “Site 1173” chapter), is the near absence of structures and dipping beds. The extreme scarcity of faults may be due to a differing response to compaction, either because of a slower rate of sedimentation above Unit III, slight differences in lithology, or differences in topography of the substrate. The virtually flat-lying beds throughout the hole and the lack of strongly disrupted intervals could be due to Site 1177 being farther oceanward with respect to the Nankai Trough compared to previous sites.

Approximately 1 m of basalt was recovered at the bottom of Hole 1177A at 831 mbsf. From 831.08 to 831.38 mbsf, the basalt pieces exhibit up to 1-cm-thick glassy rinds at the contact with overlying light green claystones (Fig. F10) and underlying coarser grained basalt. These uppermost basalt pieces show a set of fractures perpendicular to the glassy boundaries. In addition, a network of veins filled by varying proportions of calcite and chlorite is present in all the recovered basalt. Calcite veins tend to be subhorizontal or shallowly dipping but in places occupy higher angle fractures (Fig. F13). One of the veins reaches and crosscuts the contact with the sediments (Fig. F10). Calcite and chlorite veins and seams within the veins have crosscutting relationships, suggesting successive episodes of mineralization, but we were unable to determine a clear relative timing.

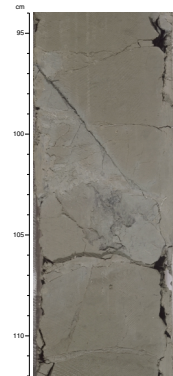
Uncalibrated Gas-Permeameter Measurements

Data collected from the gas permeameter at Site 1177 are shown in Figure F14. Plotting the data on a logarithmic scale (Fig. F14A), as was done for the other sites, reveals the relatively fine-scale variations among the poorly gas-permeable materials. However, a linear plot shows that most measurements differ little from 10^{-16} m² (Fig. F14B). The change in other physical properties reported at 410 mbsf is not reflected in the gas-permeability values. The appearance of sand with the facies change from Unit II to Unit III accounts for all the high measurements at the site. The carbonate-cemented claystones at 540 and 591 mbsf give slightly higher values, as do the altered ashes of Unit IV, but the increase is small. Numerous wood-bearing silty sands were measured in the lower part of Unit III but give identical results to the background hemipelagites. The one exception, at 696 mbsf, is unusually coarse, with wood fragments more than a centimeter long.

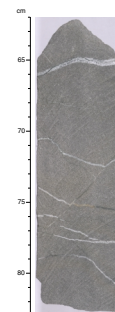
BIOSTRATIGRAPHY

Sediments recovered from Hole 1177A provide a sedimentary record from the Pliocene through the early Miocene. Calcareous nannofossils were used for developing the biostratigraphic framework according to

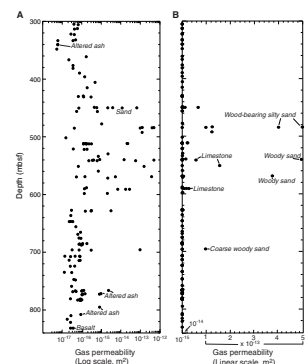
F12. Healed fault and brecciated fracture zone with greenish alteration of claystone, p. 38.



F13. Subhorizontal veins and high-angle fracture in basalt, p. 39.



F14. Gas-permeameter data plotted logarithmically and linearly, p. 40.



the zonation schemes of Martini (1971) with zonal modifications proposed by Young (1998) (Table T8). Abundance and preservation of calcareous nannofossils vary throughout the sequence. The nannofossil events recognized in Site 1177 are reported in Table T9. The epoch boundaries have been placed as in Table T10. For nannofossil ranges in Site 1177 see Table T11.

Calcareous Nannofossils

Hole 1177A was washed down to 300.20 mbsf. The sediments recovered from Hole 1177A range in age from Zone NN18 of the Pliocene to Zones NN4–NN2 of the early Miocene. Cores 190-1177A-1R to 8R bear mostly moderately to well-preserved nannofossil assemblages. Below this interval, from Core 190-1177A-9R to the bottom of the hole (832.13 mbsf), nannofossils are present only in low numbers and are poorly preserved except for Cores 190-1177A-18R to 23R with moderately preserved specimens. In general, assemblages are affected by both strong overgrowth and etching. Some intervals appear barren of nannofossils, inhibiting a zonal assignment for large sections of Site 1177. Frequent reworking of older nannofossils throughout the sequence, giving the sediments a seemingly older age, imposes further constraints on age determination.

Pliocene

The Pliocene sediments retrieved from Hole 1177A contain mostly moderately to well-preserved nannofossils (Samples 190-1177A-1R-CC [308.65 mbsf] to 7R-CC [367.11 mbsf]). The abundance of nannofossils is generally very low. The Pliocene nannofossil assemblages are dominated by different morphotypes of reticulofenestrads and discoasterids; associated are mainly *Coccolithus* spp., *Calcidiscus* spp., and sphenoliths. Reworked specimens were encountered frequently.

Sample 190-1177A-1R-CC contains *Discoaster brouweri*, the last occurrence of which defines the top of Zone NN18 (1.95 Ma) and thus assigns the top of the cored interval to be of Pliocene age. The top of Zone NN17, as marked by the last occurrence of *Discoaster pentaradiatus*, was recorded between Samples 190-1177A-4R-3, 68–69 cm, and 4R-CC. The last occurrence of *Discoaster surculus* (2.55 Ma), which defines the top of Zone NN16, was observed between Samples 190-1177A-6R-CC and 7R-4, 75–76 cm. The event defining the top of Zone NN14, the last occurrence of *Amaurolithus* spp. (4.0 Ma), was recorded between Samples 190-1177A-12R-CC and 13R-3, 75–76 cm. At this site *Discoaster asymmetricus* was only sporadically present, and most of the samples between 385.26 and 433.33 mbsf are depleted of nannofossils. Therefore, its first common occurrence, which marks the top of Zone NN13, could not be determined. The same problem applies to the base of Zone NN13, indicated by the first occurrence of *Ceratolithus cristatus*. Sample 190-1177A-14R-3, 70–71 cm, yields *Discoaster quinqueramus*, the last occurrence of which marks the top of Subzone NN11b (5.54 Ma). This event approximates the Pliocene/Miocene boundary (5.32 Ma).

Miocene

Miocene sediments (425.99 ± 7.34 to 832.13 mbsf) recovered from Hole 1177A yield poorly preserved assemblages. The Miocene nannofossils are of low abundance. Discoasterids, sphenoliths, and *Reticu-*

T8. Recognized nannofossil events, p. 73.

T9. Interval and depth constraints of calcareous nannofossil events, p. 74.

T10. Epoch boundaries, p. 75.

T11. Calcareous nannofossil range chart, p. 76.

lofenestra spp. are strongly altered by overgrowth. Reworking of nannofossils is common throughout the Miocene sediments. Reworked Paleogene specimens, mostly *Sphenolithus* spp., are confined to intervals between Samples 190-1177A-34R-CC and 35-CC (617.26–628.82 mbsf) and from Samples 190-1177A-43R-2, 66–67 cm, to 46R-2, 40–41 cm (705.86–734.40 mbsf) and exhibit strong overgrowth.

The top of Subzone NN11a as marked by the first occurrence of *Amaurolithus primus* (7.2 Ma) could not be identified because of its scarceness throughout the sequence. The presence of *Discoaster bergonii*, which is confined to a short interval (7.8–8.6 Ma) within Subzone NN11a in Sample 190-1177A-23R-1, 74–75 cm, provides an alternative datum event. The same sample yields the first *D. quinqueramus* specimens. The absence of nannofossils, except for rare and scattered specimens of *Reticulofenestra pseudoumbilicus* ($>7\ \mu\text{m}$), or zonal marker species precludes a precise zonal assignment for the interval between Samples 190-1177A-23R-CC and 32R-1, 68–69 cm. The last occurrence of *R. pseudoumbilicus* ($>7\ \mu\text{m}$), marking the top of Subzone NN10a, was observed between Samples 190-1177A-23R-CC and 26R-1, 49–50 cm. Bounding the barren interval, the last occurrence of *Coccolithus miope-lagicus* (10.9 Ma), the presence of which is basically restricted to Zone NN7 (Young, 1998), was recorded between Samples 190-1177A-32R-1, 68–69 cm, and 32R-CC (598.54 mbsf). This event approximates the boundary between the late and middle Miocene (11.2 Ma). The first occurrence of *Discoaster kugleri* marking the top of NN6 (11.8 Ma) was recorded between Samples 190-1177A-36R-1, 40–41 cm, and 36R-CC. The last occurrence of *Sphenolithus heteromorphus* (13.6 Ma), defining the top of Zone NN5, was recorded between Samples 190-1177A-39R-CC and 40R-1, 71–72 cm, as strongly altered by overgrowth and dissolution. The top of Zone NN4 (15.6 Ma), indicated by the last occurrence of *Helicosphaera ampliaperta*, was recorded between Samples 190-1177A-47R-2, 76–77 cm, and 47R-CC. The last occurrence of *Discoaster deflandrei*, which approximates the middle to lower Pliocene boundary, could not be determined because of the common reworking of *D. deflandrei*. Specimens of *Sphenolithus belemnos*, the range of which defines Zone NN3, were not identified, probably because of the poor state of preservation of the sphenoliths. The last appearance of *Discoaster druggii* (18.6 Ma), an event to occur within Zone NN3, was observed between Samples 190-1177A-50R-CC and 54R-CC. The event to define the base of Zone NN2 is the first occurrence of *D. druggii* (23.1 Ma). Because *D. druggii* is still present in the lowermost sample above basement (190-1177A-56R-2, 35–36 cm), the basal part of the cored sequence is assigned to Zones NN4–NN2 of the early Miocene.

PALEOMAGNETISM

Introduction

After measuring the natural remanent magnetization (NRM), all sections of the archive-half of the core were partially demagnetized using AF magnetization at 30 mT at 5-cm intervals to remove magnetic overprints acquired during RCB coring.

Inclinations document early Miocene to Pliocene geomagnetic polarity changes and were used in conjunction with the standard geomagnetic polarity time scale (GPTS) of Cande and Kent (1995) to date the sediments.

Paleomagnetic Results

After AF demagnetization, the stable depositional remanent magnetization was measured from 300.25 (Section 190-1177A-1R-1, 5 cm) (Fig. F15) to ~832.08 mbsf (Section 56R-3, 100 cm). The inclinations from 300.25 (Section 190-1177A-1R-1, 5 cm) to 450.25 mbsf (Section 16R-5, 35 cm) show a clear record of geomagnetic polarity changes. Below 450 mbsf, however, inclination changes provide limited information on the geomagnetic polarities because of poor core recovery. Rapid declination changes are interpreted to have been caused by rotation of individual pieces of the core during the RCB coring process.

The magnetic intensity shows a rapid repetition in values. There are five high-intensity and four low-intensity anomalies from the top to the bottom of Hole 1177A (Fig. F15). High intensity was continuously observed from the top of Hole 1177A (Section 190-1177A-1R-1, 5 cm) to 473.35 mbsf (Section 19R-1, 55 cm). A distinct low-intensity zone is abruptly present at 473.55 mbsf (Section 190-1177A-19R-1, 75 cm), and the low-intensity values terminate at 521.65 mbsf (Section 24R-1, 95 cm). After this low magnetic intensity, two high-intensity peaks are observed at 521.70–540.05 mbsf (interval 190-1177A-24R-1, 100 cm, through 25R-CC, 20 cm) and 569.35–608.15 mbsf (interval 190-1177A-29R-1, 40 cm, through 33R-1, 65 cm). These are followed by a rapid decrease in intensity values from 608.15 mbsf (Section 190-1177A-33R-1, 60 cm) to 684.85 mbsf (Section 41R-1, 45 cm). Below 684.90 mbsf (Section 190-1177A-41R-1, 45 cm), the intensity changes gradually into higher values, and this continuation of high intensity is terminated at 759.15 mbsf (Section 48R-5, 145 cm). Slightly low intensity is again seen from 759.25 mbsf (Section 190-1177A-48R-6, 5 cm) to 831.00 mbsf (Section 56R-2, 70 cm). The lower part of Hole 1177A consists mainly of volcanoclastics with high magnetic intensities in the range from 10^{-1} to 1 A/m.

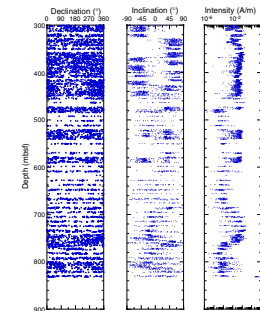
Magnetostratigraphy

Site 1177 magnetostratigraphy is based on polarity changes determined by measuring the inclination of the archive-half of the core after AF demagnetization at 30 mT. Early Miocene to Pliocene magnetic polarity changes were identified using biostratigraphic datums (calcareous nannofossils; see “Biostratigraphy,” p. 10) and correlated with the GPTS of Cande and Kent (1995) (Fig. F16). The identified chrons and subchrons are given in Table T12.

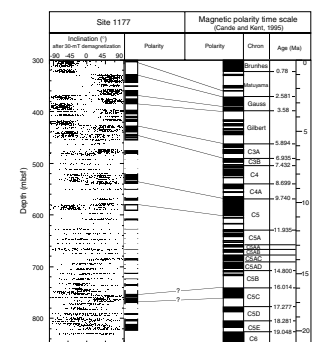
A magnetic polarity change from reversed to normal at 301.85 mbsf (Section 190-1177A-1R-2, 15 cm) is interpreted as the Reunion Event within the Matuyama Chron and is dated at 2.14 Ma (Cande and Kent, 1995). The boundary between the Matuyama and Gauss Chrons (2.581 Ma) is at 328.55 mbsf (Section 190-1177A-4R-1, 5 cm), and the boundary between the Gauss and Gilbert Chrons (3.58 Ma) is at 384.25 mbsf (Section 9R-6, 15 cm).

The termination of the Gilbert Chron and the beginning of Chron C3A (5.894 Ma) is identified at 427.45 mbsf (Section 190-1177A-14R-2, 145 cm). The boundary at 444.25 mbsf (Section 190-1177A-16R-1, 35 cm) is interpreted as the beginning of Chron C3B (6.935 Ma). A normal polarity inclination at 534.55 mbsf (Section 190-1177A-25R-3, 115 cm) is interpreted as the beginning of Chron C5 (9.74 Ma), although magnetic measurements for this interval are limited because of poor core recovery. Based on the biostratigraphic analysis, the normal inclination at

F15. Paleomagnetic declination, inclination, and intensity, p. 41.



F16. Magnetostratigraphy, p. 42.



T12. Depths and ages of magnetic chrons and subchrons, p. 82.

755.1 mbsf (Section 190-1177A-48R-3, 40 cm) may be correlated with the beginning of Chrons C5C (16.014 Ma).

Sedimentation Rates

The relationship between magnetostratigraphy and biostratigraphy is shown in Figure F17. A slight change in sedimentation rate from 6.15 to 2.96 cm/k.y. occurs at 370 mbsf (~3.3 Ma) within the top of the lower Shikoku Basin facies. Below 370 mbsf, the sedimentation rate remains stable in the lower Shikoku Basin facies (Fig. F17).

INORGANIC GEOCHEMISTRY

Fifty-two pore fluid samples were squeezed from selected 10- to 47-cm-long whole-round samples for chemical and isotopic analyses. Sample depths ranged from 306.5 to 828.8 mbsf. One sample per core was collected except from Core 190-1177A-11X, from which three samples were collected, and Cores 190-1177A-51X, 52X, and 54X, from which two samples were collected. Because of poor core recovery, no pore fluids were recovered from Cores 190-1177A-21X, 22X, 28X, and 32X.

Elemental concentrations are reported in Table T13 and plotted in Fig. F18. As at other Leg 190 sites, eight major and minor dissolved anions and cations that sensitively reflect inorganic or microbially mediated water-rock reactions were determined for each sample. The anions are Cl, Ca, Mg, Na, K, and Si, and the cations are alkalinity and sulfate. Salinity and pH were also determined. Thirty-seven samples were analyzed for ammonium and eighteen for Si.

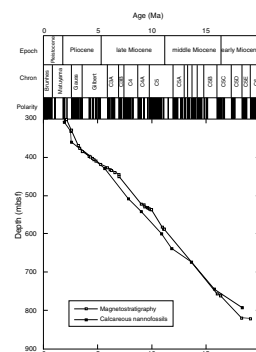
The outstanding characteristics of the pore fluids' concentration-depth profiles at Site 1177 are the sharp discontinuities that occur between and within lithostratigraphic units and a high sulfate interval that ranges across the turbidite unit, which spans over approximately the middle half of the sediment section, from 420 to 735 mbsf. The most prominent discontinuities correlate with changes in measured physical properties and suggest that either specific intervals of sediment effectively remain as closed systems with respect to vertical diffusion or that localized diagenetic reactions have begun recently. The most conspicuous interval is situated in Unit IV, between 775 and 805 mbsf. This interval has a porosity of ~60% (see "Physical Properties," p. 21) and is sandwiched between sediments with ~40%–45% porosity, the prevailing porosity being from ~450 mbsf to the bottom of the section.

Chloride

Cl concentrations were determined with a relative analytical uncertainty of 0.1% based on duplicate or triplicate titrations of all samples. Chloride concentrations are similar to modern bottom water in this region and smoothly vary within a range of ~1% between 307 and 406 mbsf. Between 406 and 421 mbsf, there is a sharp discontinuity with concentrations dropping by 2.7%. This discontinuity is just below the designated boundary of lithostratigraphic Units I and II and is coincident with a ~10% reduction in average porosity. Within the remainder of Unit II, concentrations are nearly constant.

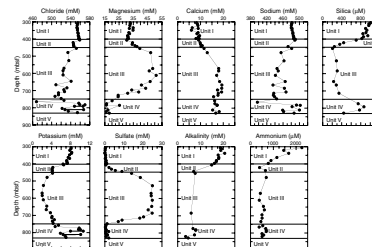
Pore fluid Cl concentrations in lithostratigraphic Units III and IV are characterized by a large range with relatively large changes occurring over short intervals. Some of the variance may be partially due to con-

F17. Age-depth plot, p. 43.



T13. Pore fluid composition, Hole 1177A, p. 83.

F18. Pore fluid composition as a function of depth, p. 44.



tamination of samples by surface seawater that is used as a drilling fluid. However, in Unit IV all of the samples have sulfate concentrations (see “**Sulfate**,” p. 15) that constrain the magnitude of drilling fluid contamination to <6%. This demonstrates that most of the Cl variance is not due to drilling fluid contamination. In Unit III, sulfate is not a highly sensitive indicator of contamination because the pore fluid sulfate concentrations are similar to surface seawater concentrations. Unit III contains numerous intervals with abundant sand, which is probably more susceptible to drilling fluid contamination. Hence, as a precaution, we have not plotted data with sulfate concentrations >25 mM in this unit, although these data are presented in T13. Further shore-based chemical and isotopic analyses should resolve this question.

Within Unit III, there is a general decrease in Cl concentrations; the lowest concentrations are ~7% lower than those of seawater. This freshening is most likely due to the dehydration of smectite and possibly is enhanced by Cl uptake into an authigenic hydrous phase. In Unit IV, Cl concentrations range from ~2% greater to 6% less than modern average seawater concentrations, and one sample has Cl concentration >15% below modern average seawater concentrations. Hydration of volcanic ash layers and the underlying basement, as well as smectite dehydration, most likely contributes to the Cl variability.

Sulfate

Sulfate concentrations are below detection limits through Unit I and the first 10 m of Unit II. They then smoothly increase through Unit II to a concentration plateau of ~25 mM at ~520 mbsf in Unit III. Concentrations drop back to zero in the 50-m interval between 700 mbsf and the Unit III/IV boundary. The sulfate depletions in Units I and IV have been driven by microbial sulfate reduction. In contrast, the near-seawater concentrations in Unit III indicate that since the time of burial, there has been relatively little microbial activity in this unit. This is probably the result of the low average sedimentation rate in Unit III (see “**Biostratigraphy**,” p. 10), which allowed microbial oxidation of the sediment organic matter and simultaneous sulfate diffusion into the turbidite section prior to burial. Indeed, the organic carbon content is very low (generally <0.5 wt%), except for woody fragments in some horizons, which are not easily utilized for microbial activity.

Along with the sharp gradients at the Unit III boundaries, the high sulfate concentrations imply that there is limited diffusive transport across these boundaries. Assuming one-dimensional vertical diffusion, diffusive flux and scale-length calculations indicate that the effective bulk diffusion across these boundaries is on the order of 1×10^{-7} cm²/s or less, more than an order of magnitude lower than diffusion coefficients calculated from porosity and formation factor data (see “**Physical Properties**,” p. 21). Based on the diffusion coefficients calculated from porosity and formation factor data, sulfate should have been depleted by diffusive transport, both upward and downward, out of the unit in <1 m.y. after burial by the Shikoku Basin sediments (~6 Ma). Alternatively, discontinuities may indicate the recent onset of a sulfate-consuming reaction in Unit IV or a sulfate-producing reaction in Unit III.

Sodium

Overall Na concentrations are similar to Cl concentrations. In Unit I, there is a limited concentration range with a smooth increase with depth; no adjacent samples vary by $>0.6\%$. In contrast, Unit III is characterized by an average concentration $\sim 4\%$ lower than in Unit I with a range of nearly 10%. The Na/Cl ratios in Unit I are greater than those of seawater, consistent with the addition of Na to the solution by ion exchange or ash alteration. The ratio varies smoothly over a range of $<1\%$ in Units II and III. In the high porosity zone in Unit IV, Na concentrations are higher than those of seawater, most likely because of Na release and hydration reactions related to ash alteration; ion exchange with clays may have played a minor role.

Potassium

Between 406 and 421 mbsf, K has a sharp discontinuity; concentrations drop by $\sim 50\%$. The K profile overall resembles that of Cl, suggesting that they are coupled by the same or related reactions. In Unit I, concentrations decrease smoothly from ~ 8 to ~ 6 mM at 409 mbsf. Similar to Cl, Unit II K concentrations, at 4 mM, are effectively invariant. In Unit III, there is a broad minimum of ~ 2 mM, centered at ~ 575 mbsf. Similar to Cl, there is a wide dispersion of concentrations in Unit IV. However, the relative concentration range is much greater; concentrations vary by approximately a factor of two with K and Cl correlated. The low concentrations and the variability of K concentrations in Unit II imply an in situ pore fluid-sediment silicate reaction with a sink for K superimposed on the dilution reflected in the Cl profile. In Unit IV, K concentrations sharply increase to approximately average seawater concentration within several horizons. This may reflect in situ dissolution of volcanic ash or sealing of pore fluids within this unusual high-porosity unit.

Magnesium and Calcium

Mg profiles are similar to sulfate profiles in that concentrations are depleted in Units I and IV and there is a broad zone with near-seawater concentrations in Unit III. In Unit I, concentrations decrease smoothly from ~ 33 mM at 306 mbsf to 30 mM at 406 mbsf (39%–44% depletion relative to modern seawater concentration). Between 406 and 421 mbsf, there is a concentration discontinuity as there is with Cl. Similar to sulfate, Mg increases in Unit II to ~ 51 mM ($\sim 94\%$ of modern seawater concentration). In Unit IV, Mg concentrations decrease to a minimum of ~ 17 mM (32% of seawater concentration). Except for a few carbonate-rich layers in Unit III, carbonate contents are low in the sediments at this site. Therefore, the formation of dolomite is most likely not responsible for the Unit I and Unit IV depletions in Mg. Instead, reactions with ash, as well as with basement, in Unit IV to form a Mg silicate are the most likely sink for Mg.

Ca concentrations are depleted by $\sim 25\%$ relative to seawater at 306 mbsf (Section 190-1177A-1R-4). This depletion may be due to the precipitation of carbonates, which is driven by the production of alkalinity that is associated with sulfate reduction at shallower depths. Concentrations then increase through Units I and II, reaching a maximum in Unit III of ~ 20 mM at 666 mbsf. In Unit IV, concentrations fall into a limited range of 15.5–17.7 mM, except in the same sample that has the

lowest Cl concentration (Section 190-1177A-49R-3). The Ca increase is most likely due to the alteration of ash and the underlying basement.

Alkalinity

Alkalinity is elevated in Unit I by 15 to 20 mM as a result of the sulfate reduction that has occurred in this unit. In the limited number of samples analyzed in the remainder of the core, it is less than ~8 mM and appears to be controlled by carbonate solubility as it varies inversely with Ca.

Silica

Silica concentrations are in equilibrium with opal-A solubility at 20°–25°C in Units I and IV; both units have about the same porosity. In Units II and III, concentrations decrease to ~200 μm , which indicates control by a mature terrigenous clay assemblage.

Ammonium

Ammonium decreases sharply through Unit I from 2250 μM at 306 mbsf to 750 mM at the Unit I/II boundary, indicating an ammonium sink which is not yet determined. Throughout the remainder of the core, ammonium concentrations vary within a limited range of 380–950 μM .

ORGANIC GEOCHEMISTRY

Monitoring of volatile hydrocarbons was conducted for safety reasons, and organic, petrological, and geochemical studies were carried out to assess the types of organic matter and the molecular compositions of the hydrocarbons found in the sediments.

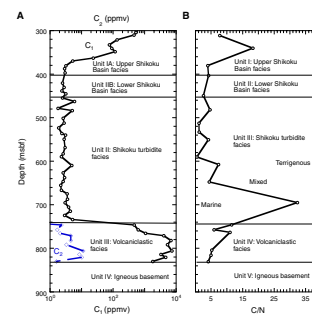
A total of 51 sediment samples were collected at Site 1177 (at ~10-m intervals) from 304.7 to 830.3 mbsf (Table T14). All sediments were analyzed for methane concentrations and light hydrocarbon compositions during headspace analyses (Fig. F19A). In addition, molecular gas compositions, TOC, inorganic carbon (carbonate), nitrogen, and sulfur analyses were performed (Table T15) (see “Organic Geochemistry,” p. 14, in the “Explanatory Notes” chapter for analytical procedures).

TOC contents for the sediment samples examined at Site 1177 ranged from 0.03 to 1.62 wt% at 695.19 mbsf, with an average value of 0.50 wt% (Fig. F20). The high average TOC value is due to the presence of terrestrial organic matter in the form of plant detritus (wood pieces), especially in the 650–750 mbsf section of the lower Shikoku turbidite facies. The distribution of sulfur was similar to that of TOC, ranging from 0 to 0.81 wt% (average = ~0.21 wt%), with the highest concentrations found at 400–520 mbsf and 650–770 mbsf (Fig. F20). The nitrogen content corresponds to a mixture of both marine and terrigenous sources contributing to the composition of the Site 1177 sediments. The two-component mixture for Site 1177 sediments is evident in the carbon/nitrogen (C/N) ratio (Fig. F19B), which clearly shows a strong component for both marine and terrigenous input, especially in the Shikoku turbidite facies (Unit III).

In contrast to Sites 1175 and 1176, inorganic carbon values were generally low at Site 1177 (0.02–2.64 wt%) with some rare high values in

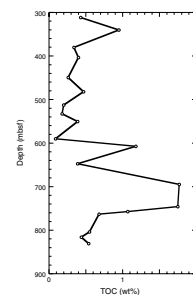
T14. Headspace gas analysis, p. 84.

F19. Methane and ethane compositions and concentrations of headspace gases and CN ratios, p. 45.



T15. Carbon, nitrogen, sulfur, and hydrogen analyses, p. 85.

F20. TOC concentrations, p. 46.



thin layers that ranged between 4.32 and 8.75 wt%. Accordingly, the bulk-carbonate values were also low (0–22 wt%) with the exception of a few samples that varied from 36 to 72 wt%; however, the overall average concentration of carbonate in the sediments was only 2.7 wt%. In general, carbonate contents were confined to very thin layers throughout the hole with higher carbonate concentrations scattered over an interval between 530 and 670 mbsf, which is characterized as a rare carbonate-cemented claystone unit within the Shikoku turbidite facies (Unit III).

Hydrocarbon Gases

Headspace gas concentrations of methane differed from the previous sites drilled during Leg 190, with low concentrations between 304 and 363 mbsf followed by an abrupt drop in methane concentrations to 1.8–5.3 ppm over a 270-m interval to 734 mbsf. The low concentrations of methane below 400 mbsf are the result of an unusually high sulfate content (see *“Inorganic Geochemistry,”* p. 14), which inhibits methanogenesis or microbial mediation of methane production throughout the upper and lower Shikoku Basin facies (Units I and II) and the Shikoku turbidite facies (Unit III). A sharp increase from low levels to ~1600 ppm was measured in the last 90 m to total depth at 830.3 mbsf, coincident with the transition from the Shikoku turbidite facies (Unit III) to the volcanoclastic facies (Unit IV). Interestingly, the Bernard $C_1/(C_2+C_3)$ ratio for the hydrocarbons at 350–400 mbsf clearly plot in the mixing zone, indicating that some hydrocarbons in these sediments were produced in situ from organic matter present in the sediments or that some hydrocarbons migrated in from a deeper source. Methane also increases through this section coincident with a sharp drop in sulfate, suggesting that methanogenesis is also occurring in these sediments. The thermal gradient (6.0°C/100 m, corresponding to ~50°C at 830.3 mbsf) in Hole 1177A, coupled with the presence of high methane concentrations, indicates that both biogenic and thermally produced hydrocarbons are present in the volcanoclastic facies sediments (Unit IV). Isotopic analyses of TOC in these samples will allow for a more detailed assessment of the nature and distributions of the hydrocarbons at Site 1177.

Conclusions

Organic geochemical analyses at this site leads to the following conclusions:

1. TOC contents for the sediments examined at Site 1177 ranged from 0.03 to 1.62 wt% with an average value of 0.50 wt%. The highest TOC values were measured in the Shikoku turbidite facies sediments (Unit III), which contained a terrestrial component characterized by plant detritus and pieces of wood.
2. Sulfur contents ranged from 0 to 0.81 wt% with the highest concentrations found between 400–520 mbsf and 650–770 mbsf.
3. C/N ratios in the Nankai sediments indicated that a mixture of both marine and terrigenous sources were contributing to the overall sediment composition at Site 1177.
4. Unlike at Sites 1175 and 1176, the inorganic carbon (~0.78 wt%) and carbonate (~2.7 wt%) contents were low with the exception

of some thin-bedded carbonate-cemented layers (containing up to 72 wt% carbonate) in the Shikoku turbidite facies (Unit III).

- Methane concentrations in sediments below the sulfate reduction zone (~4.5–734 mbsf) are consistent with a bacterial origin. The $C_1/(C_2+C_3)$ ratio for hydrocarbons in sediments below 750 mbsf plot within the mixing zone, suggesting that more than one source of hydrocarbons may be present.

MICROBIOLOGY

Twenty-three samples were obtained from Hole 1177A for direct microscopic enumeration of bacteria aboard ship. Twenty-one whole-round cores were taken for shipboard enrichment cultures, cell viability, and shore-based microbiological analysis to measure potential bacterial activities, culture microorganisms, characterize nucleic acids, and investigate fatty acid biomarkers.

Total Bacterial Enumeration

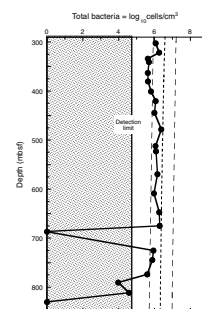
Bacteria are present in all but 2 of the 23 samples (Table T16; Fig. F21), and populations are all below the general model for bacterial populations in deep-sea sediments (Parkes et al., 1994). Between 303 and 381 mbsf (Samples 190-1177A-1R-2, 106–107 cm, to 9R-3, 109–110 cm), bacterial populations slowly decline by ~60% from 1.14×10^6 to 4.28×10^5 cells/cm³. There is a general trend of population increase (by a factor of 4.5) to 1.92×10^6 cells/cm³ at 675 mbsf (Sample 190-1177A-40R-1, 30–31 cm). A persistent and statistically significant ($t = 4.54$; $N = 6$; $P = <0.02$) increase at this depth is unexpected and presumed to relate to in situ conditions.

At 687 mbsf (Sample 190-1177A-41R-2, 99–100 cm), no cells were detected. This particular core also proved anomalous with respect to some aspects of geochemistry (see “Organic Geochemistry,” p. 17, and “Inorganic Geochemistry,” p. 14) for reasons that are currently unclear. At the next depth sampled (725 mbsf; Sample 190-1177A-45R-2, 98–99 cm) bacteria are again present, although population sizes are low and remain low to 774 mbsf (Sample 190-1177A-50R-2, 147–148 cm). Between 791 and 811 mbsf (Samples 190-1177A-52R-1, 33–34 cm, to 54R-2, 45–46 cm), bacterial populations are barely detectable, and they were not detected at all in the deepest sample at 830 mbsf (Sample 190-1177A-56R-1, 149–150 cm).

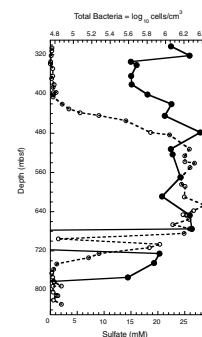
At previous sites that have been sampled for microbiology during Leg 190, a relationship is sometimes observed between bacterial populations and in situ methane concentrations (see “Microbiology,” p. 22, in the “Site 1173” chapter and “Microbiology,” p. 19, in the “Site 1175” chapter). This is not true at Site 1177. Between ~400 and 740 mbsf, high concentrations of sulfate are present in the interstitial water (IW), reaching almost seawater concentrations between 500 and 675 mbsf (see “Inorganic Geochemistry,” p. 14). Methane is only present in significant quantities either above 340 or below 740 mbsf (see “Organic Geochemistry,” p. 17). However, there is a strong correlation ($R^2 = 0.737$; $N = 14$; $P = <0.005$) between bacterial population size and IW sulfate concentration. Bacterial numbers increase from ~380 mbsf, slightly above but paralleling the increase in sulfate concentrations that initiates from ~400 mbsf (Fig. F22). This may be the result of bacterial sulfate reduction partially depleting sulfate above 500 mbsf. Bacterial

T16. Total bacterial populations in sediments, p. 87.

F21. Depth distribution of total bacterial populations, p. 47.



F22. Depth profiles of total bacteria, p. 48.



populations remain high to ~740 mbsf, where they decrease at a depth slightly below that of the decline in sulfate concentration. It is notable that the anomalous zero bacterial enumeration is mirrored in a very low anomalous sulfate concentration at 687 mbsf.

The presence of such high concentrations of sulfate so deep in the sediment is puzzling when bacteria are present at $\sim 10^6$ cells/cm³ at the same depths. Because the age of the sediments that contain this zone of elevated sulfate ranges from ~3 Ma at the top to 13 Ma at the base (see “**Biostratigraphy**,” p. 10, and “**Paleomagnetism**,” p. 12), there has been sufficient time for considerable amounts of sulfate removal by bacteria. The continued presence at high concentration implies that there is either replenishment of sulfate by fluid flow or that TOC concentrations are too low to support rapid bacterial sulfate reduction. Sulfate reduction rates will be addressed by shore-based work; however, low TOC concentrations are the likely cause of high sulfate concentrations. TOC is low for much of Hole 1177A, particularly within the elevated sulfate zone, not exceeding 0.4 wt% (and generally <0.3 wt%) between 381 and 590 mbsf (see “**Organic Geochemistry**,” p. 17). High TOC is only present within the elevated sulfate zone at 608 mbsf (0.81 wt%) and 695 mbsf (1.62 wt%), and the latter, curiously, is coincident with the anomalous bacterial population and sulfate concentration lows. However, visual inspection of the cores indicates that much of this TOC is present in the form of pieces (up to 3 cm) of wood. This is a recalcitrant material for bacterial degradation and additionally implies that the TOC is heterogeneously distributed in the sediment with the vast majority of the sediment being very TOC poor. Under these conditions it is not surprising that the IW sulfate concentrations remain elevated.

Contamination Tests

The chemical tracer test was conducted during RCB coring of Cores 190-1177A-24R and 25R. The particulate tracer was used during RCB coring of Core 190-1177A-6R. In order to estimate the amount of drilling fluid intrusion into the recovered cores, chemical and particulate tracers were deployed as previously described (Smith et al., 2000).

Chemical Tracer

Perfluoro(methylcyclohexane) was used as the perfluorocarbon tracer (PFT). Calibration of the gas chromatograph (HP 5890) with standard solutions yielded a slope of 9.2×10^{11} area units/gram of PFT. The detection limit for these samples is equivalent to 0.01 μ L of drilling fluid. The tracer was detected on the outer edge of four of the six sections of core examined (Table T17). The PFT concentrations in water collected on the catwalk from the top of Cores 190-1177A-24R and 25R were ~23 and 330 μ g/L and confirmed delivery of the tracer to the drill bit. These values are higher than the target concentration of 1 μ g/L, and the measured values were used to calculate the estimated drilling fluid intrusion. Estimates of drilling fluid intrusion into the interior of the cores range from below detection to 0.07 μ L/g (Table T17).

T17. Drilling fluid intrusion estimated based on PFT experiments, p. 88.

Particulate Tracer

Fluorescent microspheres were detected on the outside of all three sections examined in Core 190-1177A-6R (Table T18). Sections 190-1177A-6R-2 and 6R-3 contained microspheres throughout the core.

T18. Fluorescent microsphere tracer experiments, p. 89.

PHYSICAL PROPERTIES

Introduction

At Site 1177, laboratory measurements were made to provide a downhole profile of physical properties at a reference site seaward of the accretionary complex. Measurements from tectonically undeformed sediments at the reference site yield information about the initial state of sediments prior to deformation.

With the exception of short (<50 cm) or broken sections, all cores were initially passed through the multisensor track (MST) before being split. Gamma-ray attenuation (GRA) and magnetic susceptibility measurements were taken at 4-cm intervals with 2-s acquisition times for all cores. Natural gamma ray (NGR) was counted every 20 cm for 20-s intervals.

Moisture and density samples were selected from undisturbed core at a frequency of at least one per section. Measurements of dry volume and wet and dry mass were uploaded to the ODP (Janus) database and were used to calculate water content, bulk density, grain density, porosity, void ratio, and dry bulk density. *P*-wave velocities were measured on discrete sample cubes at a frequency of two to three per core when core conditions permitted. Electrical conductivity measurements were taken on the same cubes used for velocity measurements. Raw data and calculated physical properties are available from the Janus database for all MST, moisture and density, velocity, thermal conductivity, and shear strength measurements (see the “[Related Leg Data](#)” contents list). Because the electrical conductivity data are not currently available from the database, they are included in Table T19.

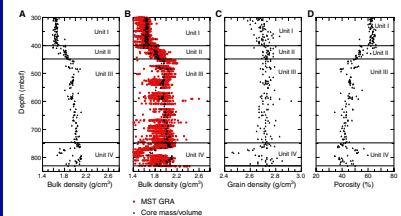
T19. Electrical conductivity and formation factor, p. 90.

Density and Porosity

Sediment bulk density was determined by both the GRA method on unsplit cores and the mass/volume method (“index properties”) on discrete samples (see “[Physical Properties](#),” p. 19, in the “Explanatory Notes” chapter). The GRA density data and the bulk densities determined by the mass/volume method are in good agreement for most of the cored interval (Fig. F23A, F23B), despite the smaller diameter and the biscuited nature of RCB cores. In general, the GRA densities are 0.1–0.2 g/cm³ lower than the bulk densities. However, between 400 and 480 mbsf, the discrete densities are generally at the low end of the range of GRA measurements. The reason for this difference is unclear. The GRA densities for a ~30-m-thick low-density interval at 765–795 mbsf within Unit IV are consistently ~0.3 g/cm³ lower than those determined by the mass/volume method. The GRA densities exhibit significant scatter, especially within lithostratigraphic Units III and IV (Shikoku turbidite facies and volcanoclastic facies).

Grain densities determined from dry mass and volume measurements increase slightly from 2.58–2.69 g/cm³ at 300 mbsf to 2.67–2.75 g/cm³ at the base of Unit I (upper Shikoku Basin facies; 402 mbsf) (Fig.

F23. Bulk density, grain density, and porosity, p. 49.



F23C). Grain densities remain nearly constant at $\sim 2.68\text{--}2.76\text{ g/cm}^3$ throughout Units II (lower Shikoku Basin facies) and III (Shikoku turbidite facies). Within Unit IV, grain densities are similar to those within Unit III but decrease to values as low as 2.43 g/cm^3 in a $\sim 30\text{-m}$ -thick interval between 765 and 795 mbsf that exhibits low bulk density and high porosity values (Fig. **F23A**, **F23D**).

Porosities within lithostratigraphic Unit I (upper Shikoku Basin facies) remain nearly constant with depth and exhibit little scatter, ranging from 60% to 65%. These values are surprisingly high for a burial depth of 300 to 400 m. Porosities within Unit II (lower Shikoku Basin facies) decrease rapidly with depth from 60%–65% at 402 mbsf to 46%–54% by ~ 450 mbsf. Unit III porosities decrease slightly with depth, from 45%–53% at ~ 450 mbsf to 40%–45% at 748 mbsf. Between 475 and 510 mbsf, porosities are consistently 38%–40%, significantly lower than those directly above and below (Fig. **F23D**). Porosities within Unit III (Shikoku turbidite facies) exhibit more scatter than within Unit I, probably as a result of lithologic variations within and between turbidite sequences. Porosities within Unit IV show considerable scatter, ranging between $\sim 36\%$ and 53%, and exhibit no clear changes with depth. An excursion to higher porosity (49%–59%) between 765 and 792 mbsf coincides with a zone of low grain density and low GRA density.

Thermal Conductivity

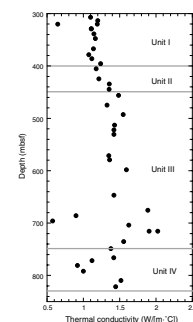
Thermal conductivity was measured on split cores using the half-space method (Fig. **F24**). In Unit I, thermal conductivity values are relatively constant and average $1.1\text{ W/(m}\cdot\text{C)}$. Thermal conductivity increases within Unit II, corresponding to a decrease in porosity. In the portion of Unit III above 600 mbsf, thermal conductivity varies between 1.4 and $1.6\text{ W/(m}\cdot\text{C)}$. Values are scattered between 600 and 748 mbsf. Values $<1.0\text{ W/(m}\cdot\text{C)}$ may reflect low-quality measurements caused by fracturing of core pieces. Within Unit IV, a drop in thermal conductivity occurs between 760 and 810 mbsf, corresponding to an interval of elevated porosity (Fig. **F23D**).

Acoustic Velocity

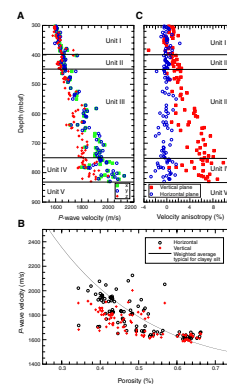
Measurements in all three directions were performed on sample cubes cut from cores. Acoustic velocity increase with depth follows a nearly constant gradient of 0.84 m/s per meter for the horizontal components (x- and y-axes) and 0.57 m/s per meter for the vertical component (z-axis) (Fig. **F25B**). The sharp decrease in porosity at the transition between lithostratigraphic Units I and II is not reflected in the acoustic velocity nor is the more progressive decrease in porosity within lithostratigraphic Unit II. The same behavior has been noted at the transition from the upper to lower Shikoku Basin facies at Site 1173.

A minor decrease in velocity of $\sim 30\text{ m/s}$ at ~ 420 mbsf stratigraphically correlates with a somewhat more pronounced kink in the acoustic velocity profile at 390 mbsf at Site 1173 and with the décollement level as defined at Site 1174 (see “**Paleomagnetism**,” p. 12). The zone of high porosity observed within lithostratigraphic Unit IV (between 765 and 790 mbsf) also displays an anomalous velocity profile. The velocity vs. porosity graph (Fig. **F25B**) shows that the velocity at a given porosity is generally lower at Site 1177 than at the eastern sites. This may be related to the lower heat flow and less advanced diagenesis at Site 1177 (Kinoshita and Yamano, 1986) (see “**Lithostratigraphy**,” p. 5). The up-

F24. Thermal conductivity, p. 50.



F25. P-wave velocity and velocity anisotropy, p. 51.



per Shikoku Basin facies (lithostratigraphic Unit I) plots above the reference curve but appears less anomalous than at Site 1173 (see Fig. F38, p. 76, in the “Site 1173” chapter); measurements plotting far away from the reference curve generally correspond to isolated samples. We note that a piece of carbonate-cemented mudstone yielded acoustic velocities of >4500 m/s in all directions and was not plotted on the graphs.

Velocity anisotropy is near 0% in Unit I but increases progressively with compaction in lithostratigraphic Units II, III, and IV to reach 6%–12% near the oceanic basement. The zone of anomalously high porosity between 765 and 790 mbsf also appears as a zone of reduced anisotropy (Fig. F25C).

Electrical Conductivity

Electrical conductivity was measured on the same sample cubes as the *P*-wave measurements with a 30-kHz two-electrode system. Electrical conductivity and formation factor (see “Physical Properties,” p. 19, in the “Explanatory Notes” chapter) measured on the sample cubes are given in Table T19. The formation factor increases between 409 and 415 mbsf, from ~3.5 above to 4–5 below for measurements along the horizontal direction (*x*- and *y*-axes) and from 3.5–4 above to 5–6 below for measurements along the vertical direction (*z*-axis). This change in properties is also reflected in the conductivity anisotropy (Fig. F26B). Vertical plane anisotropy first decreases from 10%–15% to 0%–1% between 300 and 409 mbsf but then increases to >15% at 415 mbsf. This abrupt transition occurs within lithostratigraphic Unit II. At Site 1177, increases in bulk density, formation factor, and electrical conductivity anisotropy occur across the transition from the upper to lower Shikoku Basin facies. This transition also occurs at Site 1173 but apparently at a younger stratigraphic age (3.1–3.5 Ma) than at Site 1177 (4–5 Ma; see “Paleomagnetism,” p. 12). Below 415 mbsf, the horizontal components increase slowly, reaching only 5–6 at the base of lithostratigraphic Unit III, whereas the vertical component increases steadily, reaching 10–16 at the base of lithostratigraphic Unit III. This leads to a very high anisotropy (60%–100%) in the lower part of lithostratigraphic Unit III, higher than at any depth at the other sites. The zone of anomalously high porosity and low *P*-wave velocity between 765 and 790 mbsf in lithostratigraphic Unit IV coincides with a zone of lower formation factor and anisotropy.

Formation factor measured along the *z*-axis and average formation factor measured along the *x*- and *y*-axes are plotted vs. porosity in Figure F26C and may be compared with results obtained at Site 1173 on cube samples (Fig. F26D). At Site 1173, the vertical and the horizontal formation factors were fitted independently using the generalized Archie’s law. The best-fitting laws are

$$F_h = 1.87 \phi^{-1.58}$$

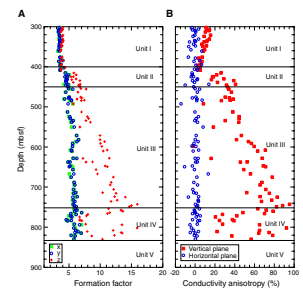
for the horizontal formation factor and

$$F_z = 1.58 \phi^{-2.17}$$

for the vertical formation factor, where ϕ is the porosity.

At Site 1177, data are compared with the same empirical relationships and plotted as reference curves (Fig. F26C). The horizontal com-

F26. Formation factor and anisotropy of electrical conductivity, p. 52.



ponent generally plots below the corresponding reference curve. The vertical component displays a high scatter and, for porosities of <50%, generally plots above the reference curve. Consequently, anisotropy at a given porosity is generally higher at Site 1177 than at Site 1173. The difference between the electrical conductivity–porosity relationships at these two sites may reflect differences in clay composition (see “Lithostratigraphy,” p. 5).

Magnetic Susceptibility

Volumetric magnetic susceptibility was measured on unsplit cores on the MST (Fig. F27). The uncorrected values of magnetic susceptibility from the Janus database were used. The magnetic susceptibility data show an increase from 20–60 × 10⁻⁵ SI at 300 mbsf to 80–150 × 10⁻⁵ SI at 450 mbsf. From below 450 mbsf to basement, the values are relatively low (0–50 × 10⁻⁵ SI) with several peaks as high as 200 × 10⁻⁵ SI. From 680 to 760 mbsf, there is a continuous increase in magnetic susceptibility values from 10–50 to 30–150 × 10⁻⁵ SI.

Natural Gamma Ray

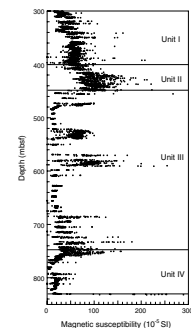
NGR results are presented in counts per second (cps) (Fig. F28). The background scatter, produced by Compton scattering, photoelectric absorption, and pair production, was measured at the beginning (6.39 cps) and subtracted from the measured gamma-ray values. In general, NGR counts are low and are consequently likely to be affected by the short counting interval and by porosity variations. The scatter of NGR data is high throughout the cored interval, with values between 10 and 60 cps. No overall downhole trend of NGR data is observed. NGR values show a slight increase from 15–40 cps at 400 mbsf to 22–50 cps at 500 mbsf. The interval between 500 and 550 mbsf is characterized by low gamma-ray values (10–40 cps). NGR values range between 10 and 60 cps below 550 mbsf, and the scatter of data increases below 600 mbsf.

Summary and Discussion

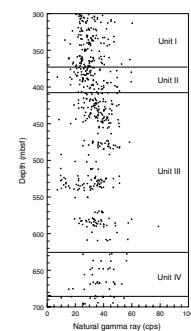
Variations in physical properties at Site 1177 correlate well with lithostratigraphic units. Units I and II are both characterized by low scatter in porosity. Unit I maintains nearly constant porosity of 60%–65%. Within Unit II (402 mbsf), porosities decrease rapidly with depth, reaching 45%–53% by 450 mbsf. Unit III is characterized by a gradual decrease in porosity with depth and by increased scatter that may be caused by lithologic variations in this turbidite-rich sequence. An excursion to lower porosity values (~40%) occurs within Unit III at 475–510 mbsf and may represent a sandy layer. Unit IV exhibits significant scatter and shows no clear trend with depth. A major excursion to high porosity (~8%–15% higher than in surrounding sediments) within Unit IV occurs in a 30-m-thick zone between 765 and 795 mbsf. This zone is also characterized by low vertical *P*-wave velocities and formation factors.

The nearly constant and relatively high porosities within Unit I are similar but 5%–8% lower than those observed in the analogous sequence (upper Shikoku Basin facies) at Site 1173. The decrease in porosity with depth in Unit II is also similar to the pattern observed within the lower Shikoku Basin facies at Site 1173.

F27. Magnetic susceptibility, p. 54.



F28. Natural gamma ray, p. 55.



SEISMIC STRATIGRAPHY

A two-dimensional seismic line, NT62-2, crosses Site 1177 and allows correlation of seismic stratigraphy with Site 1177 (Fig. F29). As with the other Leg 190 seismic ties, specific correlations should be considered preliminary at this time because the velocity structure at this site is not well known. Any inaccuracies in velocity will produce errors in depth conversion. Additional velocity work will be carried out postcruise to improve depth conversions and stratigraphic correlations.

Hole 1177A was washed to a depth of 300 mbsf before coring began. The seismic section shows that this upper section of the hole contains the outer trench facies as well as the top of the upper Shikoku Basin hemipelagic section.

Lithostratigraphic Unit I is recognized on the seismic line as a sequence bounded at its base by two strong, continuous reflections (Fig. F29). The unit is characterized by low-amplitude, discontinuous horizontal reflections.

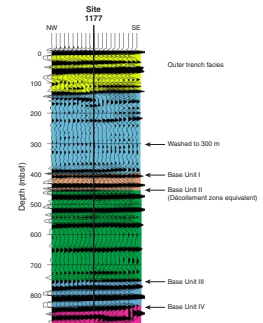
Lithostratigraphic Unit II is bounded by a strong reflection at its top and base and is <50 m thick. The reflection character is indicative of a negative impedance contrast, indicating that there is an inversion of either velocity or density at the top of the unit. This horizon is traced laterally toward the accretionary prism, where it becomes the décollement.

The series of high-amplitude, laterally continuous reflections between 450 mbsf and 750 mbsf correlates with lithostratigraphic Unit III. The strong reflections correlate with individual sand packages.

Lithostratigraphic Unit IV is correlated with the three high-amplitude, laterally continuous reflections between 750 and 850 mbsf. They are conformable at their base with the underlying basement reflection.

Basaltic basement is identified as a strong double reflection at 850 mbsf. This reflection is laterally continuous under the entire region.

F29. Three-dimensional seismic reflection line 281, p. 56.



REFERENCES

- Cande, S.C., and Kent, D.V., 1995. Revised calibration of the geomagnetic polarity timescale for the Late Cretaceous and Cenozoic. *J. Geophys. Res.*, 100:6093–6095.
- Kano, K., Kato, H., Yanagisawa, Y., and Yoshida, F., 1991. Stratigraphy and geologic history of the Cenozoic of Japan. *Geol. Surv. Jpn.*, 274:114.
- Karig, D.E., 1971. Structural history of the Mariana Island arc system. *Geol. Soc. Am. Bull.*, 82:323–344.
- Kinoshita, H., and Yamano, M., 1986. The heat flow anomaly in the Nankai Trough area. In Kagami, H., Karig, D.E., Coulbourn, W.T., et al., *Init. Repts DSDP, 87*: Washington (U.S. Govt. Printing Office), 737–743.
- Lee, M.W., Hutchinson, D.R., Collett, T.S., and Dillon, W.P., 1996. Seismic velocities for hydrate-bearing sediments using weighted equation. *J. Geophys. Res.*, 101:20347–20358.
- Martini, E., 1971. Standard Tertiary and Quaternary calcareous nannoplankton zonation. In Farinacci, A. (Ed.), *Proc. 2nd Int. Conf. Planktonic Microfossils Roma*: Rome (Ed. Tecnosci.), 2:739–785.
- Parkes, R.J., Cragg, B.A., Bale, S.J., Getliff, J.M., Goodman, K., Rochelle, P.A., Fry, J.C., Weightman, A.J., and Harvey, S.M., 1994. A deep bacterial biosphere in Pacific Ocean sediments. *Nature*, 371:410–413.
- Shipboard Scientific Party, 1975a. Site 296. In Karig, D.E., Ingle, J.C., Jr., et al., *Init. Repts. DSDP, 31*: Washington, DC (U.S. Govt. Printing Office), 191–206.
- , 1975b. Site 297. In Karig, D.E., Ingle, J.C., Jr., et al., *Init. Repts. DSDP, 31*: Washington (U.S. Govt. Printing Office), 275–316.
- , 1986. Site 582. In Kagami, H., Karig, D.E., Coulbourn, W.T., et al., *Init. Repts. DSDP, 87*: Washington (U.S. Govt. Printing Office), 35–122.
- , 1991. Site 808. In Taira, A., Hill, I., Firth, J.V., et al., *Proc. ODP, Init. Repts.*, 131: College Station, TX (Ocean Drilling Program), 71–269.
- Smith, D.C., Spivack, A.J., Fisk, M.R., Haveman, S.A., Staudigel, H., and ODP Leg 185 Scientific Party, 2000. Methods for quantifying potential microbial contamination during deep ocean coring. *ODP Tech. Note, 28* [Online]. Available from World Wide Web: <<http://www-odp.tamu.edu/publications/tnotes/tn28/INDEX.HTM>>.
- Young, J.R., 1998. Neogene. In Bown, P.R. (Ed.), *Calcareous Nannofossil Biostratigraphy* (Vol. 8): Dordrecht (Kluwer Academic), 225–265.

Figure F1. Stratigraphic column for Site 1177, showing lithostratigraphic units, ages, and characteristic lithologies.

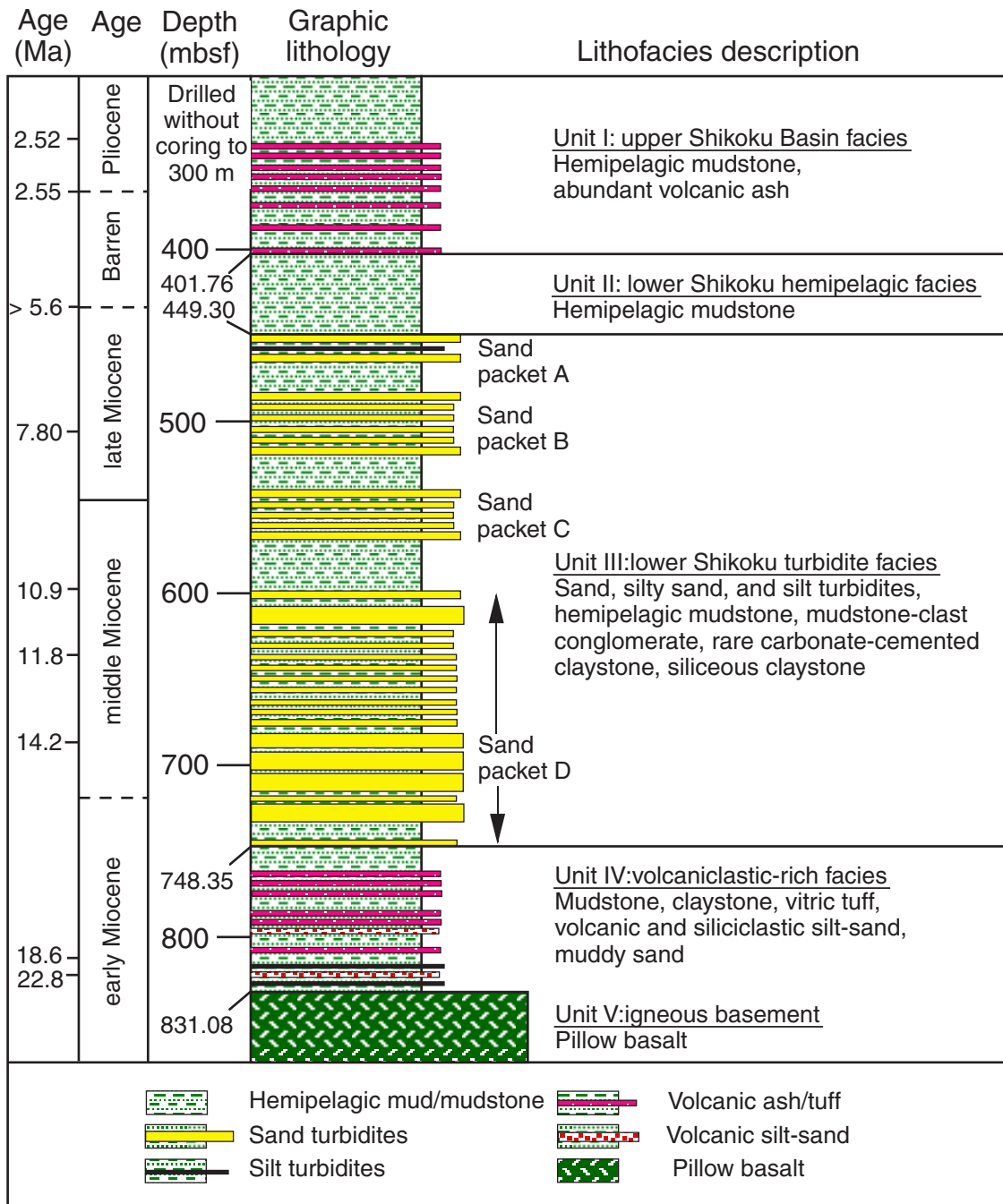


Figure F2. Distribution and thickness of volcanic-ash layers at Site 1177.

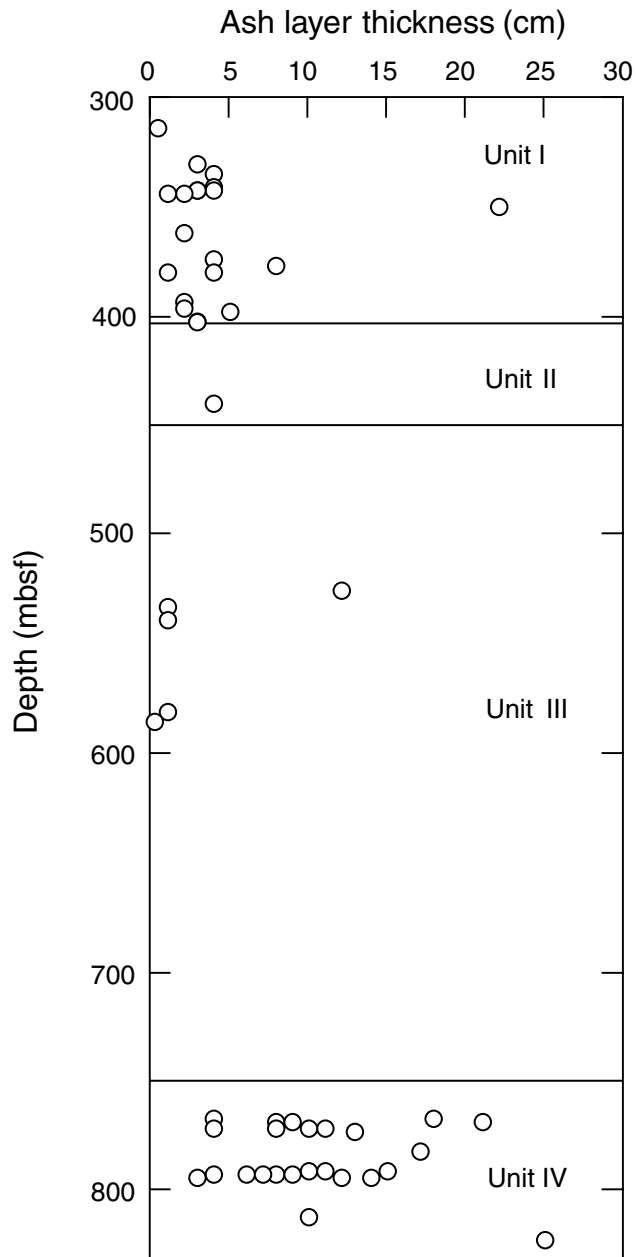


Figure F3. *Zoophycos* in silty claystone overlying a wood-rich silt from Unit III (interval 190-1177A-17R-2, 0-20 cm).

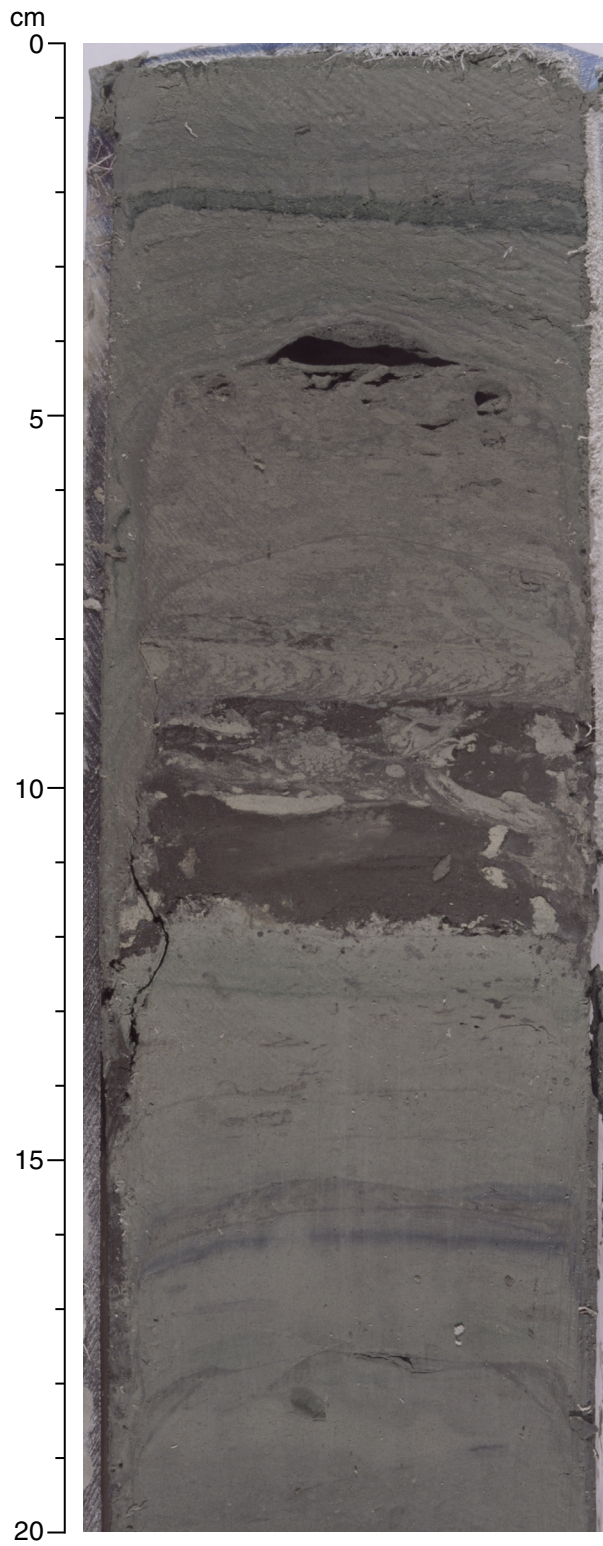


Figure F4. Wood fragments in silty claystone from Unit III (interval 190-1177A-24R-1, 75–90 cm).

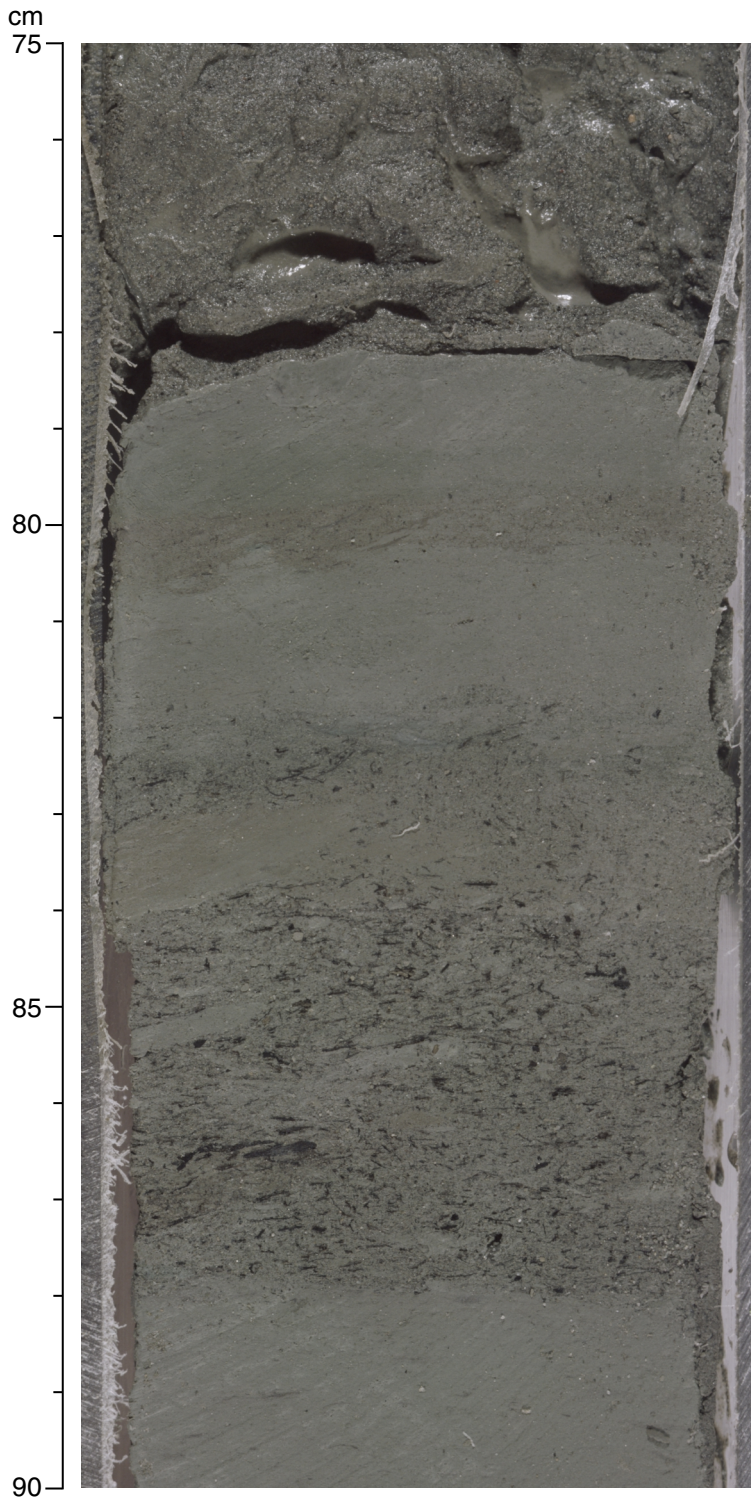


Figure F5. Laminated wood-rich sandy turbidite from Unit III interbedded with silty claystone (interval 190-1177A-43R-3, 0–25 cm).

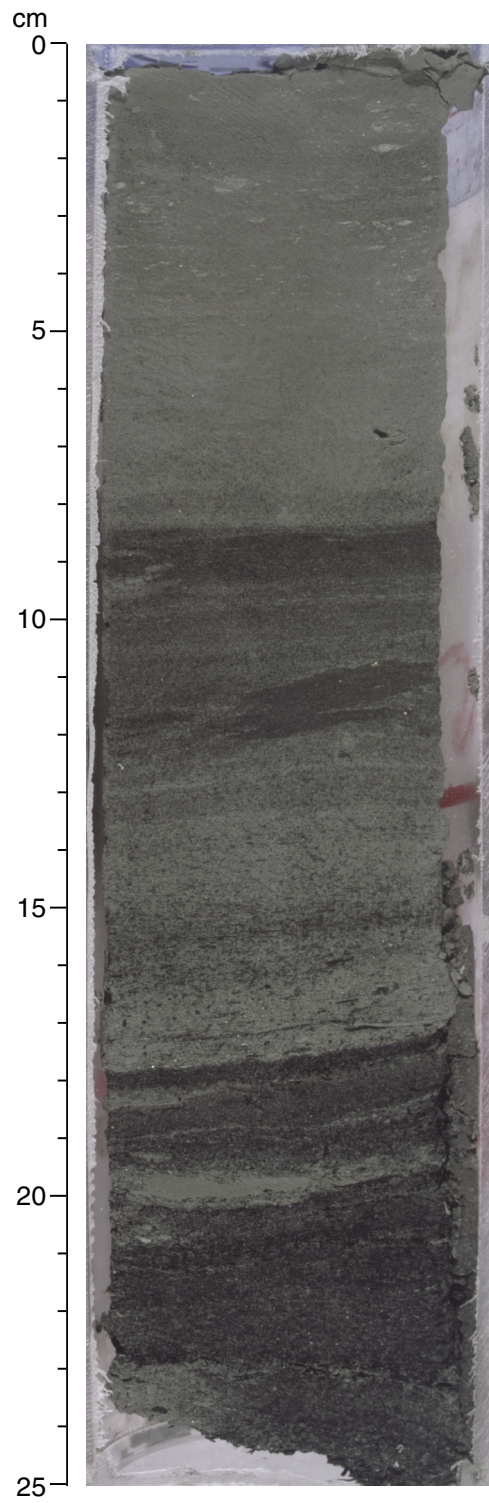


Figure F6. Siliciclastic turbidite from Unit III containing abundant plant material and rip-up clasts of silty claystone (interval 190-1177A-41R-1, 50–65 cm).

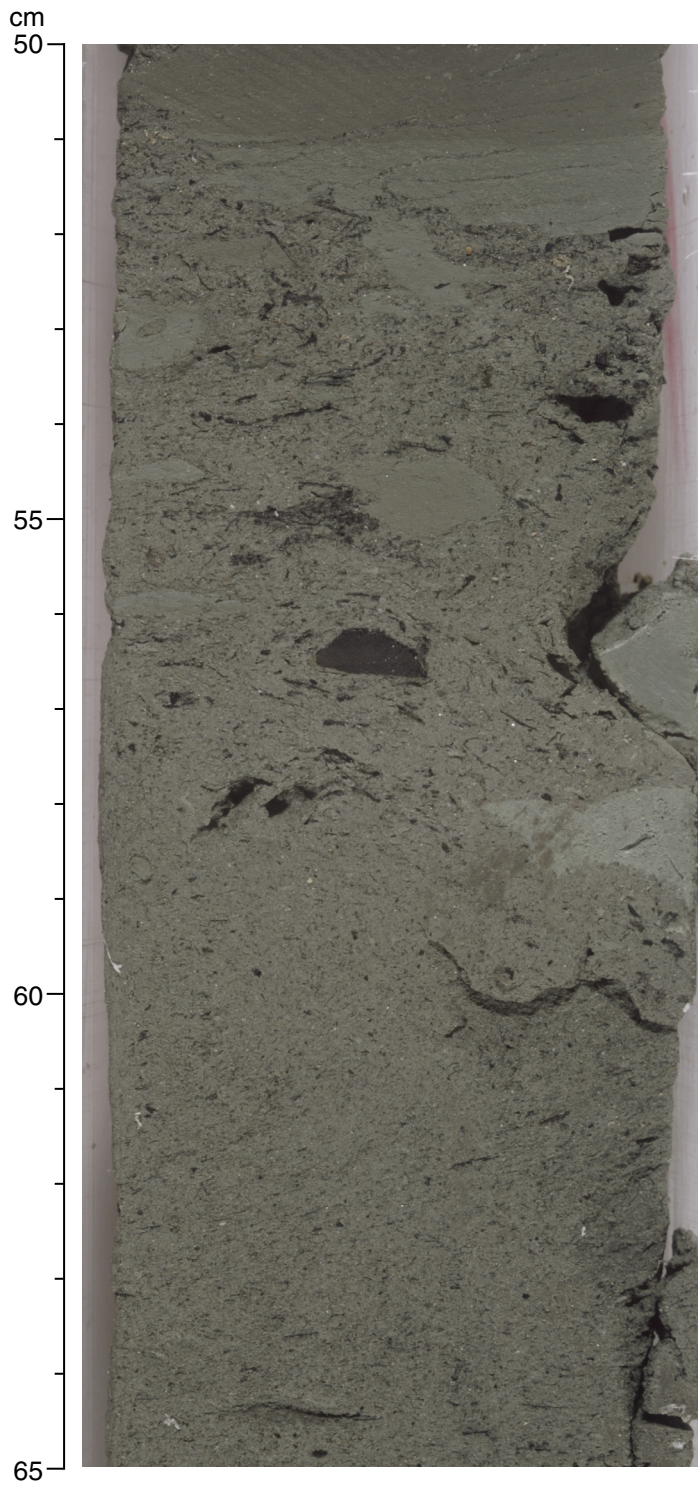


Figure F7. Siliciclastic turbidite or debris-flow deposit from Unit III containing abundant rip-up clasts of silty claystone (interval 190-1177A-46R-4, 0-30 cm).



Figure F8. Laminated and bioturbated volcanic ash from Unit IV (interval 190-1177A-49R-4, 77–101 cm).

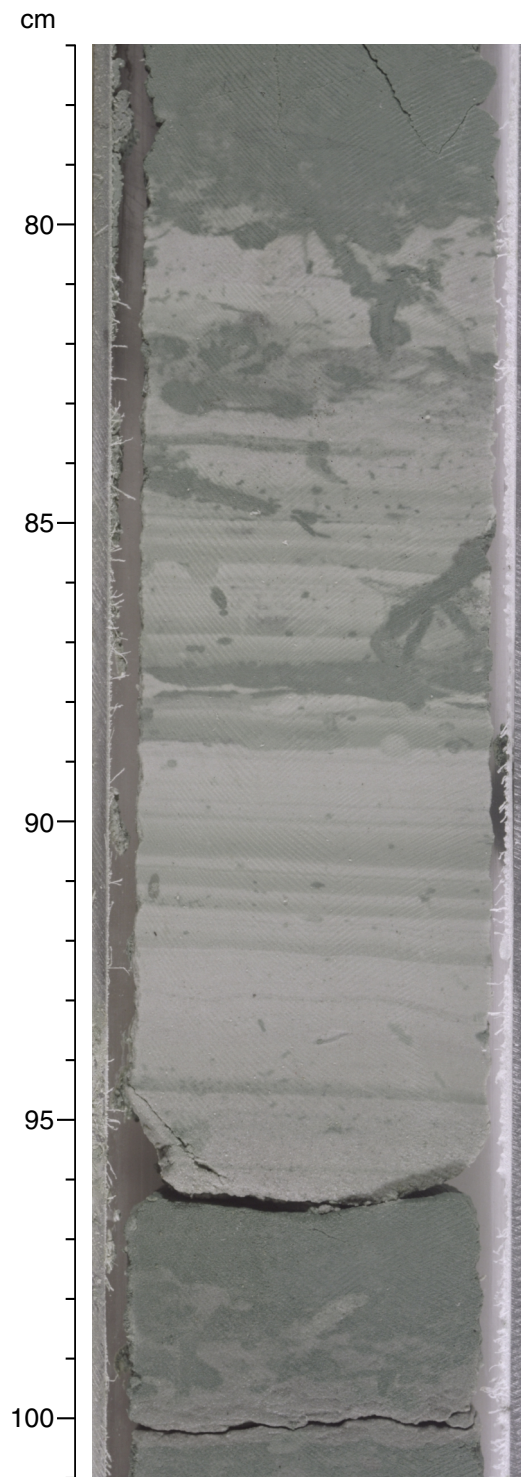


Figure F9. Contorted interbeds of volcanic ash and silty claystone from Unit IV (interval 190-1177A- 50R-2, 6-32 cm).

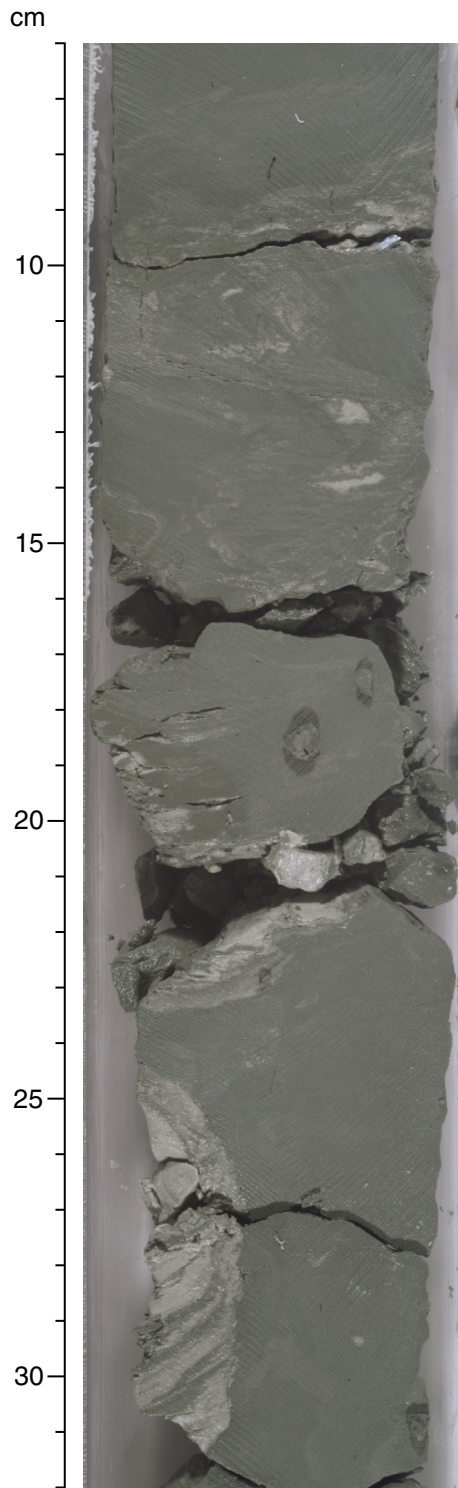


Figure F10. Contact between green basal mudstone (Unit IV) and basalt (Unit V) (interval 190-1177A-56R-3, 0–12 cm). A calcite vein crosscuts the contact between basalt and sediment (interval 190-1177A-56R-3, 0–10 cm). Note the very fine grain size and the glassy rind of the basalt.

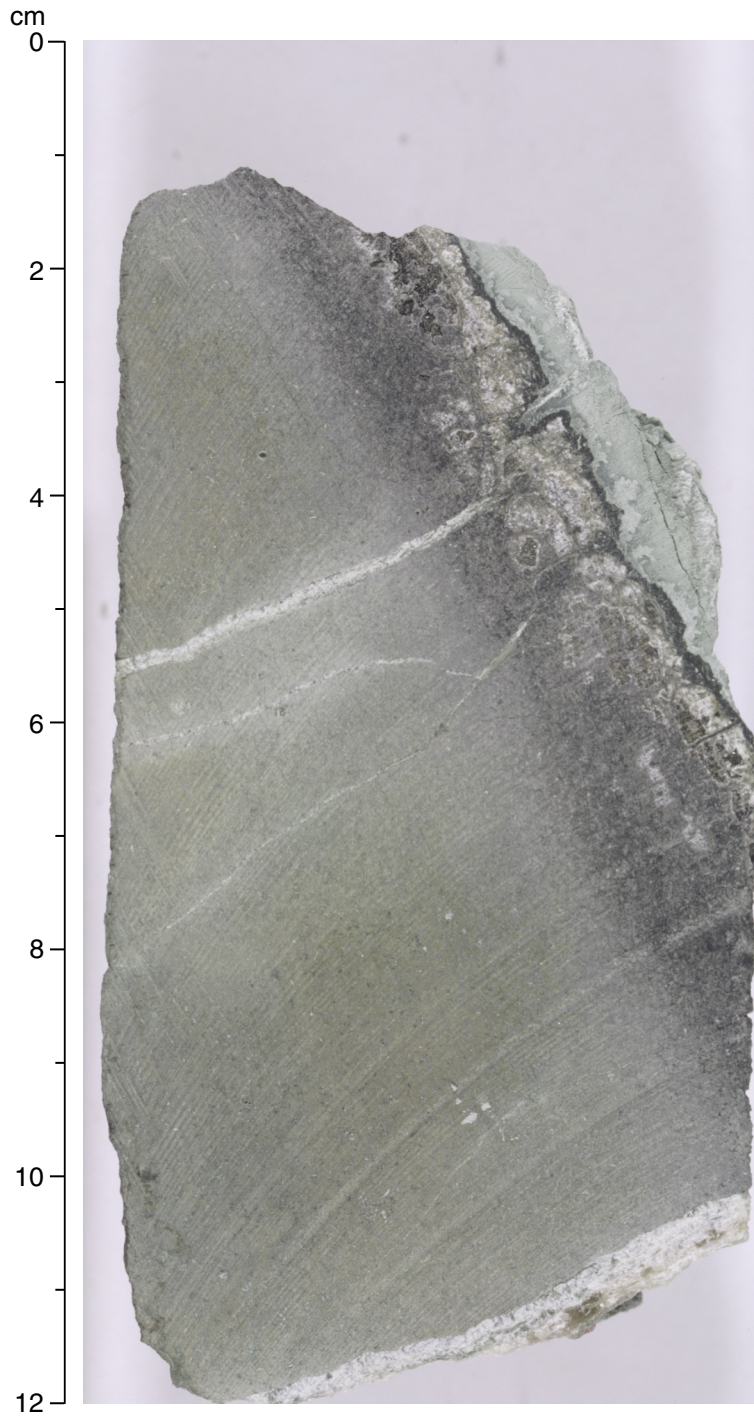


Figure F11. Relative abundances of total clay minerals, quartz, plagioclase, and calcite at Site 1177 based on X-ray diffraction analyses of random bulk powders. Also shown is the ratio of peak areas for (101) cristobalite to (100) quartz.

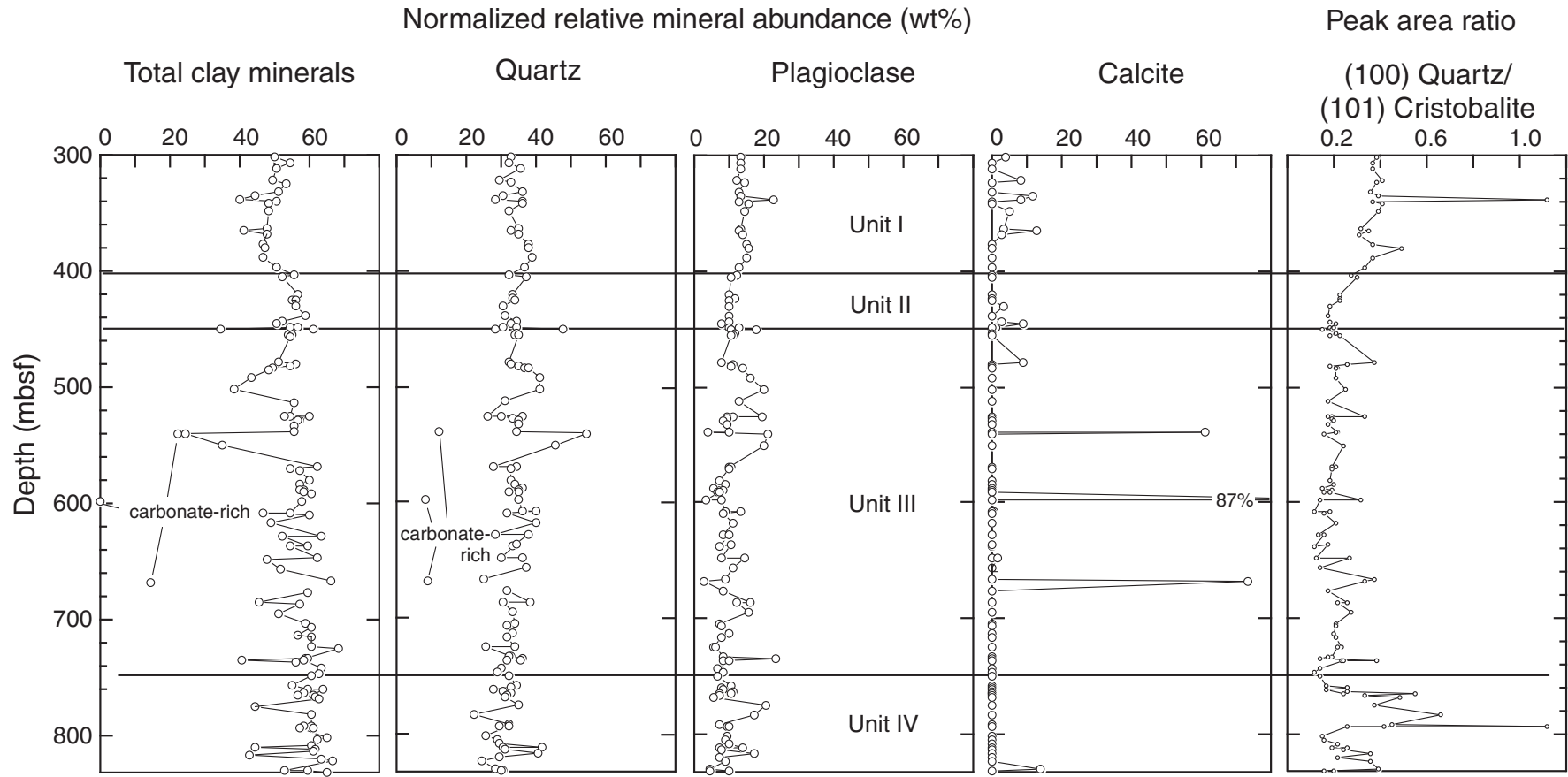


Figure F12. Healed fault (107–111 cm) and brecciated fracture zone (96–106 cm) with greenish alteration of claystone at the margins (interval 190-1177A-30R-1, 94–112 cm).

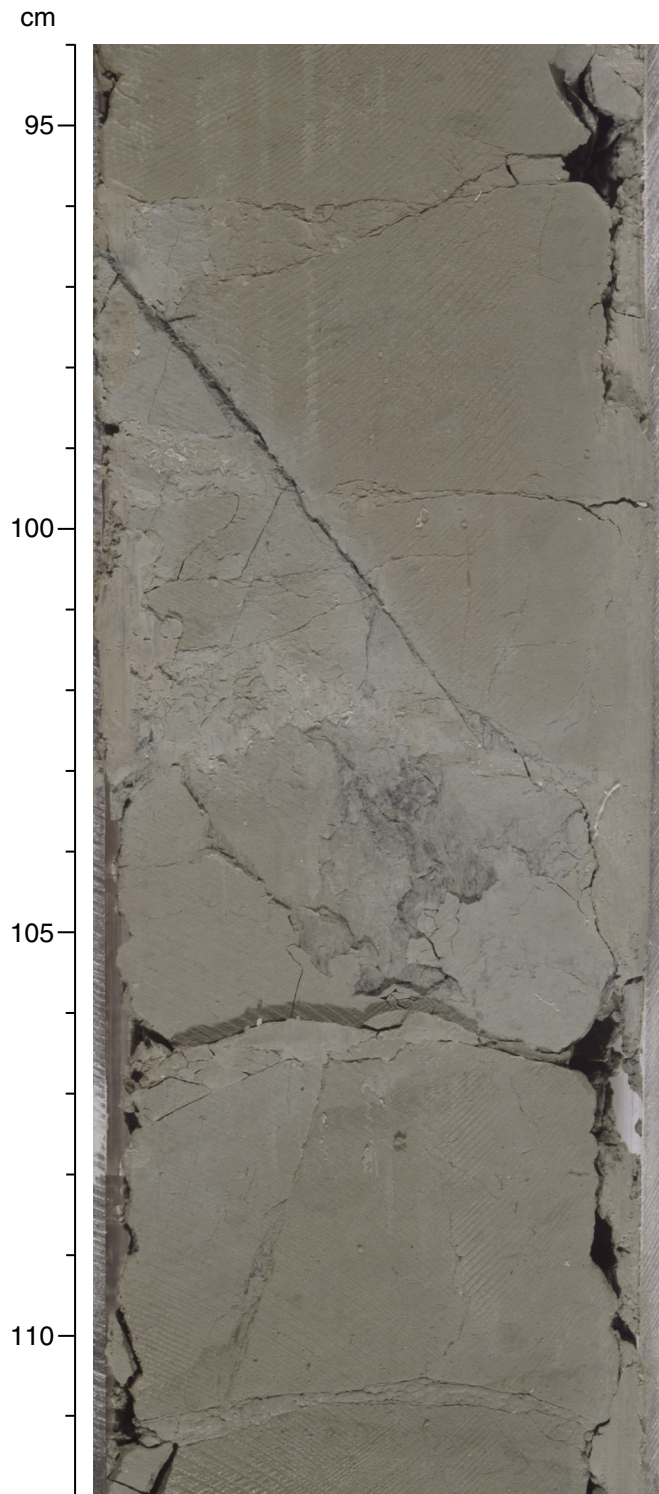


Figure F13. Subhorizontal veins and high-angle fracture in a relatively unaltered piece of basalt 60 cm below the base of the sediments (interval 190-1177A-56R-3, 62–82.5 cm). Chlorite is present as thin dark seams at 72–75 cm and in discontinuous bands in the calcite vein at 65–66 cm.

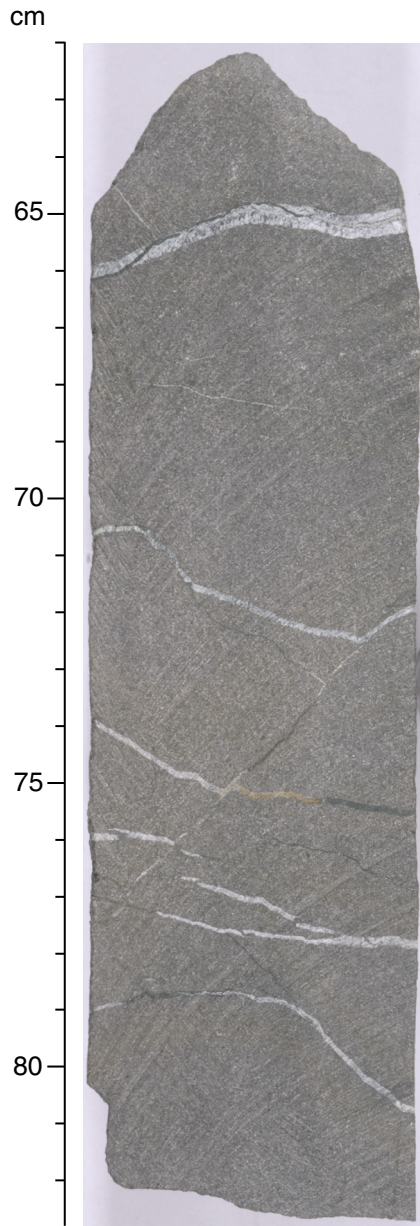


Figure F14. Gas-permeameter data from Site 1177 plotted (A) logarithmically and (B) linearly.

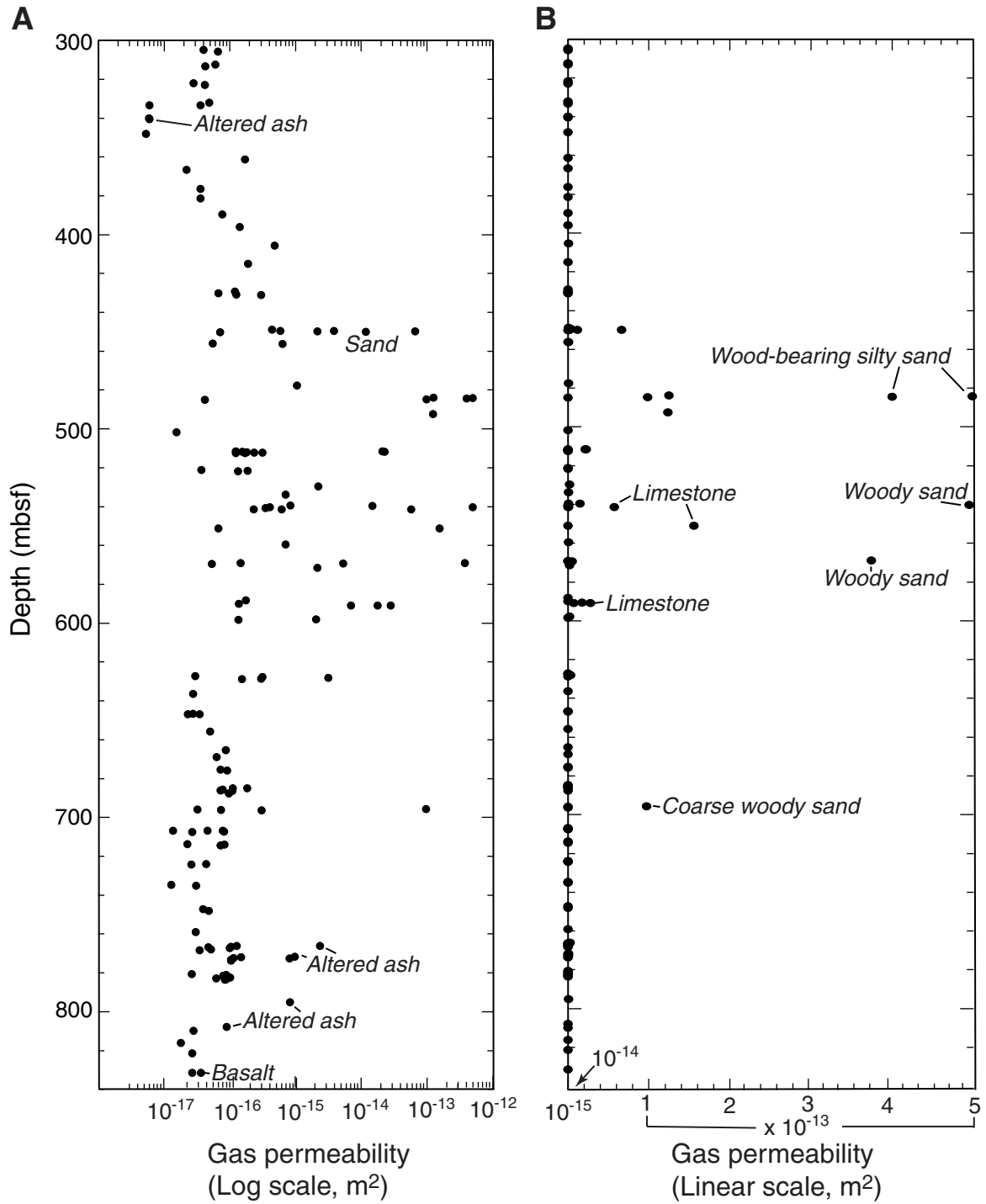


Figure F15. Paleomagnetic declination, inclination, and intensity after AF demagnetization at 30 mT at Hole 1177A. Continuous depositional remanent magnetization was observed from the top of the hole to ~450 mbsf. Scattered declinations reflect the rotation of small core pieces during RCB coring.

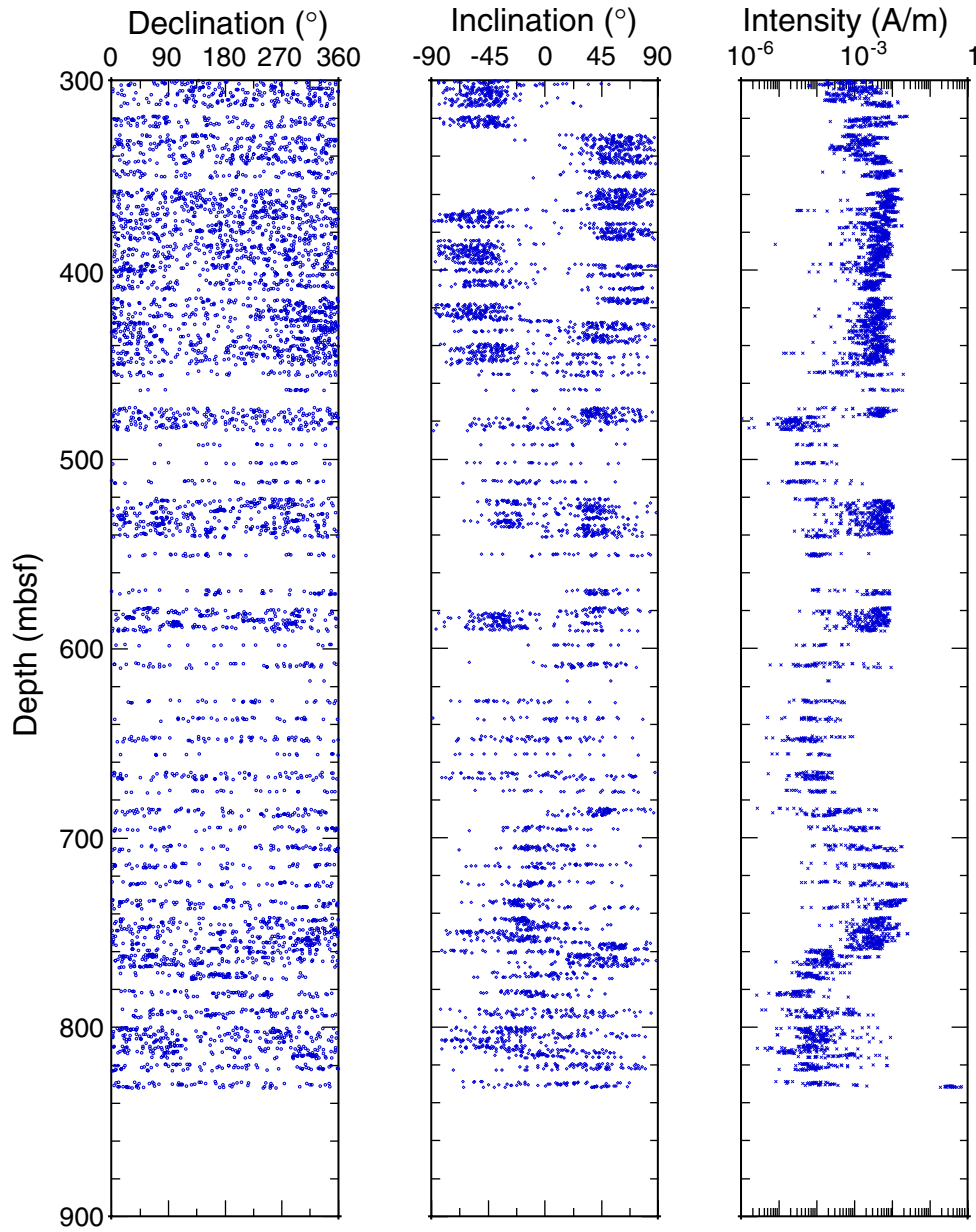


Figure F16. Site 1177 magnetostratigraphy. Detailed comparison of polarity changes with the polarity time scale of Cande and Kent (1995) was difficult because of poor core recovery below 450 mbsf. Black = normal polarity, white = reversed polarity, dashed lines = possible correlations based on biostratigraphic results.

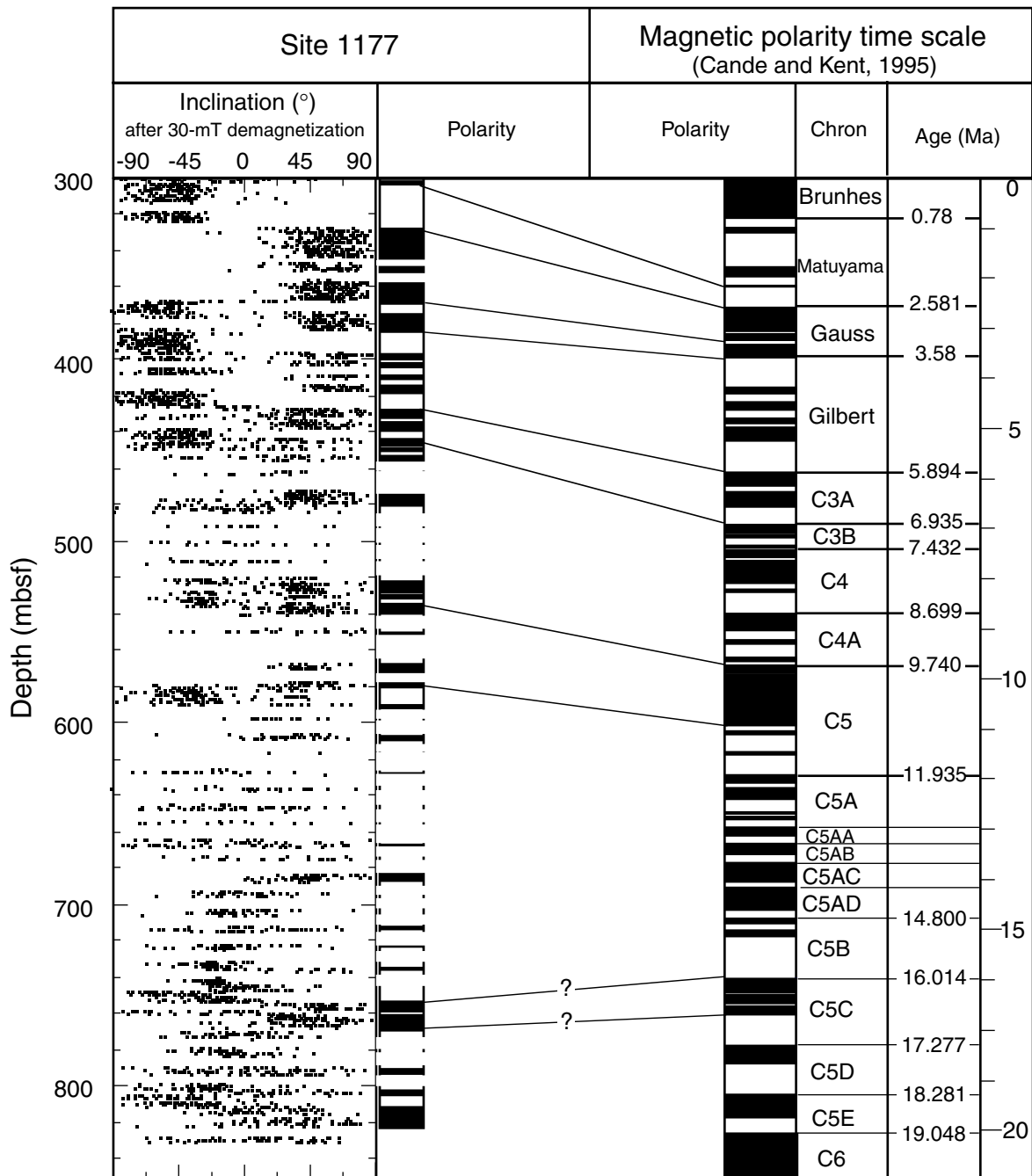


Figure F17. Site 1177 age-depth plot obtained from magnetostratigraphy and biostratigraphy. Black = normal polarity, white = reversed polarity.

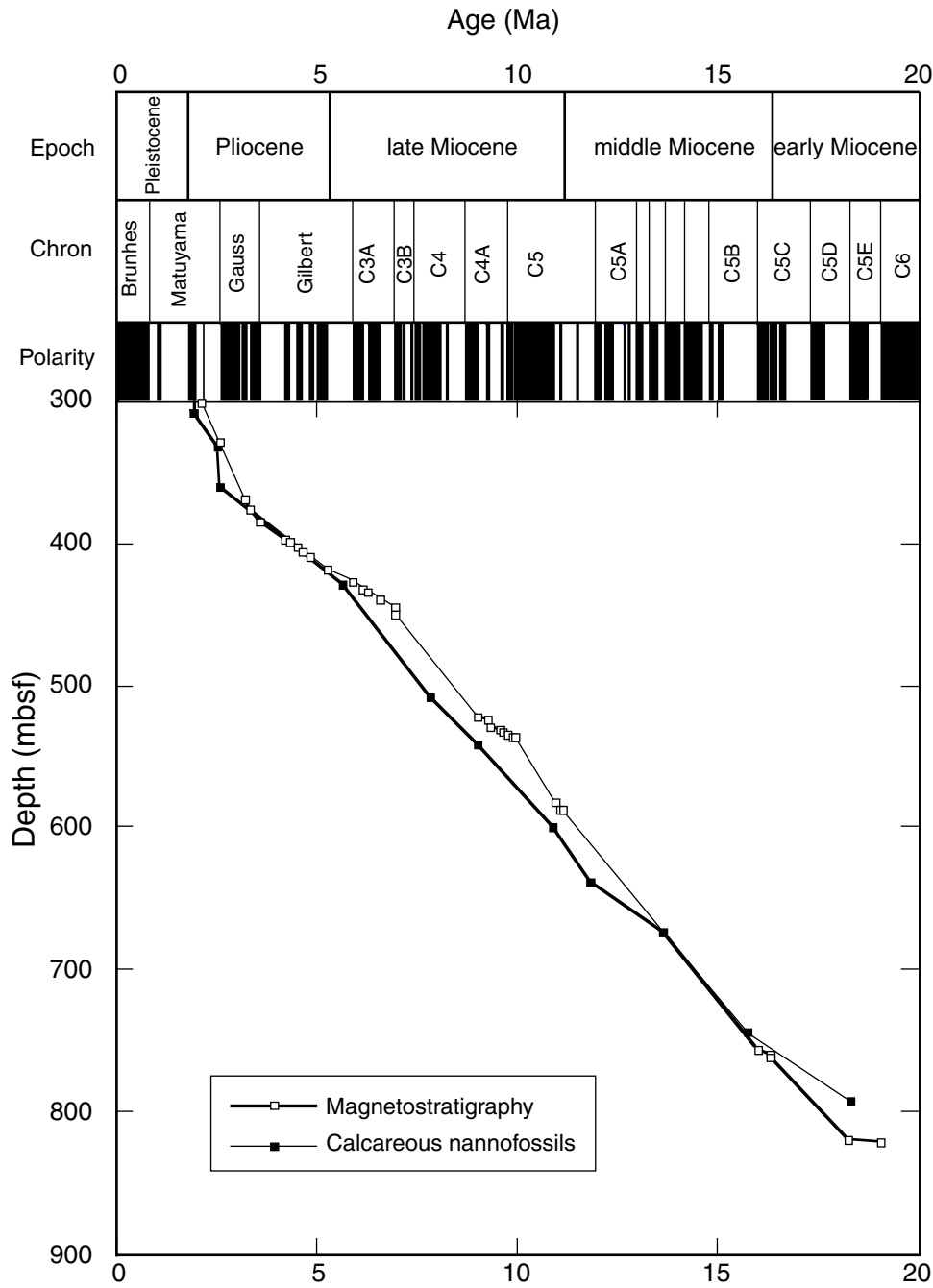


Figure F18. Pore fluid composition as a function of depth for Hole 1177A. Solid horizontal lines indicate lithostratigraphic boundaries.

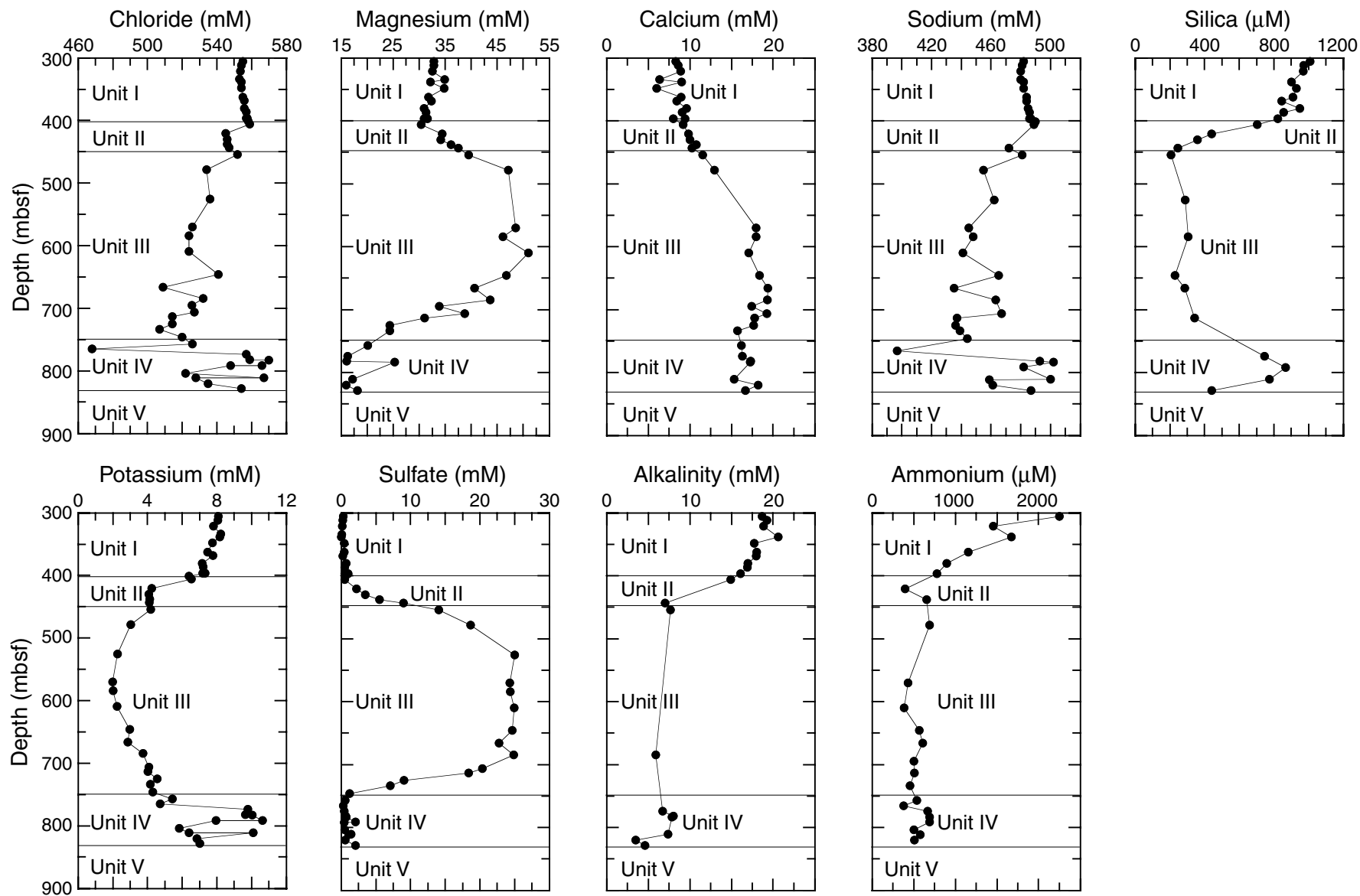


Figure F19. A. Methane and ethane compositions and concentrations of headspace gases. B. Carbon/nitrogen (C/N) ratios distributed in the sediments from Site 1177.

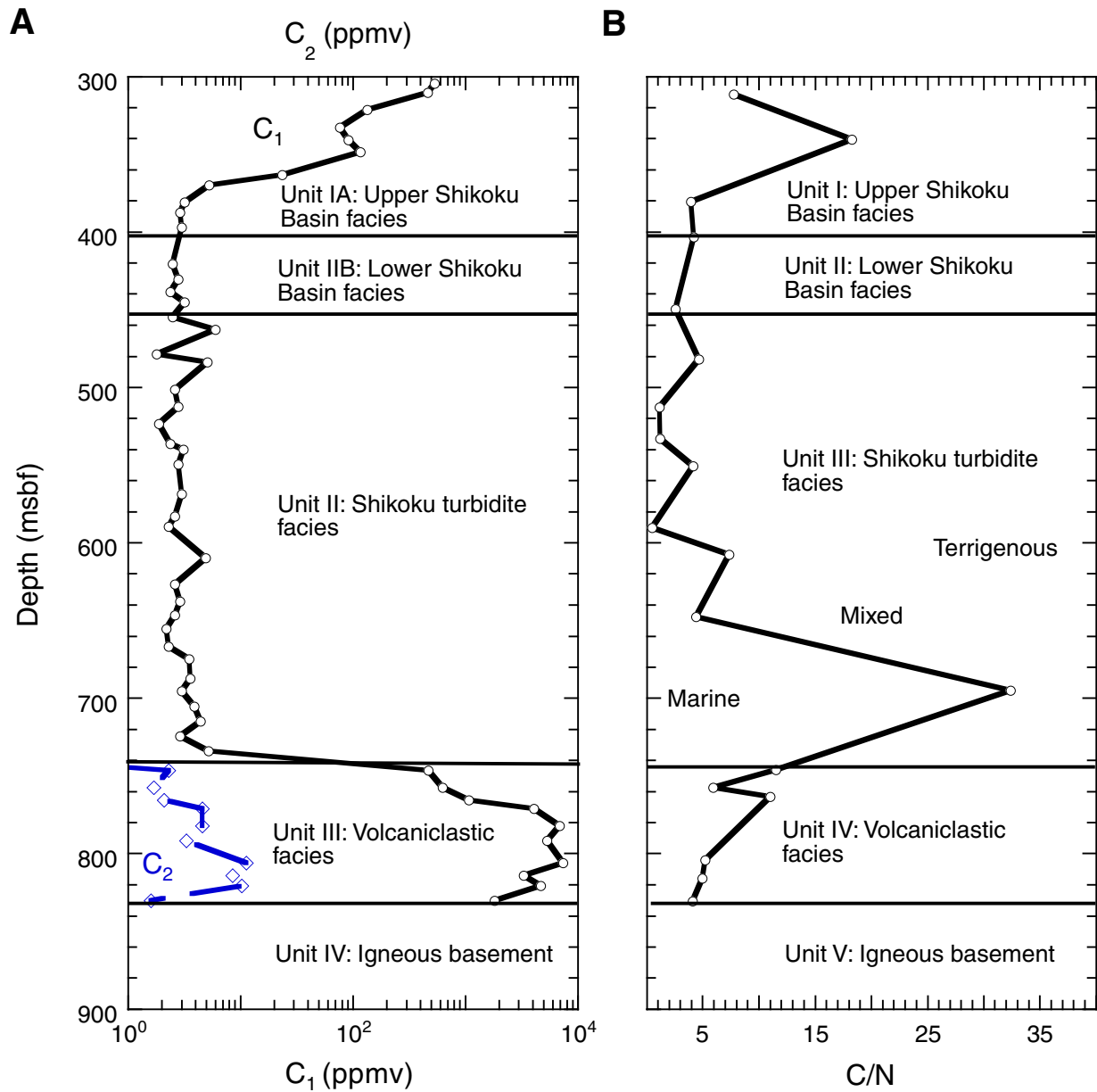


Figure F20. Total organic carbon (TOC) concentrations in sediments at Site 1177.

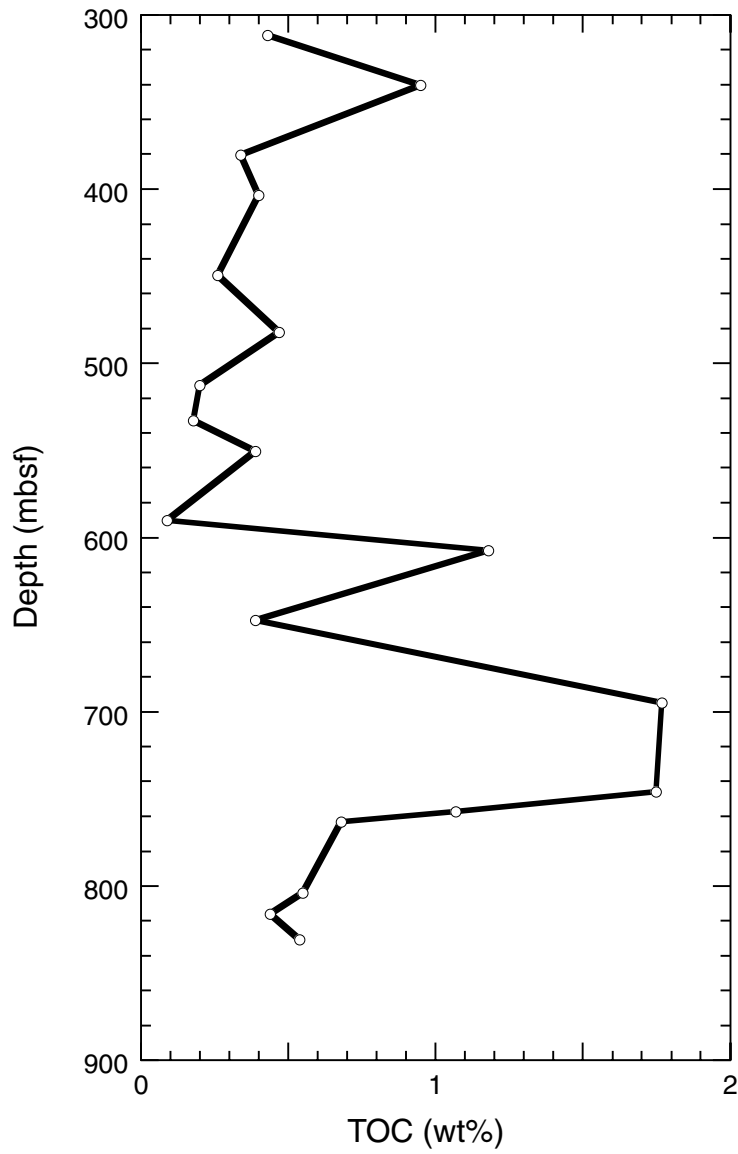


Figure F21. Depth distribution of total bacterial populations in sediment samples from Hole 1177A. The dashed line represents a general regression line of bacterial numbers vs. depth in deep-sea sediments (Parkes et al., 1994), with 95% upper and lower prediction limits shown by the lines of longer dashes. The shaded area on the left of the figure indicates where bacterial populations are too low to be detected with the acridine orange direct counts technique. The detection limit was 6×10^4 cells/cm³ (any values within this area are constructed from sums of three enumerations and have no measure of error).

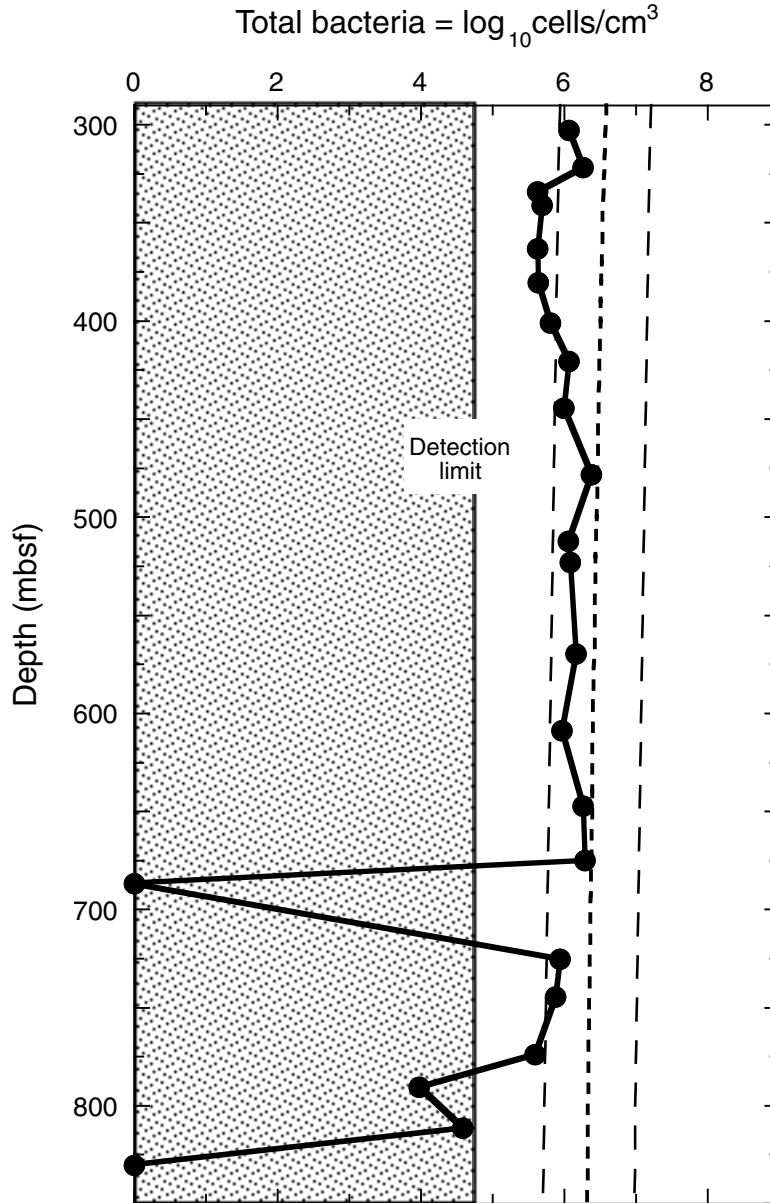


Figure F22. Depth profiles of total bacteria with an expanded section of the axis (solid circles) and interstitial water sulfate concentration (open circles).

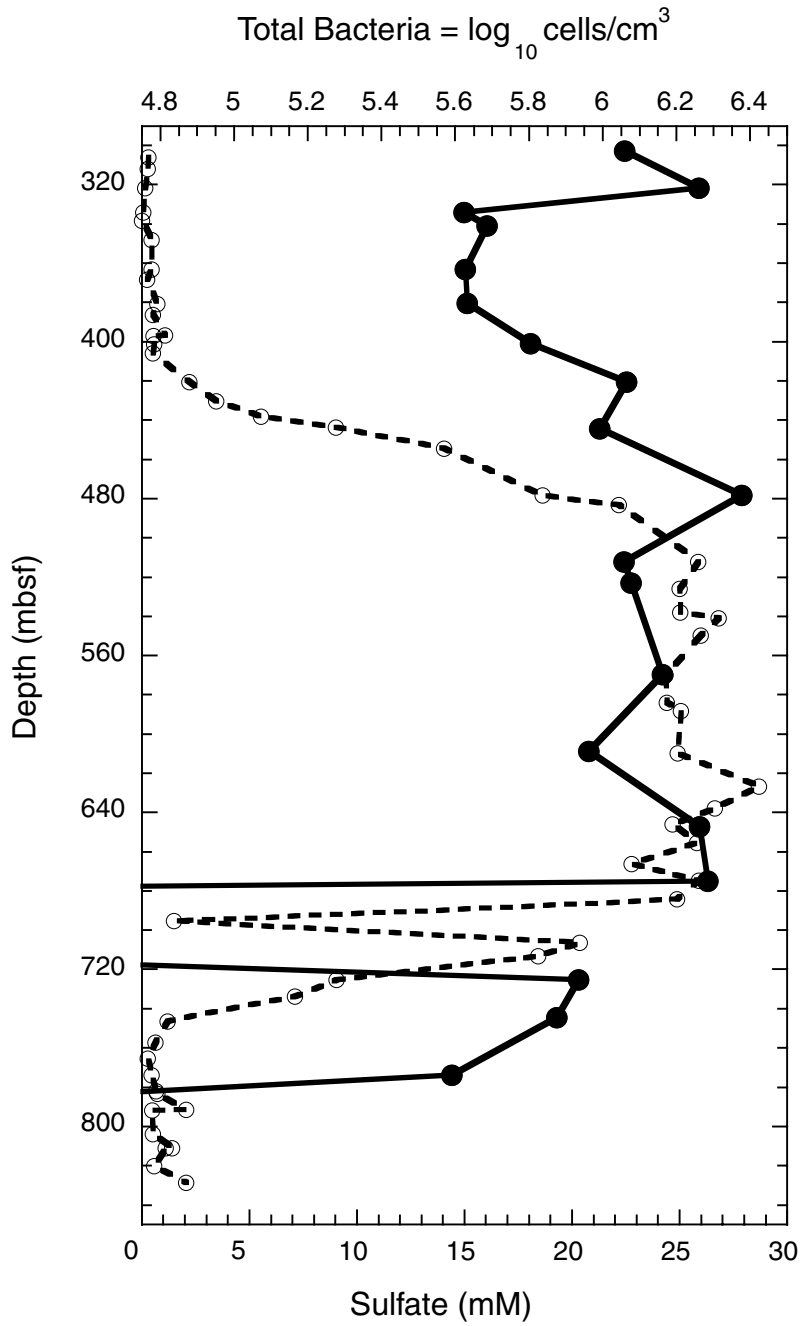


Figure F23. A. Site 1177 bulk density measurements. Lithostratigraphic Units I (upper Shikoku Basin facies), II (lower Shikoku Basin facies), III (Shikoku turbidite facies), and IV (volcaniclastic facies) are indicated. B. Gamma-ray attenuation (GRA) and mass/volume bulk density. C. Grain density. D. Porosity.

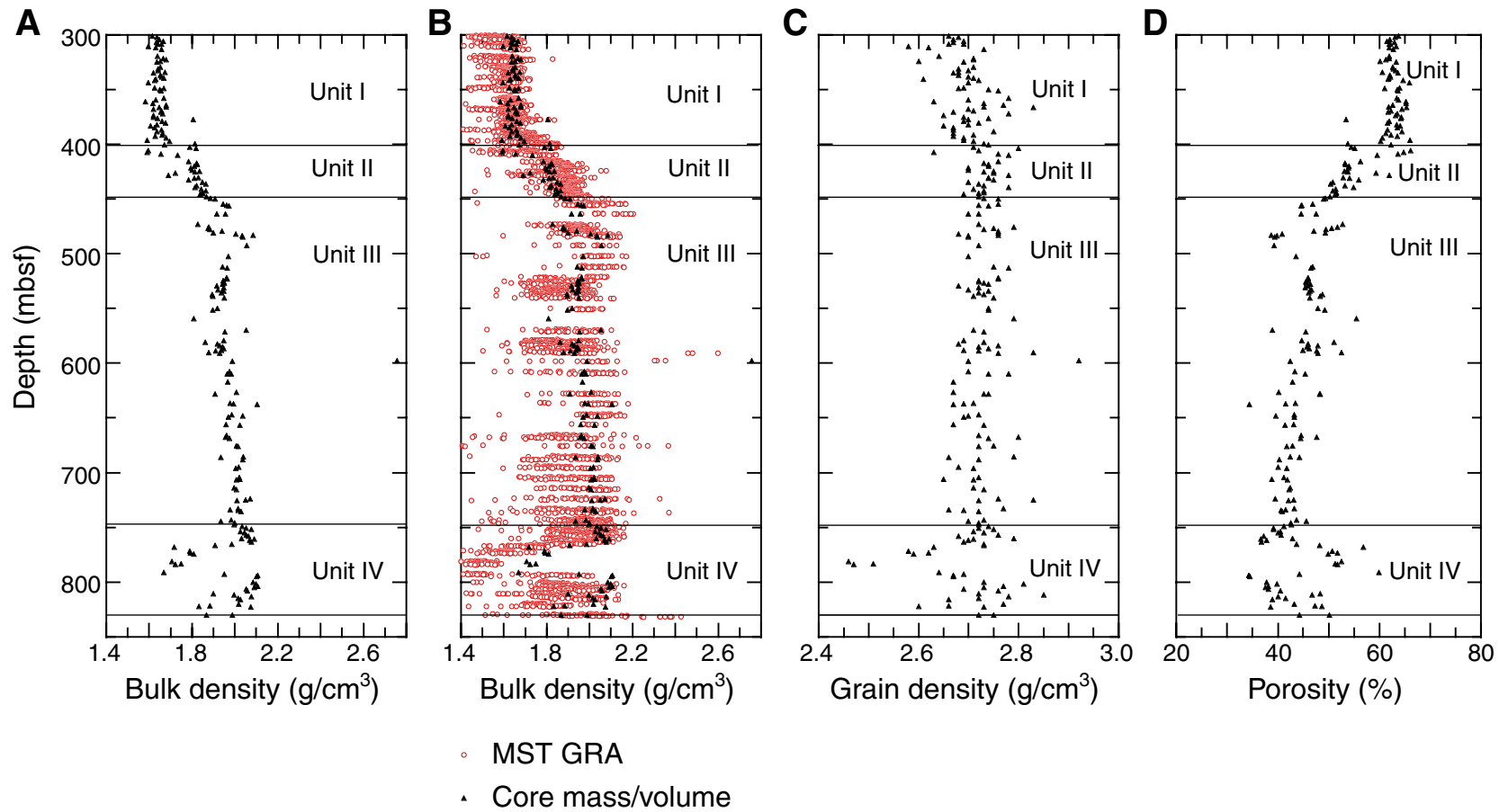


Figure F24. Site 1177 thermal conductivity.

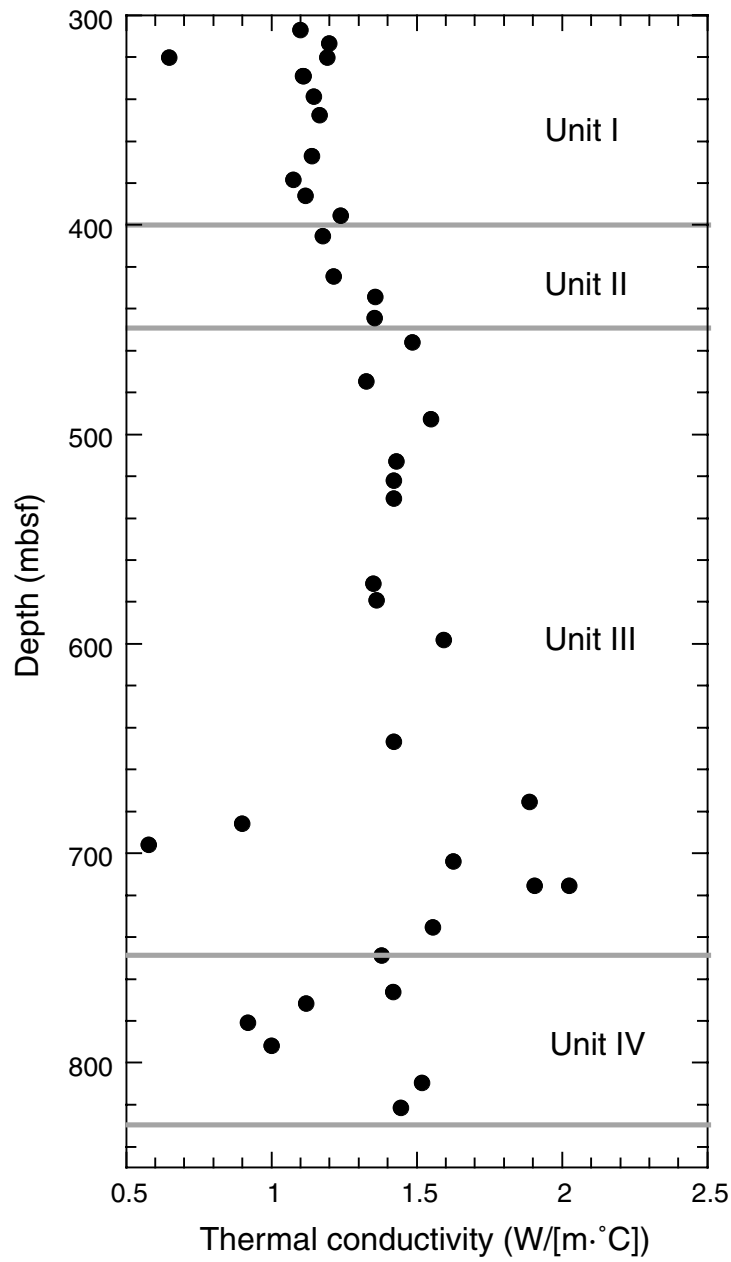


Figure F25. A. Hole 1177A *P*-wave velocity. B. Horizontal and vertical *P*-wave velocity as a function of porosity. The line represents a typical relationship for clayey silt computed from a weighted average equation (Lee et al., 1996). Units I, II, III, IV, and V refer to the lithostratigraphic units. C. *P*-wave anisotropy. The vertical plane anisotropy compares velocity along the two transverse axes (x and y) to that parallel to the core (z), whereas the horizontal plane anisotropy compares velocity of the x- and y-axes. Because cores are randomly rotated, horizontal plane anisotropy should average zero.

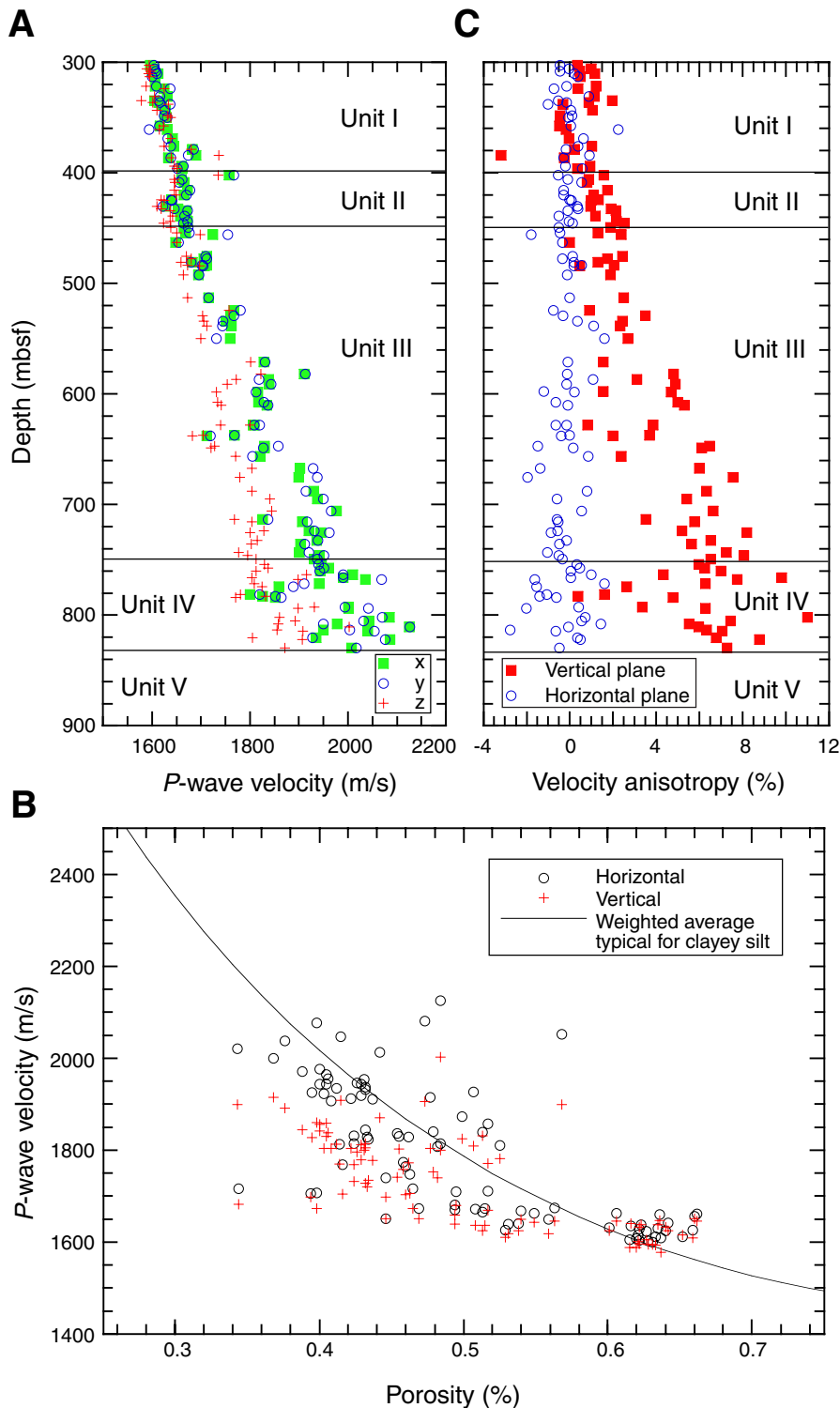


Figure F26. A. Hole 1177A formation factor. Measurements were performed in x- and y- (orthogonal to core) and z- (parallel to core) directions. B. Anisotropy of electrical conductivity in the horizontal (x- and y-axes) and vertical (z-axis) planes. (Continued on next page.)

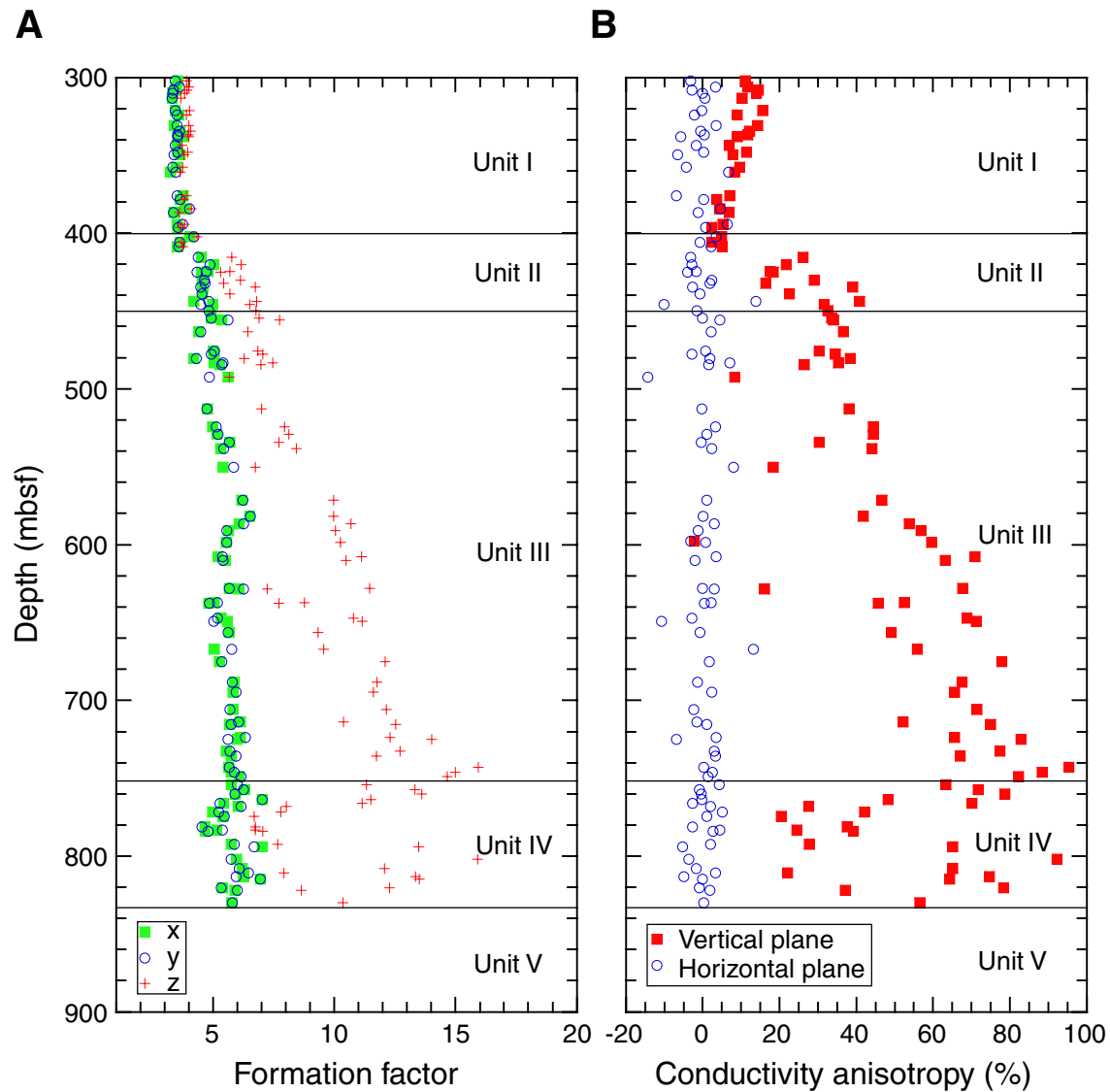
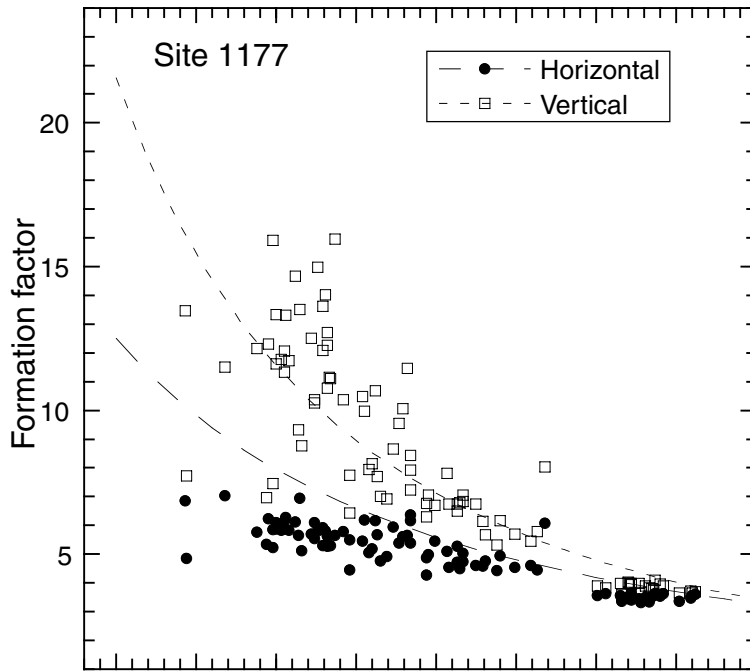


Figure F26 (continued). C. Horizontal and vertical formation factors vs. porosity, Site 1177. Curves represent best fits to generalized Archie's laws fitted at Site 1173. D. Horizontal and vertical formation factors vs. porosity, Site 1173. Curves represent power law (generalized Archie's law) fits to horizontal (dashed) and vertical (solid) components.

C



D

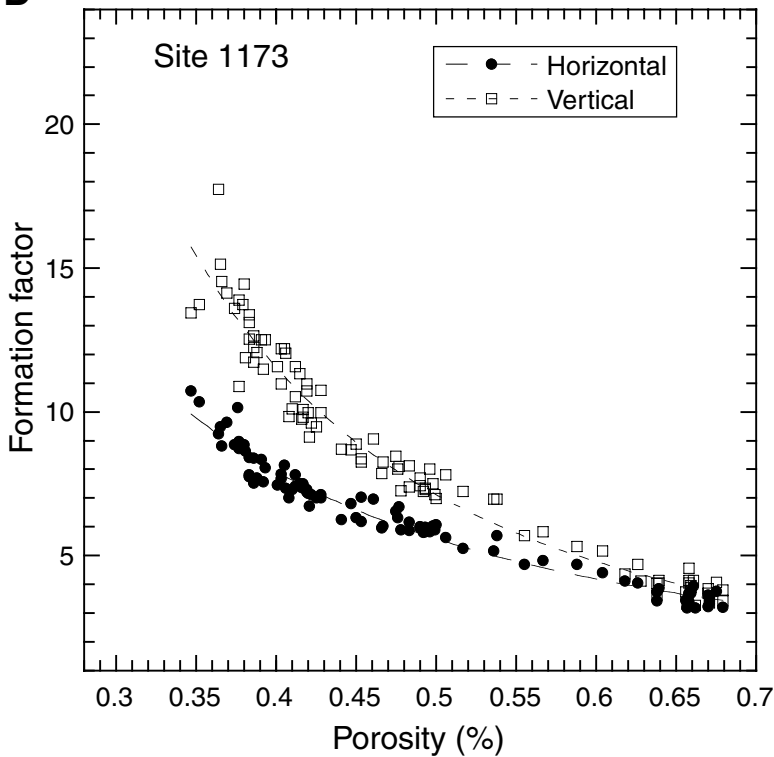


Figure F27. Site 1177 magnetic susceptibility.

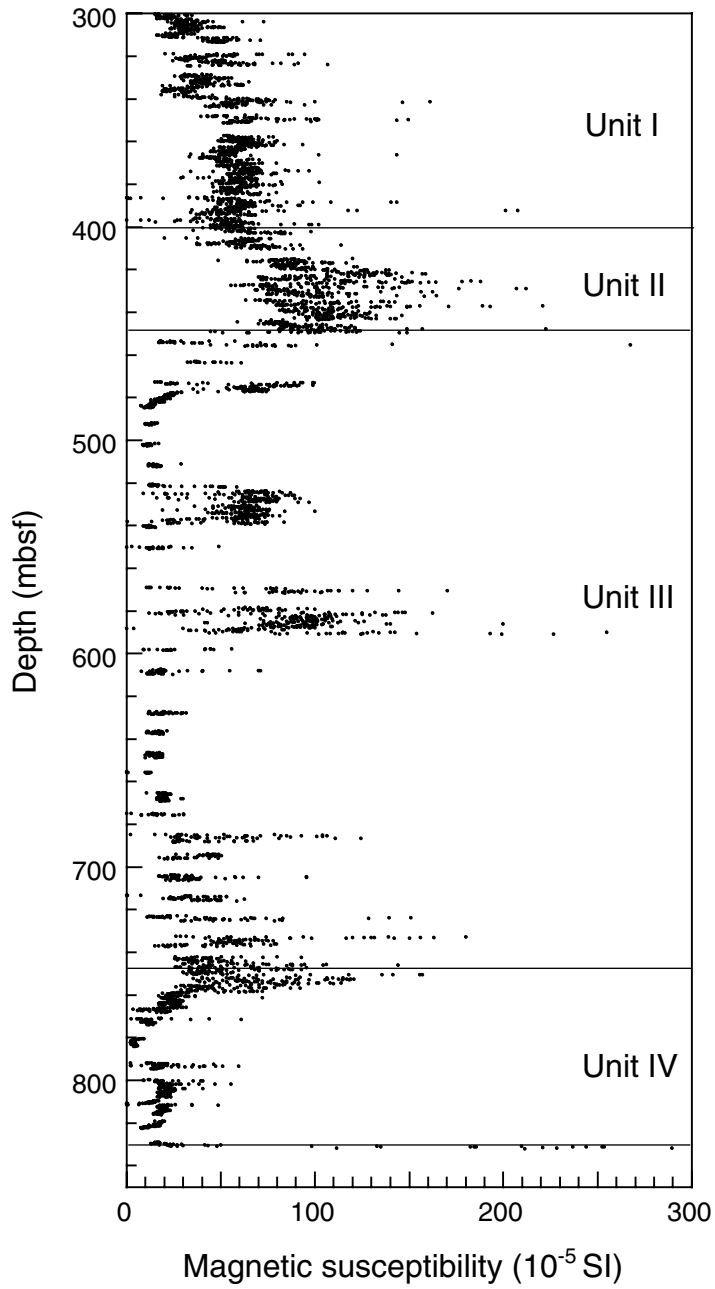


Figure F28. Site 1177 natural gamma ray.

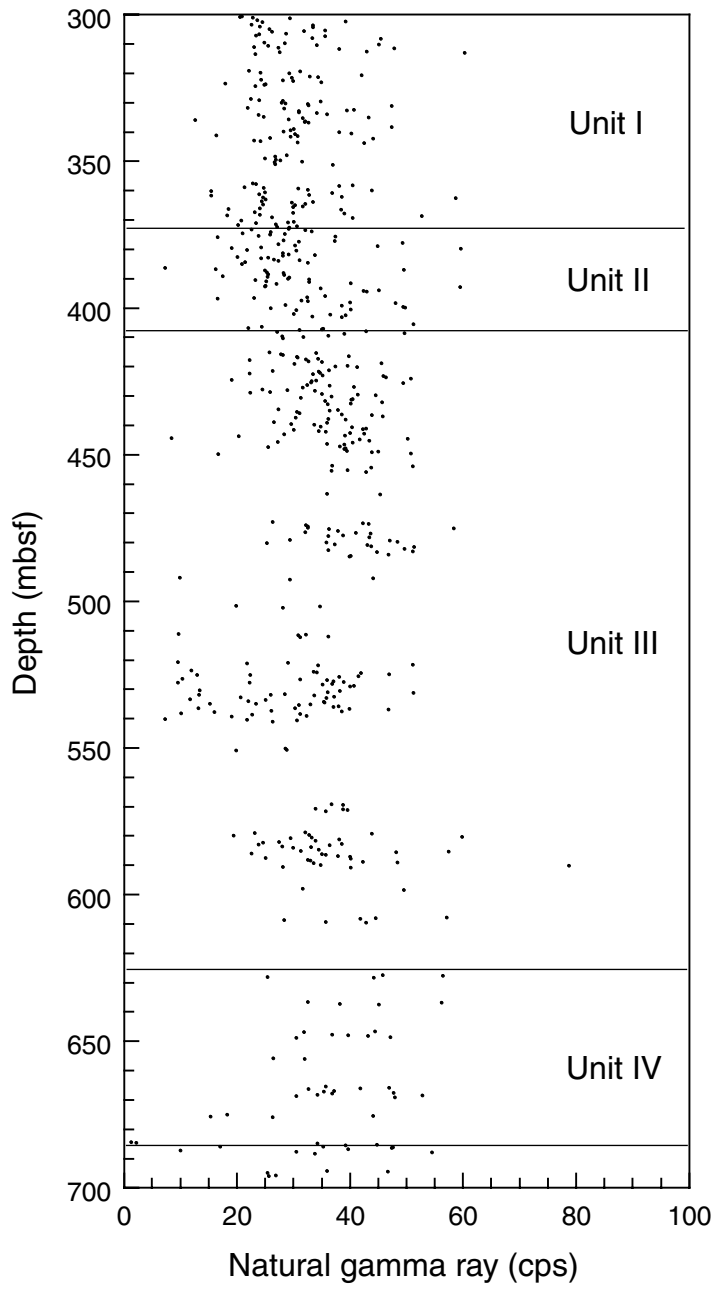


Figure F29. Three-dimensional seismic reflection line 281 across Site 1175. This line has been 3-D stacked and migrated.

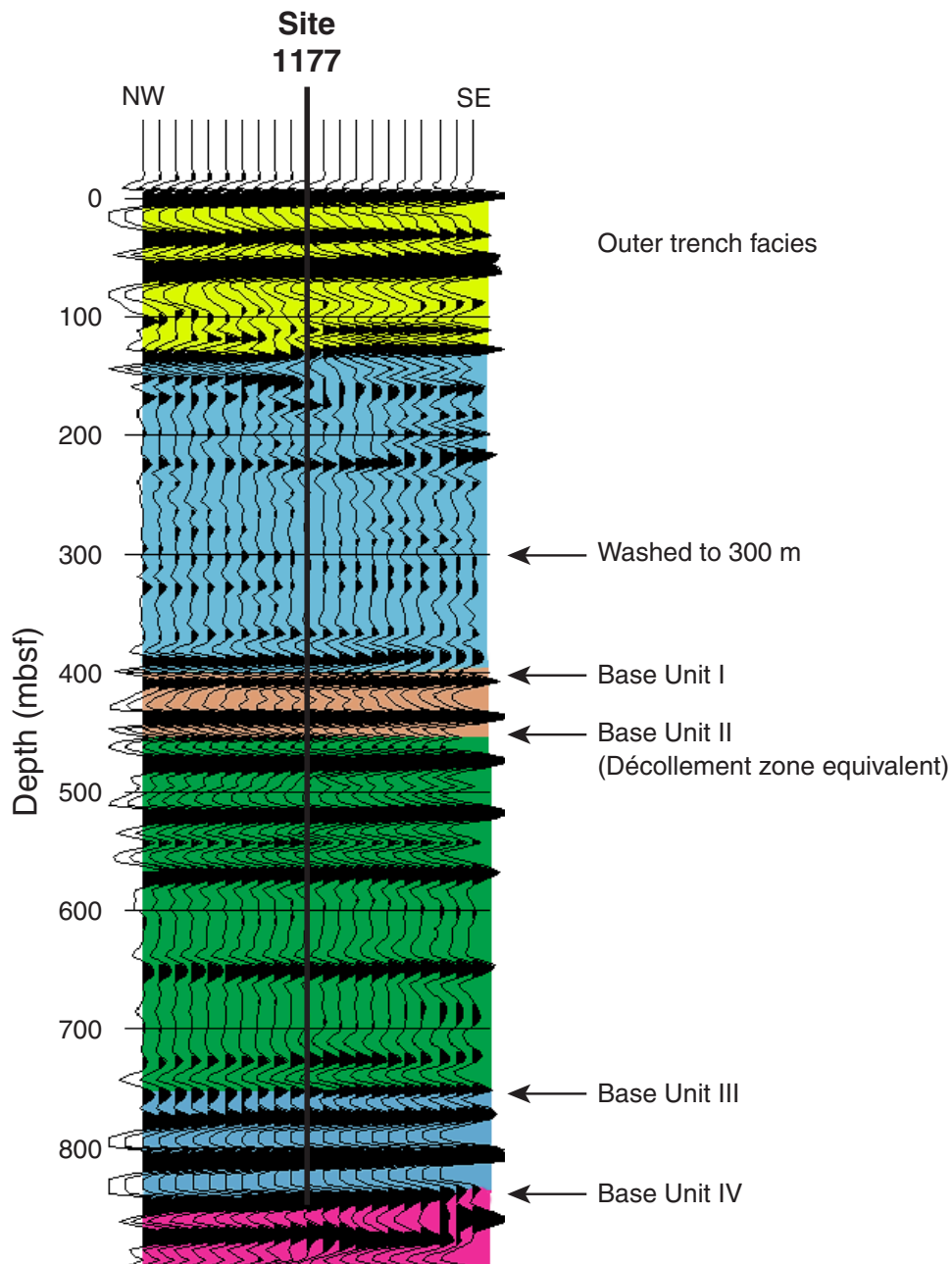


Table T1. Coring summary, Site 1177.

Core	Date (July 2000)	Time (local)	Depth (mbsf)		Length (m)		Recovery (%)	Comments
			Top	Bottom	Cored	Recovered		
190-1177A-								
NA	1	0130	0.0	300.2	NA	NA	NA	Drilled without coring; DVTP at 50.5 and 120 mbsf
1R	1	0330	300.2	309.2	9.0	8.46	94.0	
2R	1	0445	309.2	318.9	9.7	4.66	48.0	
3R	1	0610	318.9	328.5	9.6	5.97	62.2	
4R	1	0715	328.5	338.1	9.6	8.75	91.1	
5R	1	0825	338.1	347.7	9.6	6.14	64.0	
6R	1	1005	347.7	357.3	9.6	3.94	41.0	Whirl-Pak
7R	1	1125	357.3	367.0	9.7	9.82	101.2	Whirl-Pak
8R	1	1235	367.0	376.6	9.6	9.68	100.8	
9R	1	1340	376.6	386.1	9.5	8.67	91.3	
10R	1	1445	386.1	395.7	9.6	9.00	93.7	
11R	1	1549	395.7	405.3	9.6	8.23	85.7	
12R	1	1705	405.3	414.9	9.6	5.40	56.2	
13R	1	1820	414.9	424.5	9.6	9.97	103.9	
14R	1	1930	424.5	434.2	9.7	8.84	91.1	
15R	1	2045	434.2	443.9	9.7	9.90	102.1	
16R	1	2205	443.9	453.5	9.6	6.60	68.7	
17R	1	2335	453.5	463.1	9.6	2.70	28.1	
18R	2	0150	463.1	472.8	9.7	0.95	9.8	
19R	2	0245	472.8	482.4	9.6	9.67	100.7	
20R	2	0410	482.4	492.0	9.6	2.80	29.2	
21R	2	0545	492.0	501.6	9.6	0.77	8.0	
22R	2	0730	501.6	511.1	9.5	1.12	11.8	
23R	2	0850	511.1	520.7	9.6	2.15	22.4	Tracer
24R	2	1025	520.7	530.4	9.7	9.31	96.0	Tracer
25R	2	1205	530.4	540.1	9.7	9.74	100.4	
26R	2	1325	540.1	549.7	9.6	1.41	14.7	
27R	2	1500	549.7	559.4	9.7	1.67	17.2	
28R	2	1645	559.4	568.9	9.5	0.13	1.4	
29R	2	1840	568.9	578.5	9.6	2.88	30.0	
30R	2	2030	578.5	588.2	9.7	9.91	102.2	
31R	2	2235	588.2	597.8	9.6	3.17	33.0	
32R	3	0030	597.8	607.5	9.7	0.82	8.5	
33R	3	0210	607.5	617.1	9.6	2.85	29.7	
34R	3	0355	617.1	626.7	9.6	0.17	1.8	
35R	3	0620	626.7	636.3	9.6	2.13	22.2	
36R	3	0805	636.3	645.9	9.6	2.17	22.6	
37R	3	1015	645.9	655.5	9.6	3.52	36.7	
38R	3	1210	655.5	665.2	9.7	0.91	9.4	
39R	3	1420	665.2	674.8	9.6	4.26	44.4	
40R	3	1620	674.8	684.4	9.6	1.40	14.6	
41R	3	1810	684.4	694.0	9.6	4.31	44.9	
42R	3	1955	694.0	703.7	9.7	2.51	25.9	
43R	3	2140	703.7	713.3	9.6	3.47	36.1	
44R	3	2340	713.3	722.9	9.6	2.95	30.7	
45R	4	0200	722.9	732.5	9.6	2.99	31.1	
46R	4	0405	732.5	742.1	9.6	5.18	54.0	
47R	4	0625	742.1	751.7	9.6	9.06	94.4	
48R	4	0830	751.7	761.3	9.6	9.45	98.4	
49R	4	1050	761.3	771.0	9.7	7.31	75.4	Soft F/5623 m - 5627 m
50R	4	1240	771.0	780.6	9.6	3.65	38.0	
51R	4	1420	780.6	790.3	9.7	3.86	39.8	
52R	4	1620	790.3	799.9	9.6	4.91	51.1	Hard at 5664.47 m
53R	4	1840	799.9	809.5	9.6	8.40	87.5	
54R	4	2040	809.5	819.2	9.7	7.01	72.3	
55R	4	2240	819.2	828.8	9.6	3.76	39.2	
56R	5	0225	828.8	833.9	5.1	3.28	64.3	
			Totals:		533.7	282.7	53	

Notes: DVTP = Davis-Villinger temperature probe. NA = not applicable.

Table T2. Coring summary by section, Site 1177. (See table notes. Continued on next five pages.)

Core	Date (July 2000)	Time (local)	Core depth (mbsf)		Length (m)		Recovery (%)	Section	Length (m)		Section depth (mbsf)		Catwalk samples
			Top	Bottom	Cored	Recovered			Liner	Curated	Top	Bottom	
190-1177A-													
NA	1	0130	0.0	300.2	NA	NA			**** Drilled without coring ****				
1R	1	0330	300.2	309.2	9.0	8.46	94.0						
								1	1.5	1.5	300.2	301.7	
								2	1.5	1.5	301.7	303.2	WRC, WRS, WRY, BAC
								3	1.5	1.5	303.2	304.7	
								4	1.5	1.5	304.7	306.2	HS, IW
								5	1.5	1.5	306.2	307.7	BGAS
								6	0.73	0.73	307.7	308.43	
								CC(w/6)	0.23	0.23	308.43	308.66	PAL
								Totals:	8.46	8.46			
2R	1	0445	309.2	318.9	9.7	4.66	48.0						
								1	1.5	1.5	309.2	310.7	
								2	1.5	1.5	310.7	312.2	HS, BGAS, IW
								3	1.41	1.41	312.2	313.61	
								CC(w/CC)	0.25	0.25	313.61	313.86	PAL
								Totals:	4.66	4.66			
3R	1	0610	318.9	328.5	9.6	5.97	62.2						
								1	1.5	1.5	318.9	320.4	
								2	1.5	1.5	320.4	321.9	HS, BGAS, IW, BACT
								3	1.5	1.5	321.9	323.4	
								4	1.19	1.19	323.4	324.59	
								CC(w/CC)	0.28	0.28	324.59	324.87	PAL
								Totals:	5.97	5.97			
4R	1	0715	328.5	338.1	9.6	8.75	91.1						
								1	1.5	1.5	328.5	330.0	
								2	1.5	1.5	330.0	331.5	
								3	1.5	1.5	331.5	333.0	
								4	1.5	1.5	333.0	334.5	HS, BGAS, IW, BACT
								5	1.5	1.5	334.5	336.0	
								6	1.03	1.03	336.0	337.03	
								CC(w/6)	0.22	0.22	337.03	337.25	PAL
								Totals:	8.75	8.75			
5R	1	0825	338.1	347.7	9.6	6.14	64.0						
								1	0.74	0.74	338.1	338.84	IW
								2	0.76	0.76	338.84	339.6	
								3	1.5	1.5	339.6	341.1	BACT
								4	1.5	1.5	341.1	342.6	HS, BGAS
								5	1.43	1.43	342.6	344.03	
								CC(w/CC)	0.21	0.21	344.03	344.24	PAL
								Totals:	6.14	6.14			
6R	1	1005	347.7	357.3	9.6	3.94	41.0						
								1	1.0	1.0	347.7	348.7	IW
								2	0.5	0.5	348.7	349.2	HS
								3	1.5	1.5	349.2	350.7	
								4	0.7	0.7	350.7	351.4	
								CC(w/CC)	0.24	0.24	351.4	351.64	PAL
								Totals:	3.94	3.94			
7R	1	1125	357.3	367.0	9.7	9.82	101.2						
								1	1.5	1.5	357.3	358.8	
								2	1.5	1.5	358.8	360.3	
								3	1.5	1.5	360.3	361.8	
								4	1.5	1.5	361.8	363.3	IW, BACT
								5	1.5	1.5	363.3	364.8	HS, BGAS
								6	1.5	1.5	364.8	366.3	
								7	0.55	0.55	366.3	366.85	
								CC(w/7)	0.27	0.27	366.85	367.12	PAL
								Totals:	9.82	9.82			
8R	1	1235	367.0	376.6	9.6	9.68	100.8						
								1	1.5	1.5	367	368.5	
								2	1.5	1.5	368.5	370.0	IW, WRMG
								3	1.5	1.5	370.0	371.5	HS
								4	1.5	1.5	371.5	373.0	
								5	1.5	1.5	373.0	374.5	
								6	1.5	1.5	374.5	376.0	
								7	0.51	0.51	376.0	376.51	
								CC(w/7)	0.17	0.17	376.51	376.68	PAL
								Totals:	9.68	9.68			

Table T2 (continued).

Core	Date (July 2000)	Time (local)	Core depth (mbsf)		Length (m)		Recovery (%)	Section	Length (m)		Section depth (mbsf)		Catwalk samples
			Top	Bottom	Cored	Recovered			Liner	Curated	Top	Bottom	
9R	1	1340	376.6	386.1	9.5	8.67	91.3						
								1	1.5	1.5	376.6	378.1	
								2	1.5	1.5	378.1	379.6	
								3	1.5	1.5	379.6	381.1	IW, BACT
								4	1.5	1.5	381.1	382.6	HS, WRMT
								5	1.5	1.5	382.6	384.1	
								6	0.92	0.92	384.1	385.02	
								CC(w/6)	0.25	0.25	385.02	385.27	PAL, WRTB
								Totals:	8.67	8.67			
10R	1	1445	386.1	395.7	9.6	9.00	93.8						
								1	1.5	1.5	386.1	387.6	IW
								2	1.5	1.5	387.6	389.1	HS, BGAS
								3	1.5	1.5	389.1	390.6	
								4	1.5	1.5	390.6	392.1	
								5	1.5	1.5	392.1	393.6	
								6	1.19	1.19	393.6	394.79	
								CC(w/CC)	0.31	0.31	394.79	395.1	PAL
								Totals:	9.0	9.0			
11R	1	1549	395.7	405.3	9.6	8.23	85.7						
								1	1.5	1.5	395.7	397.2	IW, IW
								2	1.5	1.5	397.2	398.7	HS, BGAS
								3	1.5	1.5	398.7	400.2	
								4	1.5	1.5	400.2	401.7	IW, WRC, WRY, WRS
								5	1.5	1.5	401.7	403.2	
								6	0.45	0.45	403.2	403.65	
								CC(w/6)	0.28	0.28	403.65	403.93	PAL, WRTB
								Totals:	8.23	8.23			
12R	1	1705	405.3	414.9	9.6	5.4	56.3						
								1	0.88	0.88	405.3	406.18	IW
								2	1.5	1.5	406.18	407.68	HS
								3	1.5	1.5	407.68	409.18	
								4	1.21	1.21	409.18	410.39	
								CC(w/CC)	0.31	0.31	410.39	410.7	PAL
								Totals:	5.4	5.4			
13R	1	1820	414.9	424.5	9.6	9.97	103.9						
								1	1.5	1.5	414.9	416.4	
								2	1.5	1.5	416.4	417.9	
								3	1.5	1.5	417.9	419.4	
								4	1.5	1.5	419.4	420.9	BACT, IW
								5	1.5	1.5	420.9	422.4	HS, BGAS
								6	1.5	1.5	422.4	423.9	
								7	0.6	0.6	423.9	424.5	WRTB
								CC(w/7)	0.37	0.37	424.5	424.87	PAL, WRSR
								Totals:	9.97	9.97			
14R	1	1930	424.5	434.2	9.7	8.84	91.1						
								1	1.5	1.5	424.5	426.0	
								2	1.5	1.5	426.0	427.5	
								3	1.5	1.5	427.5	429.0	
								4	1.5	1.5	429.0	430.5	IW
								5	1.5	1.5	430.5	432.0	HS
								6	1.02	1.02	432.0	433.02	
								CC(w/6)	0.32	0.32	433.02	433.34	PAL
								Totals:	8.84	8.84			
15R	1	2045	434.2	443.9	9.7	9.9	102.1						
								1	1.5	1.5	434.2	435.7	
								2	1.5	1.5	435.7	437.2	
								3	1.5	1.5	437.2	438.7	IW
								4	1.5	1.5	438.7	440.2	HS, BGAS
								5	1.5	1.5	440.2	441.7	
								6	1.5	1.5	441.7	443.2	
								7	0.6	0.6	443.2	443.8	
								CC(w/7)	0.3	0.3	443.8	444.1	PAL, WRTB
								Totals:	9.9	9.9			
16R	1	2205	443.9	453.5	9.6	6.6	68.8						
								1	1.5	1.5	443.9	445.4	BACT, IW
								2	1.5	1.5	445.4	446.9	HS
								3	1.5	1.5	446.9	448.4	WRSR
								4	1.5	1.5	448.4	449.9	

Table T2 (continued).

Core	Date (July 2000)	Time (local)	Core depth (mbsf)		Length (m)		Recovery (%)	Section	Length (m)		Section depth (mbsf)		Catwalk samples
			Top	Bottom	Cored	Recovered			Liner	Curated	Top	Bottom	
17R	1	2335	453.5	463.1	9.6	2.7	28.1	5	0.4	0.4	449.9	450.3	PAL, SFRCC
								CC(w/5)	0.2	0.2	450.3	450.5	
								Totals:	6.6	6.6			
18R	2	0150	463.1	472.8	9.7	0.95	9.8	1	1.5	1.5	453.5	455.0	IW
								2	1.02	1.02	455.0	456.02	HS, BGAS
								CC(w/2)	0.18	0.18	456.02	456.2	PAL
19R	2	0245	472.8	482.4	9.6	9.67	100.7	1	0.81	0.81	463.1	463.91	HS
								CC(w/1)	0.14	0.14	463.91	464.05	PAL
								Totals:	0.95	0.95			
20R	2	0410	482.4	492.0	9.6	2.8	29.2	1	1.5	1.5	472.8	474.3	BACT, IW HS, BGAS HYWR PAL, SFRCC
								2	1.5	1.5	474.3	475.8	
								3	1.5	1.5	475.8	477.3	
								4	1.5	1.5	477.3	478.8	
								5	1.5	1.5	478.8	480.3	
								6	1.5	1.5	480.3	481.8	
								7	0.43	0.43	481.8	482.23	
								CC(w/7)	0.24	0.24	482.23	482.47	
Totals:	9.67	9.67											
21R	2	0545	492.0	501.6	9.6	0.77	8.0	1	1.5	1.5	482.4	483.9	SMTCR, IW
								2	1.04	1.04	483.9	484.94	SMTCR, HS
								CC(w/2)	0.26	0.26	484.94	485.2	SFRCC, PAL
22R	2	0730	501.6	511.1	9.5	1.12	11.8	Totals:	2.8	2.8			
								1	0.77	0.77	492.0	492.77	PAL
23R	2	0850	511.1	520.7	9.6	2.15	22.4	Totals:	0.77	0.77			
								1	0.84	0.84	501.6	502.44	HS
								CC(w/CC)	0.28	0.28	502.44	502.72	PAL
24R	2	1025	520.7	530.4	9.7	9.31	96.0	Totals:	1.12	1.12			
								1	1.43	1.43	511.1	512.53	BACT, HS, BGAS
								2	0.44	0.44	512.53	512.97	IW
25R	2	1205	530.4	540.1	9.7	9.74	100.4	CC(w/CC)	0.28	0.28	512.97	513.25	PAL, WRTB
								Totals:	2.15	2.15			
								1	1.5	1.5	520.7	522.2	SMTCR
								2	1.5	1.5	522.2	523.7	WRC, PLUGS, BACT
								3	1.5	1.5	523.7	525.2	HS, SMTCR
								4	1.2	1.2	525.2	526.4	IW, WRMT, CRG
								5	1.5	1.5	526.4	527.9	SMTCR, WRSR
								6	1.5	1.5	527.9	529.4	WRSR
7	0.3	0.3	529.4	529.7									
26R	2	1325	540.1	549.7	9.6	1.41	14.7	CC(w/7)	0.31	0.31	529.7	530.01	PAL
								Totals:	9.31	9.31			
								1	1.5	1.5	530.4	531.9	SMTCR
								2	1.5	1.5	531.9	533.4	WRLZ
								3	1.5	1.5	533.4	534.9	WRMG
								4	1.5	1.5	534.9	536.4	SMTCR
								5	1.5	1.5	536.4	537.9	HS, SMTCR, WRTB
								6	1.5	1.5	537.9	539.4	IW
7	0.45	0.45	539.4	539.85									
27R	2	1500	549.7	559.4	9.7	1.67	17.2	CC(w/7)	0.29	0.29	539.85	540.14	PAL
								Totals:	9.74	9.74			
								1	1.25	1.25	540.1	541.35	HS, IW, WRMT
28R	2	1500	549.7	559.4	9.7	1.67	17.2	CC(w/1)	0.16	0.16	541.35	541.51	PAL
								Totals:	1.41	1.41			
								1	1.39	1.39	549.7	551.09	HS, IW, BGAS
29R	2	1500	549.7	559.4	9.7	1.67	17.2	CC(w/CC)	0.28	0.28	551.09	551.37	PAL
								Totals:	1.67	1.67			

Table T2 (continued).

Core	Date (July 2000)	Time (local)	Core depth (mbsf)		Length (m)		Recovery (%)	Section	Length (m)		Section depth (mbsf)		Catwalk samples
			Top	Bottom	Cored	Recovered			Liner	Curated	Top	Bottom	
28R	2	1645	559.4	568.9	9.5	0.13	1.4						
								CC(w/CC)	0.13	0.13	559.4	559.53	PAL
								Totals:	0.13	0.13			
29R	2	1840	568.9	578.5	9.6	2.88	30.0						
								1	1.5	1.5	568.9	570.4	WRY, WRS, BACT, HS
								2	1.26	1.26	570.4	571.66	
								CC(w/2)	0.12	0.12	571.66	571.78	PAL
								Totals:	2.88	2.88			
30R	2	2030	578.5	588.2	9.7	9.91	102.2						
								1	1.5	1.5	578.5	580.0	
								2	1.5	1.5	580.0	581.5	
								3	1.5	1.5	581.5	583.0	WRSF
								4	1.5	1.5	583.0	584.5	HS, BGAS, IW
								5	1.5	1.5	584.5	586.0	
								6	1.5	1.5	586.0	587.5	
								7	0.63	0.63	587.5	588.13	WRTB
								CC(w/7)	0.28	0.28	588.13	588.41	PAL
								Totals:	9.91	9.91			
31R	2	2235	588.2	597.8	9.6	3.17	33.0						
								1	1.5	1.5	588.2	589.7	IW, BGAS, IW
								2	1.32	1.32	589.7	591.02	HS
								CC(w/CC)	0.35	0.35	591.02	591.37	PAL, WRSR
								Totals:	3.17	3.17			
32R	3	0030	597.8	607.5	9.7	0.82	8.5						
								1	0.82	0.82	597.8	598.62	PAL
								Totals:	0.82	0.82			
33R	3	0210	607.5	617.1	9.6	2.85	29.7						
								1	1.5	1.5	607.5	609.0	WRC, PLUGS, BACT,
								2	1.1	1.1	609.0	610.1	HS, IW
								CC(w/2)	0.25	0.25	610.1	610.35	PAL
								Totals:	2.85	2.85			
34R	3	355	617.1	626.7	9.6	0.17	1.8						
								CC(w/CC)	0.17	0.17	617.1	617.27	PAL
								Totals:	0.17	0.17			
35R	3	0620	626.7	636.3	9.6	2.13	22.2						
								1	0.52	0.52	626.7	627.22	HS, IW
								2	0.98	0.98	627.22	628.2	
								3	0.41	0.41	628.2	628.61	
								CC(w/3)	0.22	0.22	628.61	628.83	PAL
								Totals:	2.13	2.13			
36R	3	0805	636.3	645.9	9.6	2.17	22.6						
								1	1.5	1.5	636.3	637.8	WRLZ
								2	0.47	0.47	637.8	638.27	HS, IW
								CC(w/CC)	0.2	0.2	638.27	638.47	PAL
								Totals:	2.17	2.17			
37R	3	1015	645.9	655.5	9.6	3.52	36.7						
								1	0.5	0.5	645.9	646.4	IW
								2	1.0	1.0	646.4	647.4	WRC, BACT, HS, BGA
								3	1.5	1.5	647.4	648.9	
								4	0.28	0.28	648.9	649.18	
								CC(w/CC)	0.24	0.24	649.18	649.42	PAL
								Totals:	3.52	3.52			
38R	3	1210	655.5	665.2	9.7	0.91	9.4						
								1	0.67	0.67	655.5	656.17	HS, IW
								CC(w/1)	0.24	0.24	656.17	656.41	PAL
								Totals:	0.91	0.91			
39R	3	1420	665.2	674.8	9.6	4.26	44.4						
								1	1.5	1.5	665.2	666.7	IW, WRSR
								2	1.5	1.5	666.7	668.2	HS, BGAS
								3	0.99	0.99	668.2	669.19	
								CC(w/3)	0.27	0.27	669.19	669.46	
								Totals:	4.26	4.26			
40R	3	1620	674.8	684.4	9.6	1.4	14.6						
								1	1.21	1.21	674.8	676.01	HS, IW, BGAS, BACT
								CC(w/1)	0.19	0.19	676.01	676.2	PAL
								Totals:	1.4	1.4			
41R	3	1810	684.4	694.0	9.6	4.31	44.9						
								1	1.5	1.5	684.4	685.9	IW, BGAS, WRSF

Table T2 (continued).

Core	Date (July 2000)	Time (local)	Core depth (mbsf)		Length (m)		Recovery (%)	Section	Length (m)		Section depth (mbsf)		Catwalk samples
			Top	Bottom	Cored	Recovered			Liner	Curated	Top	Bottom	
42R	3	1955	694.0	703.7	9.7	2.51	25.9	2	1.5	1.5	685.9	687.4	WRY, WRC, WRY, WRS
								3	1.07	1.07	687.4	688.47	HS
								CC(w/3)	0.24	0.24	688.47	688.71	PAL
								Totals:	4.31	4.31			
43R	3	2140	703.7	713.3	9.6	3.47	36.1	1	1.5	1.5	694.0	695.5	IW
								2	0.8	0.8	695.5	696.3	HS
								CC(w/2)	0.21	0.21	696.3	696.51	PAL
								Totals:	2.51	2.51			
44R	3	2340	713.3	722.9	9.6	2.95	30.7	1	1.5	1.5	703.7	705.2	WRTB, WRMT
								2	1.5	1.5	705.2	706.7	HS, BGAS, IW
								3	0.25	0.25	706.7	706.95	
								CC(w/3)	0.22	0.22	706.95	707.17	PAL
Totals:	3.47	3.47											
45R	3	2340	713.3	722.9	9.6	2.95	30.7	1	1.5	1.5	713.3	714.8	IW
								2	1.23	1.23	714.8	716.03	HS, BGAS
								CC(w/2)	0.22	0.22	716.03	716.25	PAL
								Totals:	2.95	2.95			
46R	4	0200	722.9	732.5	9.6	2.99	31.1	1	1.5	1.5	722.9	724.4	
								2	1.26	1.26	724.4	725.66	BACT, HS, IW
								CC(w/2)	0.23	0.23	725.66	725.89	PAL
								Totals:	2.99	2.99			
47R	4	0405	732.5	742.1	9.6	5.18	54.0	1	1.5	1.5	732.5	734.0	IW, WRLZ
								2	1.5	1.5	734.0	735.5	WRSR, HS
								3	1.5	1.5	735.5	737.0	
								4	0.45	0.45	737.0	737.45	
CC(w/4)	0.23	0.23	737.45	737.68	PAL								
Totals:	5.18	5.18											
48R	4	0625	742.1	751.7	9.6	9.06	94.4	1	1.5	1.5	742.1	743.6	
								2	1.5	1.5	743.6	745.1	WRC, PLUGS, WRY, B
								3	1.5	1.5	745.1	746.6	IW, WRSR
								4	1.5	1.5	746.6	748.1	HS
5	1.5	1.5	748.1	749.6									
6	1.37	1.37	749.6	750.97									
CC(w/CC)	0.19	0.19	750.97	751.16	PAL								
Totals:	9.06	9.06											
49R	4	0830	751.7	761.3	9.6	9.45	98.4	1	1.5	1.5	751.7	753.2	
								2	1.5	1.5	753.2	754.7	
								3	1.5	1.5	754.7	756.2	
								4	1.5	1.5	756.2	757.7	IW
5	1.5	1.5	757.7	759.2	HS, BGAS								
6	1.5	1.5	759.2	760.7									
7	0.3	0.3	760.7	761.0									
CC(w/7)	0.15	0.15	761.0	761.15	PAL								
Totals:	9.45	9.45											
50R	4	1050	761.3	771.0	9.7	7.31	75.4	1	1.5	1.5	761.3	762.8	
								2	1.5	1.5	762.8	764.3	
								3	1.5	1.5	764.3	765.8	HS, BGAS, IW
								4	1.5	1.5	765.8	767.3	WRSR
5	1.13	1.13	767.3	768.43									
CC(w/5)	0.18	0.18	768.43	768.61	PAL								
Totals:	7.31	7.31											
51R	4	1240	771.0	780.6	9.6	3.65	38.0	1	1.5	1.5	771.0	772.5	HS, BGAS
								2	1.48	1.48	772.5	773.98	BACT
								3	0.67	0.67	773.98	774.65	PAL, IW
								Totals:	3.65	3.65			
51R	4	1420	780.6	790.3	9.7	3.86	39.8	1	1.5	1.5	780.6	782.1	IW
								2	1.5	1.5	782.1	783.6	HS, BGAS, IW, WRTB
								3	0.62	0.62	783.6	784.22	

Table T2 (continued).

Core	Date (July 2000)	Time (local)	Core depth (mbsf)		Length (m)		Recovery (%)	Section	Length (m)		Section depth (mbsf)		Catwalk samples
			Top	Bottom	Cored	Recovered			Liner	Curated	Top	Bottom	
52R	4	1620	790.3	799.9	9.6	4.91	51.1	CC(w/3)	0.24	0.24	784.22	784.46	PAL
								Totals:	3.86	3.86			
								1	1.5	1.5	790.3	791.8	HS, IW, BACT, PLUG
								2	1.5	1.5	791.8	793.3	IW, WRSE, CRG
								3	1.5	1.5	793.3	794.8	
53R	4	1840	799.9	809.5	9.6	8.4	87.5	4	0.41	0.41	794.8	795.21	PAL
								Totals:	4.91	4.91			
								1	1.5	1.5	799.9	801.4	
								2	1.5	1.5	801.4	802.9	WRMT
								3	1.5	1.5	802.9	804.4	BGAS, IW
54R	4	2040	809.5	819.2	9.7	7.01	72.3	4	1.5	1.5	804.4	805.9	
								5	1.5	1.5	805.9	807.4	HS
								6	0.63	0.63	807.4	808.03	
								CC(w/6)	0.27	0.27	808.03	808.3	PAL
								Totals:	8.4	8.4			
55R	4	2240	819.2	828.8	9.6	3.76	39.2	1	1.5	1.5	809.5	811.0	
								2	1.5	1.5	811.0	812.5	BACT, IW BGAS
								3	1.5	1.5	812.5	814.0	
								4	1.5	1.5	814.0	815.5	HS
								5	0.69	0.69	815.5	816.19	
56R	5	0225	828.8	833.9	5.1	3.28	64.3	CC(w/5)	0.32	0.32	816.19	816.51	PAL
								Totals:	7.01	7.01			
								1	1.5	1.5	819.2	820.7	BGAS, IW
								2	1.5	1.5	820.7	822.2	HS
								3	0.41	0.41	822.2	822.61	
56R	5	0225	828.8	833.9	5.1	3.28	64.3	CC(w/3)	0.35	0.35	822.61	822.96	
								Totals:	3.76	3.76			
								1	1.5	1.5	828.8	830.3	IW
								2	0.78	0.78	830.3	831.08	HS, BGAS
								3	1.0	1.05	831.08	832.13	
		Totals:		533.7	282.74	53							

Notes: Catwalk samples: IW = interstitial water, HS = headspace, PAL = paleontology, VAC = vacutainer. All other abbreviations are sample codes for postcruise research (see the "Sample Codes" database query). NA = not applicable. CC = core catcher (number in parenthesis indicated which section the core catcher is stored with). This table is also available in [ASCII](#) format.

Table T3. Summary of stratigraphic relations at Hole 1177A and correlation with equivalent units at Sites 808, 1173, and 1174.

Unit	Facies name	Interval (cm)		Depth (mbsf)		Thickness (m)	Stratigraphic age	Lithologic description	Processes of formation	Stratigraphic correlation		
		Top	Bottom	Top	Bottom					Site 808	Site 1173	Site 1174
		190-1177A- ***Drilled without coring from 0 to 300.20 mbsf***	190-1177A- ***Drilled without coring from 0 to 300.20 mbsf***									
I	Upper Shikoku Basin facies	1R-1, 0	11R-5, 6	300.20	401.76	Minimum 101.56	Pliocene	Hemipelagic mud, abundant volcanic ash	Hemipelagic settling and frequent volcanic ash falls derived from Honshu/Kyushu	Unit IVA	Unit II	Unit III
II	Lower Shikoku hemipelagic facies	11R-5, 6	16R-4, 90	401.76	449.30	47.54	late Miocene to Pliocene (?)	Hemipelagic mudstone, trace siliceous claystone	Hemipelagic settling	Unit IVB	Unit III	Unit IV
III	Lower Shikoku turbidite facies	16R-4, 90	47R-5, 25	449.30	748.35	299.05	early to late Miocene	Hemipelagic mudstone, abundant sand to silt turbidites, mud-clast conglomerate, rare calcareous and siliceous claystone	Hemipelagic settling, frequent terrigenous turbidity currents in abyssal fan system	NA	NA	NA
IV	Volcaniclastic-rich facies	47R-5, 25	56R-3, 0	748.35	831.08	82.73	early Miocene	Hemipelagic mudstone, volcanic ash, volcanic and siliciclastic silt to sand	Volcanic ash falls and turbidity currents from unknown source, hemipelagic settling	~13.6 Ma Unit V	~14.1 Ma Unit IV	~13.4 Ma Unit V
V	Basaltic basement	56R-3, 0	56R-3, 105	831.08	832.13	1.05	Probable early Miocene	Basalt, pillow basalt	Lavas flows at Shikoku Basin spreading ridge	~15 Ma basalt	~15 Ma basalt	Not cored

Note: NA = not applicable.

Table T4. Peak intensities and peak areas from X-ray diffraction analysis of bulk-powder sediment samples, Hole 1177A. (See table note. Continued on next two pages.)

Core, section, interval (cm)	Depth (mbsf)	X-ray diffraction peak intensity (cps)								X-ray diffraction peak area (total counts)							
		Smectite + chlorite	Illite	Chlorite + kaolinite	(101) Quartz	Plagioclase	Calcite	Quartz (100)	Cristobalite (101)	Smectite + chlorite	Illite	Chlorite + kaolinite	(101) Quartz	Plagioclase	Calcite	Quartz (100)	Cristobalite (101)
190-1177A-																	
1R-2, 84-85	302.54	54	99	92	1,642	274	167	289	103	2,872	2,305	1,743	21,396	8,909	2,647	4,123	1,581
1R-4, 130-131	306.00	67	132	129	1,765	344	0	300	97	2,767	2,977	2,323	23,368	9,575	0	4,220	1,536
2R-2, 106-107	311.76	61	115	113	1,805	314	0	291	107	2,704	2,412	2,106	23,821	8,980	0	4,269	1,582
3R-2, 120-121	321.60	55	108	101	1,595	304	253	255	107	2,821	2,674	2,153	21,506	8,849	4,519	3,468	1,404
3R-4, 85-86	324.25	60	101	102	1,629	297	34	277	109	2,721	2,609	1,975	21,570	9,449	429	4,071	1,561
4R-3, 105-106	332.55	60	110	111	1,708	314	0	283	89	3,121	2,170	2,038	22,576	8,512	0	3,678	1,312
4R-5, 21-22	334.71	60	99	104	1,518	419	330	241	84	2,538	2,059	2,122	20,102	8,911	5,187	3,362	1,312
5R-1, 35-36	338.45	28	47	40	684	279	111	135	154	1,394	848	917	9,179	7,638	2,081	2,078	2,316
5R-3, 95-96	340.55	61	98	93	1,871	312	0	325	120	2,751	2,490	1,987	25,001	8,916	0	4,560	1,655
5R-4, 65-66	341.75	41	84	99	1,490	290	0	264	100	2,274	1,842	1,882	20,204	8,690	0	3,727	1,519
6R-1, 67-68	348.37	62	89	97	1,489	367	204	301	110	3,068	2,081	1,934	20,028	9,699	2,924	4,146	1,611
7R-4, 123-124	363.03	54	104	99	1,645	298	119	303	89	2,486	2,075	2,025	22,140	8,423	2,190	4,175	1,325
7R-6, 62-63	365.42	52	87	102	1,594	285	327	279	88	2,603	1,709	2,164	21,665	8,526	5,603	3,890	1,373
8R-2, 54-56	369.04	54	97	86	1,710	329	146	291	96	2,755	2,109	1,921	22,532	9,206	2,198	4,552	1,421
9R-1, 48-49	377.08	51	82	75	1,414	349	33	250	86	2,314	1,471	1,575	18,853	7,916	345	3,751	1,375
9R-3, 108-109	380.68	49	89	81	1,682	300	30	289	133	2,555	1,841	1,948	22,287	9,201	481	4,156	2,039
10R-2, 149-150	389.09	58	73	83	1,672	299	22	281	109	2,973	1,588	1,813	22,075	9,169	266	4,413	1,608
11R-1, 133-134	397.03	71	76	69	1,487	292	0	273	95	4,117	1,570	1,590	19,962	8,917	0	4,243	1,404
11R-6, 35-36	403.55	52	118	99	1,623	278	32	310	94	3,024	2,829	2,028	21,677	8,506	543	4,561	1,242
12R-1, 56-57	405.86	51	76	64	1,597	247	26	262	80	4,277	1,697	1,617	20,861	8,013	385	4,180	1,244
13R-4, 114-115	420.54	69	72	63	1,292	468	0	237	73	7,043	2,155	1,565	20,122	10,513	0	4,631	1,050
13R-7, 46-47	424.36	54	82	80	1,731	300	0	300	82	3,965	2,714	1,716	22,669	9,457	0	4,362	986
13R-CC, 25-26	424.75	62	86	77	1,511	296	32	255	70	5,036	2,240	1,820	20,559	8,683	407	4,187	927
14R-4, 129-130	430.29	58	77	78	1,481	302	169	284	69	4,646	2,707	1,816	20,324	8,493	2,880	4,410	828
15R-3, 112-113	438.32	55	116	89	1,764	298	0	279	63	4,543	3,314	1,881	22,716	8,986	0	4,066	700
15R-CC, 10-11	443.90	61	90	88	1,829	282	172	309	72	3,758	2,539	1,978	24,220	8,163	2,630	4,810	895
16R-1, 90-91	444.80	49	77	71	1,561	239	323	264	66	4,647	2,010	1,477	20,766	6,822	5,104	4,273	890
16R-3, 117-118	448.07	55	88	75	1,688	266	135	317	67	4,139	2,475	1,918	22,802	7,888	1,897	5,025	916
16R-4, 144-145	449.84	35	76	57	1,699	319	28	314	61	2,810	4,063	1,163	22,753	8,523	415	4,474	685
16R-4, 149-150	449.89	32	68	70	4,378	713	0	621	126	1,303	2,733	1,558	51,663	15,992	0	7,367	1,441
16R-4, 66-67	449.06	51	77	66	1,569	330	0	284	68	3,214	3,085	1,774	21,325	9,526	0	4,485	906
17R-1, 114-115	454.64	50	69	74	1,815	319	0	317	73	3,157	2,792	1,685	24,421	8,855	0	4,779	1,000
17R-2, 24-25	455.24	57	80	78	1,874	313	0	335	72	2,890	3,088	1,724	25,077	8,392	0	4,702	865
17R-2, 98-99	455.98	54	74	76	2,051	339	0	356	87	3,641	3,073	1,866	27,236	9,038	0	5,306	1,180
19R-4, 118-119	478.48	52	68	49	1,303	217	278	260	131	3,656	1,826	1,127	17,238	5,805	4,157	3,808	1,419
19R-6, 42-43	480.72	50	76	70	1,774	308	0	309	94	3,858	3,003	1,448	23,742	9,274	0	4,545	1,160
19R-7, 36-38	482.16	54	76	77	2,132	315	0	382	89	3,192	3,207	1,968	27,831	8,797	0	5,681	1,043
20R-1, 106-107	483.46	41	87	82	2,366	401	52	444	111	2,681	3,192	1,912	31,658	11,115	789	6,092	1,326
20R-2, 62-63	484.52	41	85	75	2,374	390	0	430	117	2,356	2,980	1,498	30,941	10,477	0	5,833	1,206
21R-1, 37-38	492.37	42	110	94	3,261	608	36	534	130	2,349	3,227	1,965	41,996	14,457	515	6,810	1,410
22R-CC, 8-9	502.52	52	122	105	4,085	932	36	611	139	1,486	3,657	1,735	49,939	20,068	623	7,510	1,880
23R-2, 42-43	512.95	44	75	74	1,661	296	0	337	77	2,354	3,201	1,816	22,922	8,888	0	5,422	971
24R-3, 147-148	525.17	112	27	0	270	1,194	0	133	50	9,952	743	0	5,370	21,332	0	3,876	1,290
24R-4, 1-2	525.21	42	60	59	1,386	231	0	288	67	3,581	1,707	1,497	18,737	7,339	0	4,312	839
24R-4, 54-55	525.74	48	87	68	1,685	303	0	301	68	4,156	3,595	1,754	22,633	8,619	0	4,691	825
24R-5, 129-130	527.69	54	64	55	1,654	263	0	268	77	3,705	2,816	1,590	22,372	7,299	0	4,820	930

Table T4 (continued).

Core, section, interval (cm)	Depth (mbsf)	X-ray diffraction peak intensity (cps)								X-ray diffraction peak area (total counts)							
		Smectite + chlorite	Illite	Chlorite + kaolinite	(101) Quartz	Plagioclase	Calcite	Quartz (100)	Cristobalite (101)	Smectite + chlorite	Illite	Chlorite + kaolinite	(101) Quartz	Plagioclase	Calcite	Quartz (100)	Cristobalite (101)
24R-6, 129-130	529.19	65	73	56	1,417	311	34	253	67	6,909	1,897	1,245	20,049	8,994	350	4,583	905
25R-2, 130-131	533.20	49	84	61	1,730	270	0	293	61	4,055	2,720	1,510	24,034	7,775	0	5,011	869
25R-6, 108-109	538.98	49	79	63	1,694	262	0	292	80	3,841	2,575	1,485	22,553	8,041	0	4,793	1,050
25R-7, 16-17	539.56	18	23	26	561	89	1308	98	26	1,625	936	513	7,055	2,510	27,145	1,501	311
26R-1, 79-80	540.89	29	58	57	5,013	868	0	896	143	1,736	1,384	1,313	60,949	20,894	0	10,832	1,755
27R-1, 96-97	550.66	46	92	104	3,572	706	0	596	159	1,887	2,289	2,074	44,148	16,894	0	7,770	1,877
29R-1, 34-35	569.24	40	67	54	1,506	235	31	257	66	3,139	3,738	1,768	20,238	7,727	493	4,093	794
29R-1, 87-88	569.77	37	63	49	1,338	206	0	245	58	2,391	2,139	1,352	18,330	6,136	0	3,656	768
29R-2, 125-126	571.65	57	84	65	1,571	250	0	291	62	4,240	2,757	1,732	21,459	8,081	0	4,431	856
30R-2, 39-40	580.39	82	76	50	1,584	277	0	286	79	8,110	2,585	1,290	21,040	9,250	0	4,671	855
30R-4, 119-120	584.19	63	71	49	1,467	420	0	258	67	6,959	2,235	1,191	20,856	9,441	0	4,446	900
30R-7, 46-47	587.96	76	65	51	1,409	287	0	307	58	9,309	1,440	1,153	19,306	7,686	0	4,872	742
31R-1, 21-22	588.41	59	59	60	1,528	225	29	261	62	5,233	2,271	1,436	21,103	7,331	973	4,482	864
31R-2, 59-60	590.29	53	53	36	842	171	25	179	37	6,425	1,789	960	17,773	6,640	380	4,852	780
31R-CC, 11-12	591.13	56	66	48	1,332	188	0	266	47	5,634	2,716	1,155	19,276	7,137	0	4,726	854
32R-1, 6-7	597.86	0	0	0	293	26	729	45	15	0	0	0	3,357	712	23,714	587	186
32R-1, 60-61	598.40	58	66	79	1,860	230	0	322	54	5,072	2,887	1,856	24,991	7,470	0	5,374	750
33R-1, 15-16	607.65	56	69	77	1,618	199	106	288	45	4,004	2,201	1,919	22,453	6,809	1,510	4,556	546
33R-1, 87-88	608.37	40	72	69	2,758	465	36	442	102	3,085	2,882	1,635	36,115	11,641	590	6,338	1,180
33R-2, 71-72	609.71	60	90	82	1,610	209	25	335	56	4,001	3,153	1,834	21,534	6,853	329	4,786	744
34R-CC, 14-15	617.24	43	67	70	2,136	297	36	399	110	3,790	2,348	2,007	30,325	9,209	640	6,151	1,284
35R-2, 70-71	627.92	52	70	54	1,411	209	0	248	45	4,243	3,501	1,410	19,226	7,285	0	4,079	559
35R-3, 8-9	628.28	46	49	65	1,693	230	22	323	74	3,802	2,083	1,549	23,556	7,660	344	5,338	856
36R-1, 116-117	637.46	56	74	83	1,743	241	56	305	50	5,332	3,488	2,177	26,708	7,808	956	5,604	663
36R-1, 24-25	636.54	66	96	85	2,227	338	55	366	80	3,941	3,497	2,020	30,172	9,822	841	5,570	987
37R-2, 80-81	647.20	55	96	98	1,625	217	67	298	54	4,103	3,740	2,343	22,855	7,105	923	4,230	545
37R-3, 32-33	647.72	53	116	100	2,928	579	133	511	164	4,348	3,792	2,205	40,280	16,304	2,941	7,317	1,953
38R-CC, 20-21	656.37	56	97	99	2,052	320	43	388	63	4,007	2,754	1,968	29,367	9,551	610	5,827	832
39R-1, 95-96	666.15	48	68	43	1,170	233	0	219	80	5,067	3,801	1,249	15,742	8,473	0	4,166	1,547
39R-2, 142-144	668.12	25	26	0	352	49	971	54	19	1,390	958	0	4,109	1,361	34,407	876	295
40R-1, 115-116	675.95	68	107	62	2,222	244	27	316	65	5,694	4,129	1,426	28,547	9,863	480	4,947	856
41R-1, 131-132	685.71	52	134	62	3,085	492	23	602	138	3,327	3,258	1,199	38,350	15,915	224	7,704	2,002
41R-2, 99-100	686.89	73	91	51	1,600	663	0	265	64	7,321	3,056	1,188	22,211	14,255	0	4,036	883
42R-1, 119-120	695.19	57	119	53	1,916	670	0	353	94	4,712	2,757	995	26,411	14,587	0	5,072	1,410
43R-1, 5-6	703.75	65	84	52	1,544	250	28	283	65	8,462	2,197	1,233	20,885	8,926	680	4,404	924
43R-2, 118-119	706.38	56	75	47	1,313	220	0	263	66	6,174	2,613	1,107	18,538	8,145	0	4,132	863
44R-1, 39-40	713.69	53	76	50	1,685	247	0	325	66	4,960	2,717	1,205	22,524	8,937	0	4,877	971
44R-2, 72-73	715.52	37	69	37	968	151	0	187	45	4,964	1,868	829	13,753	6,035	0	3,202	656
45R-1, 127-128	724.17	48	60	33	879	132	20	182	41	5,875	1,424	751	12,842	4,909	153	3,283	780
45R-2, 86-87	725.26	51	64	36	1,072	163	0	200	45	5,262	3,765	784	15,321	6,156	0	3,293	708
46R-1, 119-120	733.69	54	73	44	1,292	240	19	243	58	6,219	2,306	990	18,560	8,228	243	4,232	812
46R-1, 21-22	732.71	63	94	59	1,594	279	27	301	54	6,596	2,781	1,223	21,105	9,102	310	4,294	770
46R-2, 125-126	735.25	59	82	59	2,499	527	32	659	88	3,498	2,450	1,307	33,395	21,801	398	8,076	1,152
46R-3, 139-140	736.89	42	36	19	660	118	0	122	47	3,908	673	458	9,012	4,444	0	2,138	818
46R-3, 9-10	735.59	69	87	52	1,558	314	26	281	80	6,381	2,966	1,140	22,086	10,584	286	4,300	1,016
46R-3, 9-10	735.59	69	87	52	1,558	314	26	281	80	6,381	2,966	1,141	22,167	10,669	286	4,378	1,059
47R-1, 38-39	742.48	59	87	63	1,267	190	0	246	47	7,055	3,235	1,526	19,117	7,864	0	4,468	627
47R-3, 101-102	746.11	50	89	68	1,269	192	27	238	40	5,061	3,204	1,654	18,510	7,696	499	4,021	462

Table T4 (continued).

Core, section, interval (cm)	Depth (mbsf)	X-ray diffraction peak intensity (cps)								X-ray diffraction peak area (total counts)							
		Smectite + chlorite	Illite	Chlorite + kaolinite	(101) Quartz	Plagioclase	Calcite	Quartz (100)	Cristobalite (101)	Smectite + chlorite	Illite	Chlorite + kaolinite	(101) Quartz	Plagioclase	Calcite	Quartz (100)	Cristobalite (101)
47R-5, 99-100	749.09	64	93	61	1,469	230	0	273	50	6,899	2,691	1,546	20,453	7,852	0	4,734	686
48R-4, 118-119	757.38	58	98	73	1,688	286	23	336	71	5,352	2,418	1,598	23,064	9,804	247	5,291	873
48R-6, 115-116	760.35	61	74	58	1,350	227	0	259	112	7,085	2,236	1,594	18,950	8,237	0	4,365	1,141
48R-7, 7-8	760.77	44	89	41	1,179	212	0	242	48	6,032	3,296	931	16,887	8,374	0	4,022	663
49R-2, 147-148	764.27	51	84	33	1,373	207	0	231	70	7,470	2,687	862	19,137	8,550	0	3,902	954
49R-2, 65-66	763.45	57	105	54	1,965	348	29	365	98	4,787	3,817	1,325	25,790	11,123	366	5,192	1,325
49R-3, 117-118	765.47	59	70	44	1,293	354	32	267	224	7,307	2,111	873	19,472	11,146	647	4,363	2,408
49R-4, 21-22	766.01	73	63	21	1,008	245	0	198	65	9,463	1,892	302	14,165	9,299	0	3,571	1,181
49R-5, 74-75	768.04	81	42	17	719	293	44	156	117	10,871	1,393	258	10,230	8,476	792	3,601	1,749
50R-3, 36-37	774.34	55	83	51	1,519	746	0	276	91	3,742	1,452	1,129	20,851	14,457	0	3,922	1,460
51R-2, 27-28	782.37	30	111	17	344	456	0	73	48	2,224	1,436	285	5,513	6,517	0	1,393	916
52R-2, 18-19	791.98	87	39	26	815	261	37	170	93	9,294	1,202	482	11,464	8,898	750	3,297	1,481
52R-2, 56-57	792.36	51	21	14	399	177	0	89	107	5,569	462	298	5,799	6,171	0	1,782	1,991
52R-3, 28-29	793.58	40	68	22	1,295	218	0	231	73	3,659	3,374	266	19,637	7,812	0	3,983	1,646
52R-3, 49-50	793.79	50	91	65	1,985	289	0	374	107	3,263	3,727	1,198	26,796	8,688	0	5,573	1,448
53R-2, 59-60	801.99	45	109	40	1,708	265	0	330	59	3,305	5,217	776	24,232	8,798	0	5,102	756
53R-3, 118-119	804.08	48	101	67	1,889	291	0	333	75	4,193	4,787	1,291	26,897	9,382	0	5,117	814
53R-6, 61-62	808.01	38	77	49	1,694	267	0	308	79	3,672	4,175	777	24,507	9,023	0	5,347	1,169
54R-1, 124-125	810.74	64	61	36	2,810	501	0	452	81	5,924	1,518	930	33,798	14,669	0	6,653	1,256
54R-2, 50-51	811.50	51	88	27	1,186	225	31	226	70	6,922	2,713	562	17,224	8,288	593	4,147	1,069
54R-3, 69-70	813.19	55	75	41	1,568	233	0	290	69	5,667	3,367	826	22,258	8,217	0	4,673	1,135
54R-5, 58-59	816.08	44	72	43	2,622	566	0	475	136	4,325	1,995	821	34,282	16,190	0	6,490	2,312
55R-1, 118-119	820.38	57	85	42	1,385	270	107	234	51	6,148	3,695	1,075	20,585	8,264	1,790	3,730	800
55R-3, 24-25	822.44	50	97	40	1,403	240	100	267	65	3,615	4,833	925	20,674	8,088	1,875	4,193	1,493
56R-1, 122-123	830.02	63	49	20	745	176	713	135	64	9,514	911	349	10,071	6,659	9,403	2,461	956
56R-2, 47-48	830.77	47	97	72	2,023	333	0	344	80	4,219	4,465	1,366	28,391	10,106	0	5,196	844
56R-2, 73-74	831.03	85	55	22	653	187	0	165	64	12,122	1,667	511	9,453	8,217	0	3,507	703

Note: This table is also available in [ASCII](#) format.

Table T5. Results of X-ray diffraction analysis of bulk-powder volcanic ash samples, Hole 1177A.

Core, section, interval (cm)	Depth (mbsf)	X-ray diffraction peak intensity (cps)												X-ray diffraction peak area (total counts)											
		Smectite	Mica	Chlorite	Clinoptilolite	Hornblende	Cristobalite	Quartz	Plagioclase	Calcite	Pyroxene	Halite	Pyrite	Smectite	Mica	Chlorite	Clinoptilolite	Hornblende	Cristobalite	Quartz	Plagioclase	Calcite	Pyroxene	Halite	Pyrite
190-1177A-																									
50R-1, 38-39	771.38	36	0	0	0	0	91	113	221	12	36	50	0	2354	0	0	0	0	1443	1627	4485	143	629	797	0
51R-1, 18-19	780.78	29	76	0	0	0	25	373	77	20	0	88	0	1909	1114	0	0	0	286	4397	2123	168	0	1113	0

Table T6. Normalized relative mineral abundances based on X-ray diffraction analysis of random bulk-sediment powders, Hole 1177A. (Continued on next page.)

Unit	Core, section, interval (cm)	Depth (mbsf)	Normalized abundance (wt%)				Peak area ratio: (101) cristobalite/ (100) quartz
			Total clay minerals	Quartz	Plagioclase	Calcite	
I	190-1177A-						
	1R-2, 84-85	302.54	50	33	13	4	0.38
	1R-4, 130-131	306.00	54	32	14	0	0.36
	2R-2, 106-107	311.76	51	36	13	0	0.37
	3R-2, 120-121	321.60	50	30	12	9	0.40
	3R-4, 85-86	324.25	53	33	14	0	0.38
	4R-3, 105-106	332.55	51	36	13	0	0.36
	4R-5, 21-22	334.71	44	30	14	12	0.39
	5R-1, 35-36	338.45	40	29	23	8	1.11
	5R-3, 95-96	340.55	51	36	13	0	0.36
	5R-4, 65-66	341.75	48	36	16	0	0.41
	6R-1, 67-68	348.37	49	32	14	5	0.39
	7R-4, 123-124	363.03	48	35	14	3	0.32
	7R-6, 62-63	365.42	41	33	13	13	0.35
	8R-2, 54-56	369.04	48	35	14	3	0.31
	9R-1, 48-49	377.08	47	38	15	0	0.37
	9R-3, 108-109	380.68	47	38	15	0	0.49
	10R-2, 149-150	389.09	47	39	15	0	0.36
	11R-1, 133-134	397.03	51	37	13	0	0.33
	Mean Unit I:		48	34	14	3	0.41
II	11R-6, 35-36	403.55	56	32	12	0	0.27
	12R-1, 56-57	405.86	52	37	11	0	0.30
	13R-4, 114-115	420.54	57	33	10	0	0.23
	13R-7, 46-47	424.36	55	33	12	0	0.23
	13R-CC, 25-26	424.75	56	34	10	0	0.22
	14R-4, 129-130	430.29	56	31	10	3	0.19
	15R-3, 112-113	438.32	59	31	10	0	0.17
	15R-CC, 10-11	443.90	52	34	10	3	0.19
	16R-1, 90-91	444.80	51	33	8	9	0.21
	16R-3, 117-118	448.07	55	34	10	1	0.18
	Mean Unit II:		55	33	10	2	0.22
III	16R-4, 144-145	449.84	61	28	11	0	0.15
	16R-4, 149-150	449.89	34	48	18	0	0.20
	16R-4, 66-67	449.06	57	30	13	0	0.20
	17R-1, 114-115	454.64	54	34	12	0	0.21
	17R-2, 24-25	455.24	55	34	11	0	0.18
	17R-2, 98-99	455.98	54	35	11	0	0.22
	19R-4, 118-119	478.48	51	32	8	9	0.37
	19R-6, 42-43	480.72	56	33	11	0	0.26
	19R-7, 36-38	482.16	54	35	11	0	0.18
	20R-1, 106-107	483.46	50	37	14	0	0.22
	20R-2, 62-63	484.52	49	38	14	0	0.21
	21R-1, 37-38	492.37	43	41	16	0	0.21
	22R-CC, 8-9	502.52	38	41	20	0	0.25
	23R-2, 42-43	512.95	56	31	13	0	0.18
	24R-3, 147-148	525.17	55	26	19	0	0.33
	24R-4, 1-2	525.21	53	36	11	0	0.19
	24R-4, 54-55	525.74	60	30	10	0	0.18
	24R-5, 129-130	527.69	57	34	9	0	0.19
	24R-6, 129-130	529.19	57	35	9	0	0.20
	25R-2, 130-131	533.20	56	35	9	0	0.17
	25R-6, 108-109	538.98	55	34	10	0	0.22
	25R-7, 16-17	539.56	22	12	4	61	0.21
	26R-1, 79-80	540.89	25	54	21	0	0.16
	27R-1, 96-97	550.66	35	45	20	0	0.24
	29R-1, 34-35	569.24	62	28	10	0	0.19
	29R-1, 87-88	569.77	55	34	11	0	0.21
	29R-2, 125-126	571.65	58	33	10	0	0.19
	30R-2, 39-40	580.39	60	33	7	0	0.18
	30R-4, 119-120	584.19	57	34	9	0	0.20
	30R-7, 46-47	587.96	58	36	6	0	0.15
	31R-1, 21-22	588.41	57	35	8	0	0.19
	31R-2, 59-60	590.29	59	35	7	0	0.16
	31R-CC, 11-12	591.13	61	32	7	0	0.18

Table T6 (continued).

Unit	Core, section, interval (cm)	Depth (mbsf)	Normalized abundance (wt%)				Peak area ratio: (101) cristobalite/ (100) quartz
			Total clay minerals	Quartz	Plagioclase	Calcite	
	32R-1, 6-7	597.86	0	9	4	88	0.32
	32R-1, 60-61	598.40	58	35	8	0	0.14
	33R-1, 15-16	607.65	54	36	9	0	0.12
	33R-1, 87-88	608.37	47	40	13	0	0.19
	33R-2, 71-72	609.71	60	32	8	0	0.16
	34R-CC, 14-15	617.24	49	40	11	0	0.21
	35R-2, 70-71	627.92	63	28	8	0	0.14
	35R-3, 8-9	628.28	52	38	10	0	0.16
	36R-1, 116-117	637.46	59	33	7	0	0.12
	36R-1, 24-25	636.54	55	35	11	0	0.18
	37R-2, 80-81	647.20	62	30	8	0	0.13
	37R-3, 32-33	647.72	48	36	14	1	0.27
	38R-CC, 20-21	656.37	52	37	11	0	0.14
	39R-1, 95-96	666.15	66	25	9	0	0.37
	39R-2, 142-144	668.12	14	9	3	74	0.34
	40R-1, 115-116	675.95	60	32	8	0	0.17
	41R-1, 131-132	685.71	46	38	16	0	0.26
	41R-2, 99-100	686.89	57	30	12	0	0.22
	42R-1, 119-120	695.19	51	34	16	0	0.28
	43R-1, 5-6	703.75	59	34	7	0	0.21
	43R-2, 118-119	706.38	60	32	8	0	0.21
	44R-1, 39-40	713.69	57	33	10	0	0.20
	44R-2, 72-73	715.52	60	32	8	0	0.20
	45R-1, 127-128	724.17	61	34	5	0	0.24
	45R-2, 86-87	725.26	68	26	6	0	0.22
	46R-1, 119-120	733.69	59	33	8	0	0.19
	46R-1, 21-22	732.71	59	32	8	0	0.18
	46R-2, 125-126	735.25	41	36	23	0	0.14
	46R-3, 139-140	736.89	56	36	8	0	0.38
	46R-3, 9-10	735.59	58	32	10	0	0.24
	46R-3, 9-10	735.59	58	32	10	0	0.24
	47R-1, 38-39	742.48	63	30	7	0	0.14
	47R-3, 101-102	746.11	63	29	8	0	0.11
	Mean Unit III		53	33	10	4	0.21
IV	47R-5, 99-100	749.09	61	33	7	0	0.14
	48R-4, 118-119	757.38	55	34	11	0	0.16
	48R-6, 115-116	760.35	59	33	8	0	0.26
	48R-7, 7-8	760.77	64	28	8	0	0.16
	49R-2, 147-148	764.27	61	32	7	0	0.24
	49R-2, 65-66	763.45	58	31	11	0	0.26
	49R-3, 117-118	765.47	57	33	10	0	0.55
	49R-4, 21-22	766.01	61	32	7	0	0.33
	49R-5, 74-75	768.04	63	31	6	0	0.49
	50R-3, 36-37	774.34	44	35	21	0	0.37
	51R-2, 27-28	782.37	61	22	17	0	0.66
	52R-2, 18-19	791.98	60	32	7	0	0.45
	52R-2, 56-57	792.36	59	32	9	0	1.12
	52R-3, 28-29	793.58	61	29	10	0	0.41
	52R-3, 49-50	793.79	57	32	10	0	0.26
	53R-2, 59-60	801.99	65	26	9	0	0.15
	53R-3, 118-119	804.08	62	29	9	0	0.16
	53R-6, 61-62	808.01	61	29	10	0	0.22
	54R-1, 124-125	810.74	44	42	14	0	0.19
	54R-2, 50-51	811.50	62	31	7	0	0.26
	54R-3, 69-70	813.19	61	31	8	0	0.24
	54R-5, 58-59	816.08	43	40	17	0	0.36
	55R-1, 118-119	820.38	63	29	7	0	0.21
	55R-3, 24-25	822.44	66	25	9	0	0.36
	56R-1, 122-123	830.02	53	29	5	14	0.39
	56R-2, 47-48	830.77	60	30	10	0	0.16
	56R-2, 73-74	831.03	65	30	5	0	0.20
	Mean Unit IV:		59	31	10	1	0.32

Table T7. Structural data, Hole 1177A. (See table note. Continued on next page.)

Core, section, interval (cm)	Depth (mbsf)	Cr az. (°)	Cr dip (°)	Pm az.	Pm plunge	Half	Identifier	Notes
190-1177A-								
1R	300.21	0	0			W	Bed	Locally, bed dips 8°
1R	300.21					W	Fracture	Subvertical fractures, drilling induced?
2R	309.21	0	0			W	Bed	
2R-1, 140-144	310.60		80				Fracture	5-mm displacement (rotated biscuit)
3R	318.91	0	0				Bed	
3R-4, 22-31	323.62	318	63				Normal fault	(22-29) offset ~1 cm
4R	328.51	0	0				Bed	Highly biscuitied
5R	338.11	0	0				Bed	Highly biscuitied
6R	347.71	0	0				Bed	
7R	357.31	0	0				Bed	
8R	367.01	0	0				Bed	
9R	376.61	0	0				Bed	
10R	386.11	0	0				Bed	
11R	395.71	0	0				Bed	
11R-2,3,4, 80-84	398.00						Breccia	Unusual texture, friable, polished fragments
11R-5, 10-14	401.80						Breccia	Early dewatering structure
12R-4	409.19		85				Fracture	Subvertical, cannot be reoriented
13R-1	414.91		12				Bed	
13R-3, 19-24	418.09		~65				Fracture	Drilling induced?
13R-6, 6-7	422.46						Microbreccia	Soft sediment deformation.
14R	424.51	0	0				Zoophycos	
14R-5, 125-135	431.75						Faults	Small offset
16R-2, 48-50	445.88						Fold	Tight fold in lamination
16R-5, 36-39	450.26						Web structure	Probably drilling induced
17R	453.51	0	0				Fracture?	
18R	463.11	0	0				Bed	Highly biscuitied
19R-2, 75-76	475.05	0	10				Bed	
19R-2, 14-18	474.44	110	71				Fracture	Drilling induced?
19R-4, 72-77	478.02	352	41				Fault	2-mm offset
19R-6, 98-101	481.28	138	65				Fault	Parallel set
21R	492.01	0	0					
22R-CC	502.45	0	0				Bed	Turbidites
22R-CC	502.45						Web structure	Normal sense
23R	511.11	0	0				Bed	Horizontal turbidites and hemipelagites
24R	520.71	0	0				Bed	Horizontal turbidites and hemipelagites
25R	530.41	0	0					
25R-5, 60-30	537.00						Stylolite	Possible?
26R	540.11	0	0				Bed	Horizontal turbidites
27R	549.71	0	0				Bed	Horizontal turbidites
28R-CC	559.41	0	0				Bed	Only sands in CC
29R	568.91	0	0				Bed	
30R	578.51	0	0				Bed	
30R-1, 95-105	579.45	180	53				Fracture	Bluish green alteration along the fracture
30R-1, 106-110	579.56	310	80	50	80		Fault	Normal, 2.5-cm offset
30R-2, 3-9	580.03	236	62				Fault	(0-60) black surface with slickenlines
30R-2, 20-20	580.20	58	53				Fault	(0-60)
30R-2, 38-38	580.38	214	58				Fault	(0-60)
30R-2, 50-50	580.50	5	45				Fault	(0-60) all brecciated zone
31R-1,2	588.21							Highly biscuitied
32R	597.81	0	0				Bed	
33R	607.51	0	0				Bed	
34R	620.00	0	0				Bed	
35R	626.71	0	0				Bed	
35R-3, 6-9	628.26						Soft sediment deformation	Fluid-escape structure?
36R	636.31	0	0				Bed	
37R	645.91	0	0				Bed	
38R	655.51	0	0				Bed	
39R	665.21	0	0				Bed	
40R	674.81	0	0				Bed	
41R	684.41	0	0				Bed	
42R	694.01	0	0				Bed	
43R	703.71	0	0				Bed	
44R	713.31	0	0				Bed	
45R	722.91	0	0				Bed	
47R-1,2,3	742.11	0	0				Bed	
47R-1, 0-25	742.10						Sedimentary breccia	
48R	751.71	0	0				Bed	Rip-up clasts
49R	761.31	0	0				Bed	

Table T7 (continued).

Core, section, interval (cm)	Depth (mbsf)	Cr az. (°)	Cr dip (°)	Pm az.	Pm plunge	Half	Identifier	Notes
50R-1, 1-56	771.01	0	0				Bed	
50R-1, 56-150	771.56							Disrupted interval, intralayer folds
50R-2, 9-32	772.59							Disrupted and folded interval, slumped?
51R	780.61	0	0				Bed	
52R	790.31	0	0				Bed	
53R	799.91	0	0				Bed	
54R-1 to 5	809.51	0	0				Bed	
54R-CC, 21-23	816.40						Normal faults	Probably drilling induced
55R-2, 112-115	821.82						Recumbent fold	Soft sediment deformation
55R-3, 1-12	822.21	0	0				Fissility	
55R-3, 16-20	822.36						Recumbent fold	Soft sediment deformation
56R	828.81	0	0				Bed	
56R-3, 3-4	831.11	309	37				Vein	1 mm wide
56R-3, 15-19	831.23	341	75				Vein	1 to 2 mm
56R-3, 28-28	831.36	42	13				Vein	1 to 2 mm wide
56R-3, 26-26	831.34	322	19				Vein	<1 mm wide
56R-3, 22-22	831.30	142	49				Contact	
56R-3, 31-44	831.39	0	12	340	12		Vein	2.5 mm wide
56R-3, 36-40	831.44	153	72				Vein	
56R-3, 67-73	831.75	39	53	14	53		Vein	Dark, fracture, 0.5 mm wide
56R-3, 80-80	831.88	71	21	46	21		Vein	White, 3 mm wide
56R-3, 66-66	831.74	180	5	155	5		Vein	White, 1 mm wide
56R-3, 70-75	831.78	164	49	139	49		Vein	Dark, <1 mm wide

Note: Cr az. = azimuth of plane in core reference frame, Cr dip = dip of plane in core reference frame, Pm az. = azimuth of plane in paleomagnetic reference frame, Pm plunge = plunge of plane in paleomagnetic reference frame.

Table T8. Nannofossil events recognized, Site 1177.

Nannofossil zones	Datum events	Age (Ma)	Depth (mbsf)	Average sedimentation rate [†] (m/m.y.)
NN19	LAD <i>Discoaster brouweri</i>	1.95	308.65	
NN18	LAD <i>Discoaster pentaradiatus</i>	2.52	331.05 ± 6.19	
NN17	LAD <i>Discoaster surculus</i>	2.55	357.09 ± 5.46	
NN14	LAD <i>Amaurolithus</i> spp.	4.0	399.50 ± 19.15	
NN11b	LAD <i>Discoaster quinquaramus</i> *	5.60	425.99 ± 7.34	
	LAD <i>Discoaster bergeni</i> *	7.80	502.30 ± 8.54	
NN10b	LAD <i>Reticulofenestra pseudoumbilicus</i> (>7 μm)*	9.0	526.92 ± 13.68	28.19
	LAD <i>Coccolithus miopelagicus</i> *	10.9	598.55 ± 0.06	
	LAD <i>Discoaster kugleri</i> *	11.8	637.58 ± 0.88	
NN5	LAD <i>Sphenolithus heteromorphus</i> *	13.6	672.48 ± 3.03	
NN4	LAD <i>Helicosphaera ampliaperta</i>	15.6	745.69 ± 1.32	
	LAD <i>Discoaster druggii</i> *	18.6	795.57 ± 20.93	

Notes: FAD = first appearance datum, LAD = last appearance datum. † = uncorrected for compaction. * = used for calculating average sedimentation rate.

Table T9. Interval and depth constraints of calcareous nannofossil events, Hole 1177A.

Event	Interval (cm)		Depth (mbsf)	
	Top	Bottom	Top	Bottom
	190-1177A-			
T <i>Discoaster brouweri</i>	1R-CC	1R-CC		308.65
T <i>Discoaster pentaradiatus</i>	4R-3, 68-69	4R-CC	324.86	337.24
T <i>Discoaster surculus</i>	6R-CC	7R-4, 75-76	351.63	362.55
T <i>Amaurolithus</i> spp.	12R-CC	13R-3, 75-76	410.69	418.65
T <i>Discoaster quinquerramus</i>	13R-3, 75-76	14R-3, 70-71	418.65	428.20
T <i>Discoaster bergonii</i>	21R-CC	23R-1, 74-75	492.76	511.84
T <i>Reticulofenestra pseudoumbilicus</i> (>7 µm)	23R-CC	26R-1, 49-50	513.24	540.59
T <i>Coccolithus miopelagicus</i>	32R-1, 68-69	32R-CC	598.48	598.61
B <i>Discoaster kugleri</i>	36R-1, 40-41	36R-CC	636.70	638.46
T <i>Sphenolithus heteromorphus</i>	39R-CC	40R-1, 71-72	669.45	675.51
T <i>Helicosphaera ampliapertura</i>	47R-2, 76-77	47R-CC	744.36	751.15
T <i>Discoaster druggii</i>	50R-CC	54R-CC	774.64	816.50

Note: T = top occurrence, B = bottom occurrence.

Table T10. Epoch boundaries, Site 1177.

Boundary	Depth (mbsf)	Event
Pliocene/Miocene	425.99 ± 7.34	T <i>Discoaster quinquerramus</i>
late/middle Miocene	598.54 ± 0.06	T <i>Coccolithus miopelagicus</i>

Note: T = top occurrence, B = bottom occurrence.

Table T12. Depths and ages of magnetic chrons and subchrons identified, Site 1177.

Depth (mbsf)		Polarity	Boundary of chron	Subchron	Age (Ma)
Top	Bottom				
301.85	302.20	N		Reunion	2.14
328.55	368.15	N	Matuyama/Gauss	C2An.1n	2.581
368.15	375.15	R		Mammoth	3.22
375.15	384.25	N		C2An.3n	3.33
384.25	397.25	R	Gauss/Gilbert	C2Ar	3.58
397.25	399.45	N		Cochiti	4.18
399.45	401.75	R		C3n.1r	4.29
401.75	405.35	N		Nunivak	4.48
405.35	409.23	R		C3n.2r	4.62
409.23	417.95	N		Sidufijall	4.8
417.95	427.45	R		C3r	5.23
427.45	431.80	N	Gilbert/C3A	C3An.1n	5.894
431.80	433.12	R		C3An.1r	6.137
433.12	439.00	N		C3An.2n	6.269
439.00	450.00	R		C3Ar	6.567
444.25	450.00	N	C3A/C3B	C3B.1n	6.935
534.55	535.40	N	C4A/C5	C5n.1n	9.74
755.10	759.35	N		C5Cn.1n?	16.014
761.10	791.95	N		C5Cn.2n?	16.327

Notes: N = normal, R = reversed. ? = uncertain chron identification.

Table T13. Pore fluid composition, Hole 1177A.

Hole, core, section, interval (cm)	Depth (mbsf)	pH (ISE)	Alk (T) (mM)	Sal (R)	Cl (T) (mM)	SO ₄ (I) (mM)	Na (I) (mM)	Mg (I) (mM)	Mg (T) (mM)	Ca (I) (mM)	Ca (T) (mM)	K (I) (mM)	H ₄ SiO ₄ (S) (μM)	NH ₄ (S) (μM)
190-1177A-														
1R-4, 135-150	306.05	7.55	18.6	32.0	555.0	0.3	482	33.0	32.8	7.72	8.3	8.10	1009	2252
2R-2, 135-150	312.05	7.54	19.3	32.5	554.0	0.3	481	32.9	32.8	8.15	8.6	8.06	972	
3R-2, 130-150	321.70	7.69	18.8	32.5	553.5	0.1	480	32.6	32.6	8.49	8.9	7.81	970	1455
4R-4, 130-150	334.30			32.5	553.0	0.1	480	32.3	34.9	8.88	6.4	8.24		
5R-1, 38-74	338.48	7.72	20.6	32.5	554.0	0.0	482	31.9	32.1	8.63	9.0	8.16	901	1674
6R-1, 70-100	348.40	7.54	17.7	32.5	554.0	0.5	482	32.0	34.8	8.85	6.0	7.75	929	
7R-4, 125-150	363.05	7.65	18.0	32.0	555.0	0.4	484	31.0	31.8	9.10	8.9	7.47	910	1157
8R-2, 0-32	368.50	7.86	18.0	32.0	556.0	0.2	484	30.5	32.4	9.31	8.4	7.77	845	
9R-3, 120-150	380.80	7.56	17.0	32.0	556.0	0.7	485	30.4	30.9	9.76	9.6	7.16	951	898
10R-1, 26-54	386.36	7.62	16.9	33.0	557.0	0.5	486	29.8	31.3	9.73	9.1	7.22	858	
11R-1, 109-119	396.79	7.74	16.1	32.0	557.0	1.1	486	30.1	31.0	9.52	9.4	7.18	824	778
11R-1, 135-150	397.05			32.0	557.5	0.5	487	29.0	31.6	9.29	8.1	7.33		
11R-4, 135-150	401.55			32.0	558.0	0.6	490	29.5		9.49		6.39		
12R-1, 59-88	405.89	7.76	14.9	32.0	559.0	0.5	489	29.3	30.3	9.62	9.2	6.53	705	
13R-4, 115-150	420.55			31.0	545.0	2.2		33.5	34.4	10.26	9.8	4.24	441	400
14R-4, 130-150	430.30			31.0	546.0	3.5		33.7	34.2	9.50	10.0	4.08	359	
15R-3, 115-150	438.35			32.0	546.0	5.6		35.3	36.2	10.38	10.8	4.12		659
16R-1, 0-48	443.90	7.90	7.0	32.5	547.0	9.0	472	36.7	37.6	10.05	10.3	4.11	247	
17R-1, 120-150	454.70	8.10	7.7	33.0	552.0	14.1	481	40.6	39.5	11.02	11.5	4.20	206	
19R-4, 120-150	478.50			33.0	534.0	18.6	455	46.5	47.1	12.36	12.9	3.03		689
20R-1, 110-150	483.50	7.57	7.5	34.0	553.0	22.2	485	44.6	44.9	12.60	12.8	4.25	314	
23R-2, 0-24	512.53			34.5	554.0	25.9	484	48.2	48.1	15.05	14.7	3.09	266	598
24R-4, 86-120	526.06			33.5	536.0	25.0		47.1		16.87		2.28	290	
25R-6, 0-30	537.90			33.5	536.0	25.0	461	46.7	47.1	17.51	17.6	2.28		458
26R-1, 95-125	541.05	8.01	7.1	34.0	550.0	27.0	484	45.0	46.3	16.63	15.4	3.11	227	
27R-1, 10-40	549.80	8.00	6.0	34.5	549.0	26.0	476	47.1	47.0	16.81	16.9	2.59		548
29R-1, 120-150	570.10			33.0	526.0	24.3	445	48.0	48.5	18.62	18.0	1.98		430
30R-4, 120-150	584.20			32.5	524.0	24.4	448	45.4	46.1	18.17	17.9	2.02	307	
31R-1, 0-13	588.20			33.5	525.0	25.0	448	47.6	47.2	17.98	17.9	2.20		
33R-2, 78-110	609.78			35.5	524.0	24.9	441	50.8	51.0	16.95	17.1	2.25		383
35R-1, 22-52	626.92	7.71	5.4	35.5	559.0	28.7	488	48.1	47.2	18.04	17.5	3.56	230	548
36R-2, 0-47	637.80	7.73	6.0	34.5	558.5	27.1	487	43.5	46.3	19.03	17.8	3.41		582
37R-1, 0-50	645.90			33.5	541.0	24.7	462	44.3	46.8	19.98	18.4	2.99	231	564
38R-1, 0-20	655.50			35.0	559.0	25.8	493	38.6	37.1	20.20	19.8	3.82		843
39R-1, 120-150	666.40			31.5	509.0	22.8	437	38.1	40.7	20.04	19.4	2.85	286	608
40R-1, 0-30	674.80			34.5	558.5	26.2	492	39.6	40.4	19.32	19.5	4.47	335	950
41R-1, 0-30	684.40	7.74	5.9	35.0	532.0	24.9	457	43.9	43.6	19.39	19.3	3.74		
42R-1, 121-150	695.21			32.5	525.5				33.8		17.4			502
43R-2, 120-150	706.40			32.5	527.0	20.4	453	37.8	38.8	19.06	19.3	4.07		
44R-1, 0-30	713.30			31.5	514.5	18.4	455	35.2	31.1	18.20	17.8	4.02	344	506
45R-2, 99-126	725.39			31.5	514.5	9.1	450	26.5	24.4	17.98	17.7	4.57		
46R-1, 125-150	733.75			30.5	507.0	7.1	443	25.0	24.3	17.11	15.7	4.17		458
47R-3, 125-150	746.35			29.0	520.0	1.2		21.7		16.80		4.30		
48R-4, 120-150	757.40			30.0	526.0	0.6	455	20.4	20.1	16.49	16.2	5.42		536
49R-3, 120-150	765.50			26.5	468.0	0.3		18.3		14.69		4.74		381
50R-3, 0-35	773.98	8.14	6.8	32.0	557.0	0.5	489	19.0	16.3	17.46	16.3	9.77	746	665
51R-1, 135-150	781.95	7.88	8.0	32.0	559.0	0.7	491	19.3	16.1	17.30	17.3	9.63		
51R-2, 134-150	783.44	7.93	7.8	32.2	570.0	0.7	483	19.0	25.3	17.76	17.3	10.02		693
52R-1, 130-141	791.60			32.0	566.0	2.1		19.7		16.74		10.63		693
52R-2, 0-17	791.80			30.7	548.0	0.5		19.0		17.13		7.95	869	
53R-3, 120-150	804.10			28.5	522.0	0.5		19.2		16.41		5.82		500
54R-2, 0-20	811.00	8.10	7.4	32.0	567.0	1.4	500	18.9	17.2	16.00	15.3	6.39	776	
54R-2, 20-45	811.20			30.0	528.0	1.1		19.2		15.69		10.08		580
55R-1, 120-150	820.40	8.21	3.5	30.0	535.0	0.6	461	19.9	16.0	15.70	18.2	6.84		508
56R-1, 0-30	828.80	7.82	4.6	31.0	554.0	2.1	486	21.3	18.2	16.63	16.7	7.02	443	

Note: ISE = ion selective electrode, Alk = alkalinity, T = titration, Sal = salinity, I = ion, S = spectrophotometry.

Table T14. Headspace gas analysis, Hole 1177A.

Core, section, interval (cm)	Depth (mbsf)	Sample method	C ₁ /C ₂	C ₁ (ppm)	C ₂ (ppm)	C ₂ = (ppm)	C ₃ (ppm)	C ₃ = (ppm)
190-1177A-								
1R-4, 0-5	304.70	HS		536	0.0	0.0	0.0	0.0
2R-2, 0-5	310.70	HS		464	0.0	0.0	0.0	0.0
3R-2, 130-150	321.70	HS		134	0.0	0.0	0.0	0.0
4R-4, 0-5	333.00	HS		77	0.0	0.0	0.0	0.0
5R-4, 0-5	341.10	HS		91	0.0	0.0	0.0	0.0
6R-2, 0-5	348.70	HS		117	0.0	0.0	0.0	0.0
7R-5, 0-5	363.30	HS		24	0.0	0.0	0.0	0.0
8R-3, 0-5	370.00	HS	18	5	0.3	0.0	0.0	0.0
9R-4, 0-5	381.10	HS		3	0.0	0.0	0.0	0.0
10R-2, 0-5	387.60	HS		3	0.0	0.0	0.0	0.0
11R-2, 0-5	397.20	HS		3	0.0	0.0	0.0	0.0
13R-5, 0-5	420.90	HS		3	0.0	0.0	0.0	0.0
14R-5, 0-5	430.50	HS		3	0.0	0.0	0.0	0.0
15R-4, 0-5	438.70	HS		2	0.0	0.0	0.0	0.0
16R-2, 0-5	445.40	HS		3	0.0	0.0	0.0	0.0
17R-2, 0-5	455.00	HS		3	0.0	0.0	0.0	0.0
18R-1, 0-5	463.10	HS		6	0.0	0.0	0.0	0.0
19R-5, 0-5	478.80	HS		2	0.0	0.0	0.0	0.0
20R-2, 0-5	483.90	HS		5	0.0	0.0	0.0	0.0
22R-1, 0-5	501.60	HS		3	0.0	0.0	0.0	0.0
23R-1, 140-143	512.50	HS		3	0.0	0.0	0.0	0.0
24R-3, 0-5	523.70	HS		2	0.0	0.0	0.0	0.0
25R-5, 0-5	536.40	HS		2	0.0	0.0	0.0	0.0
26R-1, 0-5	540.10	HS		3	0.0	0.0	0.0	0.0
27R-1, 0-5	549.70	HS		3	0.0	0.0	0.0	0.0
29R-1, 0-5	568.90	HS		3	0.0	0.0	0.0	0.0
30R-4, 0-5	583.00	HS		3	0.0	0.0	0.0	0.0
31R-2, 0-5	589.70	HS		2	0.0	0.0	0.0	0.0
33R-2, 78-110	609.78	HS		5	0.0	0.0	0.0	0.0
35R-1, 22-52	626.92	HS		3	0.0	0.0	0.0	0.0
36R-2, 0-47	637.80	HS		3	0.0	0.0	0.0	0.0
37R-2, 0-5	646.40	HS		3	0.0	0.0	0.0	0.0
38R-1, 0-5	655.50	HS		2	0.0	0.0	0.0	0.0
39R-2, 0-5	666.70	HS		2	0.0	0.0	0.0	0.0
40R-1, 0-5	674.80	HS		4	0.0	0.0	0.0	0.0
41R-3, 0-5	687.40	HS		4	0.0	0.0	0.0	0.0
42R-2, 0-5	695.50	HS		3	0.0	0.0	0.0	0.0
43R-2, 0-5	705.20	HS		4	0.0	0.0	0.0	0.0
44R-2, 0-5	714.80	HS		4	0.0	0.0	0.0	0.0
45R-2, 0-5	724.40	HS		3	0.0	0.0	0.0	0.0
46R-2, 0-5	734.00	HS		5	0.0	0.0	0.0	0.0
47R-4, 0-5	746.60	HS	204	469	2.3	0.0	0.0	0.0
48R-5, 0-5	757.70	HS	372	632	1.7	0.0	0.7	0.0
49R-3, 120-150	765.50	HS	514	1080	2.1	0.0	0.0	0.0
50R-1, 0-5	771.00	HS	887	4079	4.6	0.0	0.0	0.0
51R-2, 0-5	782.10	HS	1495	6875	4.6	0.0	0.0	0.0
52R-1, 125-130	791.55	HS	1614	5325	3.3	0.0	0.0	0.0
53R-5, 0-5	805.90	HS	657	7426	11.3	0.0	0.0	0.0
54R-4, 0-5	814.00	HS	389	3309	8.5	0.0	0.0	0.0
55R-2, 0-5	820.70	HS	457	4703	10.3	0.0	0.0	0.0
56R-2, 0-5	830.30	HS	1138	1821	1.6	0.0	0.0	0.0

Note: HS = headspace.

Table T15. Carbon, nitrogen, sulfur, and hydrogen analyses, Hole 1177A.
(See table note. Continued on next page.)

Core, section, interval (cm)	Depth (mbsf)	Inorganic C (wt%)	CaCO ₃ (wt%)	TOC (wt%)	Organic C (wt%)	N (wt%)	S (wt%)	H (mg HC/g of sediment)
190-1177A-								
1R-2, 85-86	302.55	0.20	1.69	NA	NA	NA	NA	NA
1R-4, 133-134	306.03	0.12	1.00	NA	NA	NA	NA	NA
2R-2, 107-108	311.77	0.08	0.68	0.43	0.35	0.04	0.00	0.63
3R-2, 122-123	321.62	0.57	4.81	NA	NA	NA	NA	NA
3R-4, 84-85	324.24	0.13	1.14	NA	NA	NA	NA	NA
4R-3, 106-107	332.56	0.30	2.55	NA	NA	NA	NA	NA
4R-5, 18-19	334.68	0.00	0.00	NA	NA	NA	NA	NA
5R-1, 36-37	338.46	0.25	2.15	NA	NA	NA	NA	NA
5R-3, 96-97	340.56	0.11	0.96	0.95	0.84	0.04	0.04	0.72
5R-4, 66-67	341.76	0.03	0.28	NA	NA	NA	NA	NA
6R-1, 66-67	348.36	0.69	5.80	NA	NA	NA	NA	NA
7R-4, 124-125	363.04	0.18	1.55	NA	NA	NA	NA	NA
7R-6, 63-64	365.43	0.65	5.49	NA	NA	NA	NA	NA
8R-2, 54-56	369.04	0.19	1.59	NA	NA	NA	NA	NA
9R-3, 108-109	380.68	0.09	0.78	0.34	0.25	0.06	0.14	0.73
10R-2, 149-150	389.09	0.08	0.72	NA	NA	NA	NA	NA
11R-1, 132-133	397.02	0.08	0.71	NA	NA	NA	NA	NA
11R-6, 36-37	403.56	0.12	1.06	0.4	0.28	0.06	0.00	0.7
12R-1, 55-56	405.85	0.08	0.74	NA	NA	NA	NA	NA
13R-4, 113-114	420.53	0.08	0.72	NA	NA	NA	NA	NA
13R-7, 45-46	424.35	0.08	0.74	NA	NA	NA	NA	NA
13R-CC, 23-24	424.73	0.24	2.04	NA	NA	NA	NA	NA
14R-4, 130-131	430.30	0.40	3.40	NA	NA	NA	NA	NA
15R-3, 112-113	438.32	0.09	0.75	NA	NA	NA	NA	NA
15R-CC, 10-11	443.90	0.20	1.69	NA	NA	NA	NA	NA
16R-1, 91-92	444.81	0.90	7.57	NA	NA	NA	NA	NA
16R-3, 118-119	448.08	0.30	2.52	NA	NA	NA	NA	NA
16R-4, 65-66	449.05	0.05	0.44	NA	NA	NA	NA	NA
16R-4, 143-144	449.83	0.01	0.16	0.26	0.24	0.09	0.36	0.70
17R-1, 113-114	454.63	0.24	2.05	NA	NA	NA	NA	NA
17R-2, 25-26	455.25	0.07	0.61	NA	NA	NA	NA	NA
17R-2, 87-98	455.87	0.06	0.50	NA	NA	NA	NA	NA
19R-4, 118-119	478.48	0.60	5.02	NA	NA	NA	NA	NA
19R-6, 42-43	480.72	0.03	0.30	NA	NA	NA	NA	NA
19R-7, 36-38	482.16	0.06	0.54	0.47	0.4	0.08	0.81	0.59
20R-1, 107-108	483.47	0.12	1.06	NA	NA	NA	NA	NA
20R-2, 61-62	484.51	0.01	0.16	NA	NA	NA	NA	NA
21R-1, 37-38	492.37	0.09	0.75	NA	NA	NA	NA	NA
22R-CC, 6-7	502.50	0.07	0.64	NA	NA	NA	NA	NA
23R-2, 41-42	512.94	0.08	0.67	0.20	0.11	0.09	0.28	0.77
24R-1, 87-88	521.57	0.16	1.40	NA	NA	NA	NA	NA
24R-1, 139-140	522.09	2.64	22.01	NA	NA	NA	NA	NA
24R-4, 1-2	525.21	1.52	12.66	NA	NA	NA	NA	NA
24R-4, 54-55	525.74	0.06	0.50	NA	NA	NA	NA	NA
24R-5, 129-130	527.69	0.09	0.79	NA	NA	NA	NA	NA
24R-6, 129-130	529.19	0.15	1.31	NA	NA	NA	NA	NA
25R-2, 129-130	533.19	0.07	0.65	0.18	0.11	0.08	0.00	0.72
25R-6, 107-108	538.97	0.05	0.47	NA	NA	NA	NA	NA
25R-7, 17-18	539.57	6.94	57.84	NA	NA	NA	NA	NA
26R-1, 79-80	540.89	0.10	0.85	NA	NA	NA	NA	NA
27R-1, 96-97	550.66	0.10	0.89	0.39	0.29	0.07	0.14	0.65
29R-1, 33-34	569.23	0.10	0.84	NA	NA	NA	NA	NA
29R-1, 87-88	569.77	4.32	35.98	NA	NA	NA	NA	NA
29R-2, 125-126	571.65	0.15	1.26	NA	NA	NA	NA	NA
30R-4, 118-119	584.18	0.07	0.62	NA	NA	NA	NA	NA
30R-7, 45-46	587.95	0.08	0.69	NA	NA	NA	NA	NA
31R-1, 20-21	588.40	0.05	0.47	NA	NA	NA	NA	NA
31R-2, 60-61	590.30	0.05	0.48	0.09	0.03	0.06	0.09	0.87
31R-CC, 12-13	591.14	0.06	0.52	NA	NA	NA	NA	NA
32R-1, 7-8	597.87	8.75	72.90	NA	NA	NA	NA	NA
32R-1, 61-62	598.41	0.14	1.17	NA	NA	NA	NA	NA
33R-1, 14-15	607.64	0.37	3.09	1.18	0.81	0.11	0.47	0.78
33R-1, 86-87	608.36	0.11	0.93	NA	NA	NA	NA	NA
33R-2, 70-71	609.70	0.10	0.89	NA	NA	NA	NA	NA
34R-CC, 15-16	617.25	0.16	1.37	NA	NA	NA	NA	NA
35R-2, 70-71	627.92	0.09	0.78	NA	NA	NA	NA	NA

Table T15 (continued).

Core, section, interval (cm)	Depth (mbsf)	Inorganic C (wt%)	CaCO ₃ (wt%)	TOC (wt%)	Organic C (wt%)	N (wt%)	S (wt%)	H (mg HC/g of sediment)
35R-3, 7-8	628.27	0.05	0.46	NA	NA	NA	NA	NA
36R-1, 24-25	636.54	0.17	1.47	NA	NA	NA	NA	NA
36R-1, 116-117	637.46	0.31	2.60	NA	NA	NA	NA	NA
37R-2, 81-82	647.21	0.26	2.18	NA	NA	NA	NA	NA
37R-3, 33-34	647.73	0.08	0.72	0.39	0.31	0.07	0.24	0.52
38R-CC, 19-20	656.36	0.59	4.95	NA	NA	NA	NA	NA
39R-1, 94-95	666.14	0.04	0.35	NA	NA	NA	NA	NA
39R-2, 140-142	668.10	7.98	66.49	NA	NA	NA	NA	NA
40R-1, 115-116	675.95	0.41	3.48	NA	NA	NA	NA	NA
41R-1, 131-132	685.71	0.11	0.96	NA	NA	NA	NA	NA
41R-2, 99-100	686.89	0.39	3.29	NA	NA	NA	NA	NA
42R-1, 119-120	695.19	0.15	1.31	1.77	1.62	0.05	0.52	0.60
43R-1, 6-7	703.76	0.48	4.07	NA	NA	NA	NA	NA
43R-2, 119-120	706.39	0.56	4.70	NA	NA	NA	NA	NA
44R-1, 40-41	713.70	0.65	5.48	NA	NA	NA	NA	NA
44R-2, 73-74	715.53	0.54	4.53	NA	NA	NA	NA	NA
45R-1, 127-128	724.17	2.04	17.01	NA	NA	NA	NA	NA
45R-2, 86-87	725.26	1.09	9.11	NA	NA	NA	NA	NA
46R-1, 20-21	732.70	0.49	4.13	NA	NA	NA	NA	NA
46R-1, 118-119	733.68	0.55	4.62	NA	NA	NA	NA	NA
46R-2, 125-126	735.25	0.12	1.00	NA	NA	NA	NA	NA
46R-3, 8-9	735.58	0.37	3.14	NA	NA	NA	NA	NA
47R-3, 101-102	746.11	0.37	3.16	1.75	1.38	0.12	0.48	0.84
47R-5, 99-100	749.09	0.50	4.19	NA	NA	NA	NA	NA
48R-4, 118-119	757.38	0.36	3.00	1.07	0.71	0.12	0.15	0.73
48R-6, 115-116	760.35	0.06	0.55	NA	NA	NA	NA	NA
49R-2, 64-65	763.44	0.23	1.99	0.68	0.44	0.04	0.10	0.69
49R-2, 146-147	764.26	0.06	0.56	NA	NA	NA	NA	NA
49R-3, 118-119	765.48	0.09	0.77	NA	NA	NA	NA	NA
49R-4, 22-23	766.02	0.06	0.57	NA	NA	NA	NA	NA
49R-5, 75-76	768.05	0.10	0.89	NA	NA	NA	NA	NA
50R-1, 38-39	771.38	0.06	0.53	NA	NA	NA	NA	NA
50R-3, 36-37	774.34	0.04	0.41	NA	NA	NA	NA	NA
51R-1, 19-20	780.79	0.06	0.51	NA	NA	NA	NA	NA
51R-2, 26-27	782.36	0.06	0.57	NA	NA	NA	NA	NA
51R-2, 112-113	783.22	0.19	1.64	NA	NA	NA	NA	NA
52R-2, 18-19	791.98	0.05	0.43	NA	NA	NA	NA	NA
52R-2, 56-57	792.36	0.14	1.17	NA	NA	NA	NA	NA
52R-3, 28-29	793.58	0.03	0.29	NA	NA	NA	NA	NA
52R-3, 49-50	793.79	0.08	0.71	NA	NA	NA	NA	NA
53R-2, 58-59	801.98	0.07	0.61	NA	NA	NA	NA	NA
53R-3, 117-118	804.07	0.07	0.62	0.55	0.47	0.09	0.10	0.67
53R-6, 62-63	808.02	0.08	0.70	NA	NA	NA	NA	NA
54R-1, 124-125	810.74	0.08	0.67	NA	NA	NA	NA	NA
54R-3, 68-69	813.18	0.07	0.62	NA	NA	NA	NA	NA
54R-3, 69-70	813.19	0.16	1.35	NA	NA	NA	NA	NA
54R-5, 57-58	816.07	0.08	0.69	0.44	0.35	0.07	0.22	0.47
55R-1, 118-119	820.38	0.28	2.33	NA	NA	NA	NA	NA
55R-3, 24-25	822.44	0.34	2.90	NA	NA	NA	NA	NA
56R-1, 122-123	830.02	1.72	14.35	NA	NA	NA	NA	NA
56R-2, 47-48	830.77	0.08	0.74	0.54	0.45	0.11	0.21	0.63
56R-2, 73-74	831.03	0.06	0.52	NA	NA	NA	NA	NA

Note: TOC = total organic carbon, HC = hydrocarbon.

Table T16. Total bacterial populations in sediments, Site 1177.

Depth (mbsf)	Bacterial cells (cells/cm ³)
302.76	1.14×10^6
321.69	1.82×10^6
334.19	4.20×10^5
341.09	4.84×10^5
363.04	4.22×10^5
380.69	4.28×10^5
401.03	6.37×10^5
420.54	1.16×10^6
444.38	9.79×10^5
478.49	2.38×10^6
512.52	1.14×10^6
523.24	1.19×10^6
569.78	1.44×10^6
608.71	9.14×10^5
647.23	1.82×10^6
675.10	1.92×10^6
686.89	BD
725.38	8.59×10^5
744.65	7.51×10^5
773.97	3.89×10^5
790.63	9.44×10^3
811.45	3.82×10^4
830.29	BD

Note: BD = below detection ($\sim 6 \times 10^4$ cells/cm³).

Table T17. Drilling fluid intrusion estimated based on PFT tracer experiments, Hole 1177A.

Core, section	Total sample weight (g)			Bulk density (g/cm ³)	PFT peak area			Drilling fluid (μL)/sediment (g)		
	Outside	Quarter	Center		Outside	Quarter	Center	Outside	Quarter	Center
190-1177A-										
24R-1	18.049	18.224	19.056	1.96	230.6	0	145.0	0.02	BD	BD
24R-3	19.945	18.041	16.777	1.95	126.9	18.4	241.6	BD	BD	0.07
24R-5	17.797	ND	18.001	1.95	153.1	ND	102.7	0.01	ND	BD
25R-1	17.753	18.428	18.111	1.95	59.8	0	0	BD	BD	BD
24R-4	18.303	17.422	19.685	1.94	2934.5	94.9	28.6	0.03	BD	BD
24R-5	17.787	17.805	18.198	1.90	5079.5	0	0	0.07	BD	BD

Note: ND = no data, BD = below detection.

Table T18. Fluorescent microsphere tracer experiments, Hole 1177A.

Core, section	Total sample weight (g)			Microspheres/sediment (g)			Microspheres/sediment (g)		
	Outside	Quarter	Center	Outside	Quarter	Center	Outside	Quarter	Center
190-1177A-									
6R-1	1.22	1.16	1.48	114	BD	BD	93	BD	BD
6R-2	1.58	1.21	1.08	722	80	280	457	66	260
6R-3	2.85	1.78	1.69	37	144	780	13	81	460

Note: BD = below detection (0.01 µL drilling fluid).

Table T19. Electrical conductivities and formation factor data for cubes, Hole 1177A. (See table note. Continued on next page.)

Core, section, interval (cm)	Depth (mbsf)	Conductivity (S/m)			Temp (°C)	Formation factor		
		x	y	z		x	y	z
190-1177A-								
1R-2, 76	302.46	1.51	1.56	1.37	25.4	3.54	3.43	3.89
1R-4, 129	305.99	1.53	1.48	1.34	25.4	3.49	3.61	3.99
1R-6, 57	308.27	1.55	1.59	1.36	25.4	3.45	3.35	3.93
2R-1, 123	310.43	1.61	1.61	1.40	25.6	3.34	3.33	3.83
2R-3, 119	313.39	1.62	1.62	1.46	25.6	3.30	3.32	3.67
3R-2, 120	321.60	1.56	1.56	1.33	25.8	3.45	3.44	4.03
3R-4, 82	324.22	1.50	1.53	1.38	25.8	3.59	3.51	3.89
4R-2, 120	331.20	1.58	1.53	1.35	25.7	3.40	3.52	3.99
4R-5, 19	334.69	1.49	1.50	1.32	26.0	3.63	3.61	4.09
4R-6, 79	336.79	1.53	1.52	1.36	26.0	3.53	3.55	3.98
5R-1, 5	338.15	1.44	1.52	1.36	26.1	3.75	3.55	3.99
5R-5, 116	343.76	1.54	1.57	1.45	26.1	3.50	3.44	3.72
6R-1, 56	348.26	1.53	1.53	1.36	26.1	3.53	3.54	3.96
6R-3, 66	349.86	1.48	1.58	1.41	25.6	3.63	3.40	3.80
7R-1, 37	357.67	1.54	1.61	1.43	25.6	3.48	3.33	3.75
7R-3, 73	361.03	1.65	1.55	1.47	25.6	3.24	3.46	3.64
8R-7, 17	376.17	1.43	1.54	1.38	25.9	3.76	3.51	3.90
9R-2, 40	378.50	1.48	1.48	1.43	25.9	3.63	3.64	3.77
9R-6, 32	384.42	1.40	1.34	1.31	25.9	3.85	4.03	4.11
10R-1, 65	386.75	1.60	1.62	1.50	26.1	3.39	3.35	3.61
10R-6, 66	394.26	1.54	1.45	1.42	26.1	3.51	3.74	3.82
11R-1, 67	396.37	1.51	1.50	1.47	25.5	3.54	3.57	3.64
11R-5, 55	402.25	1.32	1.27	1.23	25.5	4.06	4.21	4.34
12R-1, 54	405.84	1.48	1.49	1.45	25.6	3.63	3.61	3.70
12R-3, 126	408.94	1.52	1.49	1.43	25.5	3.52	3.60	3.75
13R-1, 68	415.58	1.18	1.21	0.92	25.2	4.52	4.38	5.78
13R-4, 82	420.22	1.06	1.09	0.86	25.0	5.02	4.88	6.16
13R-CC, 19	424.69	1.11	1.12	0.93	25.1	4.80	4.73	5.68
14R-1, 59	425.09	1.18	1.23	1.00	25.2	4.51	4.34	5.31
14R-4, 124	430.24	1.18	1.15	0.87	25.4	4.53	4.64	6.14
14R-6, 46	432.46	1.16	1.14	0.98	25.2	4.57	4.66	5.44
15R-1, 31	434.51	1.16	1.19	0.79	25.4	4.60	4.48	6.74
15R-4, 56	439.26	1.17	1.18	0.94	25.3	4.56	4.53	5.70
15R-CC, 14	443.94	1.27	1.11	0.78	25.3	4.20	4.82	6.79
16R-2, 33	445.73	1.08	1.19	0.83	25.7	4.98	4.50	6.50
16R-4, 121	449.61	1.09	1.10	0.79	25.3	4.90	4.83	6.77
17R-1, 115	454.65	1.09	1.09	0.78	25.6	4.92	4.92	6.91
17R-2, 96	455.96	1.00	0.95	0.69	25.5	5.37	5.62	7.74
18R-1, 26	463.36	1.22	1.19	0.83	25.6	4.40	4.49	6.44
19R-2, 126	475.56	1.07	1.06	0.79	25.7	5.01	5.05	6.83
19R-4, 60	477.90	1.06	1.09	0.76	25.7	5.05	4.91	7.05
19R-6, 46	480.76	1.27	1.25	0.85	25.7	4.22	4.30	6.29
20R-1, 108	483.48	1.07	0.99	0.72	25.8	5.04	5.41	7.46
20R-2, 59	484.49	1.01	1.00	0.77	25.6	5.29	5.37	6.96
21R-1, 33	492.33	0.96	1.10	0.95	25.6	5.61	4.86	5.66
23R-2, 31	512.84	1.13	1.13	0.77	25.6	4.76	4.75	7.00
24R-3, 78	524.48	1.08	1.04	0.68	25.7	4.97	5.14	7.94
24R-6, 119	529.09	1.04	1.03	0.66	25.7	5.16	5.21	8.14
25R-3, 96	534.36	0.95	0.95	0.70	25.8	5.68	5.66	7.71
25R-6, 76	538.66	1.01	0.99	0.64	25.8	5.32	5.45	8.43
27R-1, 44	550.14	1.00	0.92	0.80	25.8	5.40	5.85	6.75
29R-2, 88	571.28	0.87	0.86	0.54	25.6	6.17	6.23	9.98
30R-3, 44	581.94	0.82	0.82	0.54	25.6	6.52	6.53	9.98
30R-6, 75	586.75	0.88	0.86	0.50	25.6	6.07	6.26	10.69
31R-CC, 10	591.12	0.93	0.94	0.52	24.6	5.64	5.57	10.06
32R-1, 62	598.42	0.95	0.94	0.51	24.6	5.53	5.57	10.25
32R-1, 2	597.82	0.04	0.05	0.05	24.7	120.39	116.62	115.94
33R-1, 15	607.65	1.01	0.98	0.47	24.6	5.20	5.39	11.11
33R-CC, 2	610.12	0.95	0.97	0.50	24.6	5.51	5.40	10.49
35R-2, 74	627.96	0.94	0.94	0.46	25.1	5.66	5.66	11.46
35R-3, 6	628.26	0.88	0.85	0.73	25.1	6.07	6.25	7.23
36R-1, 113	637.43	1.05	1.03	0.61	25.2	5.06	5.17	8.77
36R-2, 1	637.81	1.10	1.10	0.69	25.3	4.83	4.85	7.72
38R-CC, 22	656.39	0.94	0.94	0.57	25.1	5.67	5.63	9.33
37R-2, 68	647.08	1.00	1.02	0.49	25.1	5.33	5.19	10.78

Table T19 (continued).

Core, section, interval (cm)	Depth (mbsf)	Conductivity (S/m)			Temp (°C)	Formation factor		
		x	y	z		x	y	z
37R-4, 14	649.04	0.95	1.06	0.48	25.1	5.59	5.02	11.15
39R-2, 58	667.28	1.05	0.92	0.56	25.1	5.05	5.77	9.56
40R-1, 65	675.45	1.01	0.99	0.44	25.1	5.26	5.35	12.09
41R-3, 83	688.23	0.91	0.92	0.45	25.1	5.86	5.79	11.77
42R-1, 76	694.76	0.90	0.88	0.45	24.4	5.81	5.94	11.62
43R-2, 63	705.83	0.90	0.92	0.43	24.2	5.83	5.69	12.15
44R-1, 41	713.71	0.85	0.86	0.50	24.2	6.14	6.05	10.38
44R-2, 73	715.53	0.92	0.91	0.42	24.3	5.67	5.73	12.52
45R-1, 98	723.88	0.85	0.82	0.42	24.2	6.13	6.34	12.31
45R-2, 82	725.22	0.87	0.93	0.37	24.4	6.01	5.61	14.03
46R-1, 15	732.65	0.95	0.92	0.41	24.5	5.54	5.70	12.71
46R-3, 14	735.64	0.91	0.88	0.45	24.5	5.74	5.94	11.73
47R-1, 106	743.16	0.93	0.93	0.33	24.8	5.65	5.66	15.95
47R-3, 96	746.06	0.92	0.90	0.35	24.6	5.73	5.87	14.98
47R-5, 99	749.09	0.87	0.86	0.36	24.7	6.08	6.16	14.67
48R-2, 79	753.99	0.92	0.88	0.47	25.0	5.75	6.00	11.32
48R-4, 118	757.38	0.84	0.85	0.40	25.0	6.30	6.25	13.31
48R-6, 111	760.31	0.89	0.90	0.39	25.0	5.93	5.91	13.61
49R-2, 75	763.55	0.75	0.75	0.46	25.0	7.04	7.02	11.51
49R-4, 39	766.19	0.97	1.00	0.48	25.0	5.44	5.29	11.16
49R-5, 65	767.95	0.88	0.86	0.66	25.0	6.02	6.15	8.03
50R-1, 66	771.66	1.07	1.01	0.68	25.0	4.97	5.22	7.81
50R-3, 37	774.35	0.98	0.97	0.79	25.0	5.41	5.47	6.69
51R-1, 70	781.30	1.14	1.17	0.79	25.0	4.66	4.54	6.74
51R-2, 111	783.21	1.03	0.98	0.79	25.0	5.16	5.39	6.74
51R-3, 40	784.00	1.13	1.10	0.75	25.0	4.68	4.80	7.05
52R-2, 75	792.55	0.92	0.90	0.69	25.0	5.74	5.86	7.67
52R-3, 75	794.05	0.75	0.79	0.39	25.0	7.04	6.68	13.47
53R-2, 62	802.02	0.89	0.92	0.33	25.0	5.97	5.76	15.92
53R-6, 62	808.02	0.86	0.87	0.44	25.0	6.19	6.09	12.06
54R-1, 117	810.67	0.85	0.82	0.67	25.1	6.25	6.47	7.93
54R-3, 88	813.38	0.85	0.89	0.40	25.2	6.25	5.95	13.34
54R-4, 87	814.87	0.77	0.77	0.39	25.2	6.94	6.94	13.52
55R-1, 117	820.37	0.99	1.00	0.43	25.2	5.39	5.34	12.27
55R-2, 121	821.91	0.90	0.89	0.61	25.1	5.89	6.00	8.65
56R-1, 117	829.97	0.92	0.91	0.51	25.1	5.78	5.80	10.36

Note: x, y, z = probe axis.